ON THE REPAIR OF IMPACT-DAMAGED PRESTRESSED CONCRETE BRIDGE GIRDERS

by

Jarret Lee Kasan

Bachelor of Science, University of Pittsburgh, 2007

Master of Science, University of Pittsburgh, 2009

Submitted to the Graduate Faculty of

Swanson School of Engineering in partial fulfillment

of the requirements for the degree of

Doctor of Philosophy

University of Pittsburgh

2012

UNIVERSITY OF PITTSBURGH

SWANSON SCHOOL OF ENGINEERING

This dissertation was presented

by

Jarret Lee Kasan

It was defended on

January 30, 2012

and approved by

Dr. James M. Thompson, P.E., Associate Teaching Professor, Department of Civil and
Environmental Engineering, Carnegie Mellon University

Dr. William W. Clark, Professor, Department of Mechanical Engineering and Materials
Science

Dr. Melissa Bilec, Assistant Professor, Department of Civil and Environmental Engineering

Dr. John Brigham, Assistant Professor, Department of Civil and Environmental Engineering

Dissertation Director: Dr. Kent A. Harries, Associate Professor, Department of Civil and
Environmental Engineering

ON THE REPAIR OF IMPACT-DAMAGED PRESTRESSED CONCRETE BRIDGE GIRDERS

Jarret Lee Kasan, PhD

University of Pittsburgh, 2012

Prestressed concrete (PC) bridges are susceptible to catastrophic damage (often from over-height vehicle impact); the extent of which is often difficult to assess until it has progressed to the point of collapse. Impact damage occurs when a vehicle's height is greater than the vertical clearance between the roadway and overpass and the vehicle strikes the overpass. Impact damage ranges in severity, but generally does not cause immediate collapse of the structure. However, when untreated, impact damage can result in further or accelerated deterioration often resulting in significant prestressing steel corrosion.

Performing a structural repair requires confidence that the member in need of repair is behaving as anticipated. In doing so, the member should be viewed from a perspective different than conventional engineering assessment practices. For example, the contribution to section capacity of strands which have been exposed or severed due to over-height vehicle impact are neglected in conventional member assessment. This assessment practice has been found to be overly conservative because strands 'redevelop' their prestressing force upon entering sound concrete. Furthermore, due to the unanticipated composite action occurring between an AB girder and the barrier wall/curb slab assembly, many AB members that conventionally behave uniaxially are behaving asymmetrically and biaxial bending effects must be considered when

determining flexural capacity. Additionally, few (often one) girders are damaged due to the localized nature of impact-damage. Therefore, a rating factor expression was developed to quantify damage to individual girders.

Overall, this dissertation presents new approaches to the assessment, analysis and repair of PC girders. Employment of these assessment and analysis techniques allows for more accurate quantification of in-service member behavior, thus allowing for the most appropriate solution (member/bridge repair or replacement) to be selected. This approach is demonstrated through a case study analysis of a previous experimentally tested girder. Lastly, an approach to determining repair technology limitations (based on geometric and mechanical constraints) through an impact-damaged AB girder repair example is provided.

TABLE OF CONTENTS

LIST OF TABLES

LIST OF FIGURES

NOMENCLATURE

The following abbreviations and notation are used in this work.

Abbreviations

AASHTO   American Association of State Highway and Transportation Officials

AB   Adjacent Box Beam

ACI   American Concrete Institute

CFRP   Carbon Fiber Reinforced Polymer

FRP   Fiber Reinforced Polymer

NCHRP   National Cooperative Highway Research Program

RF   Rating Factor

Notation

A_{cg} concrete cross sectional area

$A_{cg,C}$ concrete cross sectional area, composite section

A_f FRP cross sectional area

A_{ps} Prestressed reinforcement area in the tension zone

b   width of compression face of member

b_w width member web(s)

C_E environmental reduction factor

c	distance from extreme concrete compression fiber to the neutral axis
cg strands	center of gravity of strands, measured from bottom of member
d_f	effective depth of FRP flexural reinforcement
d_p	distance from the extreme concrete compression fiber to centroid of prestressed reinforcement
E_c	modulus of elasticity of concrete
E_f	tensile modulus of elasticity of FRP
E_{ps}	tensile modulus of elasticity of prestressing steel, taken as 28500 ksi
e	eccentricity of prestressing steel with respect to centroidal axis of member
f_c'	specified compressive strength of concrete
f_{DC}	stress due to dead load and components and attachments
f_{DW}	stress due to wearing course
f_{LL+IM}	stress due to live load
f_{fe}	effective stress in FRP; stress level attained at section failure
f_{fu}	design ultimate tensile strength of FRP
f_{fu}^*	ultimate tensile strength of the FRP material as reported by the manufacturer
f_{gcp}	gross stress in concrete due to prestressing and beam self-weight
f_{pb}	compressive stress due to effective prestress
f_{pe}	effective prestress in prestressed steel reinforcement
f_{ps}	stress in prestressed reinforcement at nominal strength
f_{pu}	specified tensile strength of prestressing tendons
g	AASHTO live load distribution factor
J	St. Venant's torsional inertia

I_x	moment of inertia of section
$I_{x,C}$	moment of inertia of composite section
M	moment due to eccentric prestressing force in strands
M_{cr}	cracking moment
M_{DC}	moment on girder due to dead load components and attachments
M_D	moment on girder due to dead load components (including member self-weight) and attachments
M_{DW}	moment on girder due to wearing surface
M_{LL+IM}	controlling live load moment
M_n	nominal flexural strength of girder
M_{nf}	contribution of FRP to nominal flexural strength of girder
M_{np}	contribution of prestressing steel to nominal flexural strength of girder
M_u	design ultimate flexural strength of girder
N_b	number of beams in bridge
n	number of plies of FRP reinforcement
P_e	effective force in prestressing reinforcement (after all losses)
r	radius of gyration of a section
S_b	section modulus of the bottom of the member
S_t	section modulus of the top of the member
$S_{b,C}$	section modulus of the bottom of the composite member
$S_{t,C}$	section modulus of the top of the composite member
t_f	nominal thickness of one ply of FRP reinforcement
y_b	distance from extreme bottom fiber to the section centroid

y_t	distance from top fiber to the section centroid
α	empirical constant to determine an equivalent rectangular stress distribution in concrete
β_1	ratio of depth of equivalent rectangular stress block to depth of neutral axis
Δf_{pES}	prestress loss due to elastic shortening
Δf_{pLT}	prestress loss due to long term effects
Δf_{pT}	total prestress loss
ε_{bi}	strain level in concrete substrate at time of FRP installation (tension is positive)
ε_c	strain level in concrete
$\varepsilon_c{}'$	maximum strain of unconfined concrete corresponding to f'$_c$; may be taken as 0.003
ε_{cu}	ultimate axial strain of unconfined concrete
ε_{fd}	debonding strain of externally bonded FRP reinforcement
$\varepsilon_{fd}{}^*$	debonding strain of externally bonded PT FRP reinforcement
ε_{fe}	effective strain level in FRP reinforcement attained at failure
ε_{fu}	design rupture strain of FRP reinforcement
$\varepsilon_{fu}{}^*$	ultimate rupture strain of FRP reinforcement
ε_{pe}	effective strain in prestressing steel after losses
ε_{pi}	initial strain level in prestressed steel reinforcement
ε_{pnet}	net strain in flexural prestressing steel at limit state after prestress force is discounted (i.e.: excluding strains due to effective prestress force after losses)
ε_{ps}	strain in prestressed reinforcement at nominal strength
ε_{pt}	strain induced in FRP reinforcement by PT

ε_t tensile strain in the member

γ_{DC} AASHTO dead load and components and attachments factor

γ_{DW} AASHTO wearing course factor

γ_{LL+IM} AASHTO live load factor

ψ_f FRP strength reduction factor

This dissertation reports values in US units (inch-pound) throughout. The following "hard" conversion factors have been used:

1 inch = 25.4 mm

1 kip = 4.448 kN

1 ksi = 6.895 MPa

Reinforcing bar sizes are reported using the designation given in the appropriate reference. A bar designated using a "#" sign (e.g.: #4) refers to the standard inch-pound designation used in the United States where the number refers to the bar diameter in eighths of an inch.

ACKNOWLEDGEMENTS

I am pleased and excited to note my gratitude to my advisor, Dr. Kent A. Harries. His encouragement, motivation and guidance have been vital in developing this document in its present form. Also, his insight has been valuable in developing my skills and understanding of structural design concepts and he should be credited for such. I must thank him for the exorbitant amount of time he has spent with me on this project and motivating me to perform at my best.

Equally significant, I would like to thank Dr. John Brigham, Dr. Melissa Bilec, Dr. William Clark and Dr. James Thompson for serving on my committee. The encouragement and suggestions provided by Dr. Bilec and Dr. Clark are greatly appreciated. The technical insights and comments provided by Dr. Brigham and Dr. Thompson greatly benefitted this document as well as my understanding of structural mechanics and design considerations. Additionally, the motivation Dr. John Oyler provided since my time as an undergraduate student as well as our technical discussions have been invaluable and instrumental in shaping my interest in structural engineering. I would like to thank all of these individuals for their role in my academic career.

I would also like to thank my colleagues, Mr. Michael Richard, Mr. Derek Mitch, Mr. Feng Mu, Mr. Manik Barman and Mr. Charles Hager for their help and support.

Finally, special thanks go to my parents, Eli and Linda, siblings, Melissa, Eli and Kevin and Sam and Danielle for all of their love, support and encouragement over the years. Without them, I would be lost. Thank you for everything.

1.0   INTRODUCTION

The deteriorating condition of the nation's bridge infrastructure cannot be overstated. Prestressed concrete (PC) bridges, however, generally contradict this trend. These, often newer, structures have thus far demonstrated exceptional durability and represent only a small fraction of deficient bridges in the nation (FHWA 2007). Nonetheless, PC bridges are susceptible to potentially catastrophic damage (often from over-height vehicle impact); the extent of which is often difficult to assess until it has progressed to the point of collapse (Harries 2009). Impact damage occurs when a vehicle's height is greater than the vertical clearance between the roadway and overpass and the vehicle strikes the overpass. Examples of impact damage can be seen in Figure 1-1. Impact damage ranges in severity, but generally does not cause collapse of the structure at the time of impact. However, when untreated, impact damage can result in further or accelerated deterioration often resulting in significant prestressing steel corrosion. The combination of impact damage and subsequent corrosion can potentially be catastrophic (Harries 2006); hence the motivation of this study.

While PC bridges generally perform well (in Pennsylvania, only 7.8% of prestressed bridge superstructures are rated as deficient as opposed to an inventory-wide value of 13.7%), adjacent box (AB) girder bridges are the exception, representing a disproportionate number of

'problem' bridges and therefore requiring a disproportionate allocation of maintenance resources. In Pennsylvania, there is an inventory of 1997 AB bridges; these average over 40 years old. Of these, 355 (18%) are structurally deficient based on their superstructure rating only (PennDOT 2007 and Kasan 2009). Typically, structural deficiencies in AB bridges result from inherent design issues and over-height vehicle impact damage. For example, common detailing and construction practices during most AB bridge construction in Pennsylvania (1960's), along with improperly performing shear keys, have resulted in exterior AB girders behaving independently from the adjacent girders and compositely with the barrier wall/curb slab assembly, in an asymmetrical manner. The issue of asymmetric behavior is exacerbated when considering impact damage. Therefore, repair of impact damaged AB girders should take priority when considering PC girder repair methods. Consequently, many of the topics described in this dissertation are discussed specifically in terms of AB girders (Chapters 3, 4 and 5). As a whole, this dissertation describes a new approach (and its limitations) to assessment, analysis and repair technique for PC structures which is valid for any girder type.

Generally speaking, it is common practice that aging and structurally damaged PC bridge members are taken out of service and replaced. This, however, is not an efficient use of materials and resources since the member can often be repaired *in situ*. Recently, emphasis has been placed on repairing these girders, ultimately saving both economic and monetary resources and reducing the length of time in which the structure is out of service for girder/bridge replacement.

Performing a repair design requires the designer to be confident that the member is behaving as anticipated in service. In doing so, it may be necessary to view the member from a perspective different than conventional engineering assessment practices. For example, typical engineering assessment practice suggests the contribution to section capacity of strands which

have been exposed or severed due to vehicle impact are neglected in member assessment. The work in this document suggests that this is overly conservative because strands 'redevelop' their prestressing force upon entering sound concrete. Also, contrary to conventional practices, a biaxial analysis approach to determining the flexural capacity of an adjacent box (AB) girder which is behaving compositely with the barrier wall/curb slab assembly is described. Typically bridge structures are not analyzed considering their neutral axes being rotated from the horizontal, many in-service AB members are behaving asymmetrically requiring that biaxial bending be included in the analysis so as not to overestimate the member's capacity. Equally significant, the manner in which member assessment (establishing a rating factor) proceeds is also modified. The localized nature of impact damage typically results in few (often only one) damaged girders. Therefore, a rating factor method was developed to quantify the damage for individual girders. This method allows for the target capacity to be varied, thus allowing for the possibility of bridge posting, if acceptable. With this new paradigm regarding member behavior and assessment, actual *in situ* member behavior can be more accurately quantified, thus allowing for the most appropriate solution (repair or replacement of the member/bridge) to be selected.

There are numerous repair techniques proposed by entrepreneurial and academic institutions which restore PC girder flexural strength and save both material and economic resources. Of course, not all repair methods are viable in every situation and thus each must be assessed based on girder geometry, repair method applicability and the objectives of the repair scenario. This document also provides a methodology for determining repair technology limitations through an example repair of an impact-damaged AB girder. Although only a single repair type for a single repair technology is described, the approach is applicable to other girder shapes and repair technologies. This portion of the dissertation, develops the methodology

required for the completion of NCHRP 20-07, an ongoing project which will address additional member shapes and repair technologies.

It is anticipated that the guidance presented in this dissertation will benefit State agency and bridge design personnel when considering repair or replacement of damaged PC girders.

1.1   MOTIVATION OF PROPOSED WORK

Collisions between over-height vehicles and bridges are becoming more commonplace (Fig. 1). Recent catastrophic collapses including Lake View Drive onto I-70 in Washington PA (Fig. 1a) and the McIlvaine Road vehicle collision only 8 miles east of Lake View Drive (Fig. 1b) have led to a re-evaluation of the condition of many prestressed structures resulting in new postings and in some cases emergency decommissioning of structures. Collision damage, however, is generally far from catastrophic (Fig. 1c) although sound repair techniques are critical if additional damage (typically related to corrosion) is to be mitigated

Although there are many research and case studies addressing repair of prestressed bridge girders, there is little comprehensive guidance available. NCHRP Project 12-21, ultimately completed in 1985 and published as *NCHRP Report 280: Guidelines for Evaluation and Repair of Prestressed Concrete Bridge Members* (Shanafelt and Horn 1985) remains the most comprehensive national study to address the evaluation and repair of prestressed bridge members. A 1996 Texas study (Feldman et al. 1996) and a 2004 Wisconsin study (Tabatabi et al. 2004) have updated the earlier guides but are limited in scope: the TXDOT study addresses only impact damage while the WIDOT study focuses primarily on corrosion mitigation techniques at girder ends in cases where strengthening or structural retrofit is largely unnecessary. Extant

4

studies are necessarily out-of-date: i) they do not address the present state of the now 25-50 year-old prestressed concrete infrastructure and the inherent deterioration associated with this aging; ii) they do not address some of the newer methods of assessing the structural capacity and, importantly, residual prestress forces; iii) they are not consistent with present evaluation practices (AASHTO 2011); and, iv) they do not address some of the newer methods of retrofit including those using FRP materials and prestressed FRP materials.

To partially address these deficiencies, the author aided in preparation of a detailed report for Pennsylvania DOT entitled *Repair Methods for Prestressed Bridges* (Harries et al. 2009). While directed primarily at post-NCHRP Report 280 repair methods and focusing heavily on prestressed box girder structures, this PennDOT project and report forms a strong foundation for the present proposed study. Harries et al. provided: i) a detailed review of assessment techniques; ii) an extensive review of repair/rehabilitation and retrofit techniques including those addressed in NCHRP Report 280 and developed subsequently; iii) results from a North American survey of current state of practice; iv) 22 prototype repair examples; and v) a set of best practices recommendations. While the Harries et al. report provides a sound foundation for the present study, it is limited in scope, provides only cursory guidance.

The use of these new repair technologies has benefitted the bridge industry by increasing the number of structures which can be repaired as opposed to being replaced or posted. Examples of such bridge repairs are presented by Tumialan et al. (2001), Schiebel et al. (2001), Klaiber et al. (2003), Herman (2005), Toenjes (2005), Kim et al. (2008), Sika (2008a), Kasan (2009), Enchayan (2010), Pakrashi et al. (2010) and Yang et al. (2011), among others. Despite these demonstrations, little attention has been paid to the selection of appropriate repair measures and the limitations of these; this is often referred to as the 'repair or replace?' question. The objective

this work is to develop a methodology to approaching repair design aimed at providing justification for the solution of the 'repair or replace' question in the context of present AASHTO practice. As part of this work, novel assessment techniques (i.e.: redevelopment of severed prestressed strands and analysis of eccentrically loaded AB girders) and the application of these techniques will be discussed.

1.2   SCOPE AND OBJECTIVE OF DISSERTATION

It is the goal of this dissertation to provide a rational approach to addressing analysis and structural repair issues relating to impact-damaged PC bridge girders. It is acknowledged that some findings presented in this document are specific to AB bridge structures, since this class of PC structure is in the most critical need (Kasan 2009). However, the approach to the issues described here can be applied to other girder shapes. Examples have been provided to demonstrate the implementation of findings described in this document (Chapters 2 and 3) to show applicability in analysis (Chapter 4) and for the determination of repair technology limitations (Chapter 5). Findings are described in context of the examples provided, but the approach can be extended to other girder types and repair technologies, and thus are useful beyond the current study.

1.3   OUTLINE OF DISSERTATION

As a whole, this dissertation addresses issues associated with repair of impact damaged PC girders, particularly focusing on analysis issues and limitations of repair techniques. Chapter 2 discusses the concept of prestressing strand redevelopment after having been exposed or severed due to impact or other damage. Chapters 3, 4 and 5 discuss methodologies to approach various topics pertaining to AB bridge structures since this bridge type exhibits exorbitant structural deficiency rates in Pennsylvania (PennDOT 2007) and in surrounding states. An approach to accounting for behavioral asymmetry of AB girders and associated analysis concerns is presented in Chapter 3. Chapter 4 presents a case study which utilizes the findings of Chapters 2 and 3 in an effort to predict the behavior of an AB girder. This chapter also demonstrates implementation of the findings of Chapters 2 and 3. Lastly, Chapter 5 presents a method for quantifying repair technology limitations. This is validated through an example which utilizes externally bonded carbon fiber reinforced polymers (EB-CFRP) to repair an impact damaged AB girder. Chapter 5 also discusses the approach to rating an impact-damaged member since this damage type often affects only a single girder as opposed to the entire structure. The girder rating approach described here also allows for rapid comparison between the repair technologies' effect on member capacity.

1.4   DISCLAIMER

This document presents engineering design examples; use of the results and/or reliance on the material presented is the sole responsibility of the reader. The contents of this document are not

intended to be a standard of any kind and are not intended for use as a reference in specifications, contracts, regulations, statutes, or any other legal document. The opinions and interpretations expressed are those of the author and other duly referenced sources. The designs presented have not been implemented nor have they been sealed by a professional engineer.

a) Lake View Drive collapse onto I-70. Impact damage led to significant strand loss, subsequent corrosion and eventual collapse under girder self-weight.
[Pittsburgh Post-Gazette]

b) Impact damage to facia beam of Crawford Lane over I-70. [Kasan]

c) Bridge over I-26 north of Columbia SC showing evidence of significant vehicle impact. [Harries]

Figure 1-1 Examples of damage associated with vehicle impact.

2.0   REDEVELOPMENT OF PRESTRESSING FORCE IN SEVERED PRESTRESSING STRANDS

The deteriorating condition of the nation's bridge infrastructure cannot be overstated. PC bridges, however, generally contradict this trend. These, often newer, structures have thus far demonstrated exceptional durability and represent only a small fraction of deficient bridges in the nation (FHWA 2007). Nonetheless, PC bridges are susceptible to potentially catastrophic damage; the extent of which is often difficult to assess until it has progressed to the point of collapse (Harries 2009). Deterioration of PC bridges usually results from corrosion of the strand in a region where the concrete has been damaged, often by vehicle impact (Harries et al. 2009). An example of such damage is shown in Figures 2-1c and d. Due to its refined chemistry and typically small diameter, prestressing steel is particularly susceptible to corrosion (ACI 222 2001). Provided sound cover concrete is present to ensuring resistance to chloride attack, the passivating layer on the prestressing strand is maintained and corrosion is mitigated. Examples of this are shown in Figure 2-1 which shows observed damage from the collapsed Lake View Drive Bridge reported by Harries (2009). In Figure 2-1a, a 3/8 in. (9.5 mm) diameter strand is entirely corroded at the location of an older vehicle impact; the steel crumbled to the touch. A short distance away, where the strand re-enters sound concrete, the corrosion is only 'surface' corrosion. Finally, at the location at which the strand was again encased in sound concrete, only 'bright' steel is found. A similar situation is seen in Figure 2-1b, showing the soffit of a box

girder following testing to failure (Harries 2009). In this case, the lowest layer of strands in the box, having a clear cover of only 1.25 in. (32 mm) and partially exposed due to spalling likely resulting from vehicle impacts, exhibits marked corrosion. The second layer of steel, 1.5 in. (38 mm) above the lower layer remains 'bright'.

Figures 2-1c and d show representative damage to prestressed box girders (Harries 2009). The damage shown in Figure 2-1c was almost certainly initiated by a recent vehicle impact and does not exhibit significant corrosion yet. Left unpatched, the damage in Figure 2-1c is likely to progress to that shown in Figure 2-1a. Figure 2-1d shows relatively typical soffit corrosion. In this case, the initial cause of the damage is less clear although the corrosion is most certainly accelerated by salt-spray from the road below. In the structure shown, the vertical clearance to the Interstate carriageway below was only 14.5 ft (4.42 m) making both vehicle impact and salt spray problematic (Harries 2009).

Damage such as that seen in Figure 2-1 clearly affects the capacity of the individual girder and therefore the bridge. Furthermore, when damage is caused by vehicle impact, it will often be located in the critical middle third of the flexural span. When rating a girder exhibiting such damage, typically a sections approach will be used and the contribution of the severed and corroded strands will be neglected. While this is an adequate approach at the affected section, it is conservative elsewhere along the span assuming fully bonded strands are used. The severed or corroded strand, once it re-enters sound concrete, continues to be bonded to the concrete; thus stress transfer between the concrete and strand is possible. If this is the case, the strand may be 'redeveloped' (in the sense of 'development length') by bond transfer at a distance from the damage location. By the same argument, the prestress force in a bonded strand is not lost at a distance from the damage, since it too may be 'redeveloped'. If the beneficial effects of

11

accounting for the redeveloped strand are to be used in load rating or assessing the need for repair or replacement of a PC girder or bridge, the effectiveness of the 'redevelopment', indeed its existence, must be established. This Chapter presents a study verifying that redevelopment of prestressing force does, in fact, occur and the code prescribed transfer length values remain valid for this phenomena.

2.1   DEVELOPMENT AND TRANSFER LENGTHS

Conceptually, this 'redevelopment' is no different than the original stress transfer from the tensioned strand to the concrete section at the ends of the member at the time of prestress force release. Only in this case the free end of the strand is not at the end of the member but at the edge of the damaged region. Thus, the concept of transfer length and development length should remain valid (ACI 318 2008; AASHTO 2007).

Ewald Hoyer utilized the redevelopment effect in the 1940's in his work with "piano-string-concrete" (Marrey and Grote 2003). Hoyer (1939) developed a system to prestress thin, hard-drawn wires and thus created the most successful (prior to 1945) commercial PC operation. Smaller beams were cut to length from larger, previously cast members. Instead of losing their tension, the wires would expand elastically at each cut and re-anchor themselves (Marrey and Grote 2003). This elastic expansion relies on the radial forces which develop over the transfer length of the wire, as in Figure 2-2; this phenomenon is aptly termed the 'Hoyer effect'. The expansive radial forces engage both friction and mechanical interaction (in the case of deformed bars or twisted strand) causing the wires to anchor themselves after the cut. Moreover, the

'redevelopment' of the thin wires utilized by Hoyer is essentially the same principal as described in this study for severed prestressing strands, as will be shown.

In a PC element, the stress in the prestressing steel may be assumed to vary linearly from zero at the point where bonding commences to the effective stress after losses, f_{pe}, at the end of the transfer length, ℓ_{tr}. In a member loaded to its capacity, strand stress may be assumed to increase linearly from the end of the transfer length to the development length, ℓ_d, reaching the stress at nominal resistance, f_{ps}, at the development length. This idealized relationship is shown in Figure 2-3. The transfer length for bonded seven wire strand is given as 60 strand diameters ($60d_b$) by AASHTO (2007) and as shown in Equation 2-1 by ACI (2008).

$$\ell_{tr} = 0.33 f_{pe} d_b \qquad \text{(ksi and in.)} \qquad \text{(Eq. 2-1)}$$

$$\ell_{tr} = 0.05 f_{pe} d_b \qquad \text{(MPa and mm)} \qquad \text{(Eq. 2-1)}$$

For typical cases, f_{pe} is on the order of 180 ksi (1240 MPa), thus both AASHTO and ACI requirements give the same transfer length. The development length, also measured from the point at which bond commences, is given by both AASHTO and ACI as:

$$\ell_d = K(f_{ps} - 0.66 f_{pe}) d_b \qquad \text{(ksi and in.)} \qquad \text{(Eq. 2-2)}$$

$$\ell_d = 0.145 K(f_{ps} - 0.66 f_{pe}) d_b \quad \text{(MPa and mm)} \qquad \text{(Eq. 2-2)}$$

Where K = 1.0 except for members deeper than 24 in. (610 mm) designed based on AASHTO where K = 1.6. Both transfer and development length recommendations were developed in the 1950's and 1960's and adopted by ACI and AASHTO in 1963 and 1973, respectively (Tabatabai and Dickson 1993). The κ factor was introduced by AASHTO in 1988 to address perceived worst-case characteristics of older strand material (AASHTO 2007). All previous calculations assume a conventional minimum concrete cover over the strand; for flexural members, this is typically 1.5 in. (38 mm) (ACI 318 2008; AASHTO 2007).

2.1.1 Effects of Concrete Properties on Transfer Length

Transfer of prestressing force and strand development is affected by concrete material properties. Concrete of good quality and higher strength will transfer prestressing force more efficiently than poor quality or lower strength concrete (Mitchell et al. 1993 and Oh et al. 2001). In other words, strand transfer length decreases with increasing concrete strength.

Concrete consolidation occurs during member casting which, in turn, influences the bond characteristics of reinforcing bars based on their casting position. This phenomenon, commonly referred to as the "top bar" effect, is often discussed for conventionally reinforced members but is equally significant in prestressed reinforcement. Top cast prestressed reinforcement will have greater initial slip upon release of prestressing force and thus exhibit slightly greater prestressing force losses as compared to bottom cast reinforcement (Wan et al. 2002). In most PC bridge girders, the prestressing reinforcement is located toward the bottom of the section. Therefore, 'redevelopment' of severed strand prestressing force will occur in the consolidated concrete at the bottom of the section and thus will not generally be prone to the bond quality issues associated with top cast reinforcement. Therefore the strand will redevelop its prestressing force in a manner similar to that by which the original prestressing force transfers to the section.

2.1.2 Effects of Concrete Cover on Transfer Length

Harries (2006) noted significant variation in concrete cover for the 3/8" (9.5 mm) prestressing strand in the Lake View Drive girders (also in the test girder). Despite specified clear cover of 1.25 in. (31.8 mm), *in situ* clear cover as small as 0.57 in. (14.5 mm) was observed. The effect of reduced concrete cover on prestress force transfer has been found to increase the transfer length

(Oh et al. 2001). There is physically less concrete for the strand prestressing force to transfer into, thus yielding greater transfer lengths. Another way of considering the effect of reduced cover is that the stiffness of the concrete surrounding the strand is reduced, resulting in longer transfer lengths. Recall that code-prescribed transfer lengths were developed based on standard concrete cover thicknesses (see above). Although this issue is beyond the scope of the current study, its importance to strand transfer length and 'redevelopment' of prestressing force is acknowledged.

2.1.3   Effects of Strand End Slip on Transfer Length

Strand end slip is the relative slip between the prestressing strand and concrete. This is typically measured at the end of the member during the release of the original prestressing force. This measurement is used to determine the effective prestressing force, or the amount of prestressing force which is transferred to the member (Oh et al. 2001 and Wan et al. 2002). Strand end slip is dependent on the location of the reinforcement (whether it be top or bottom cast), the rate at which prestressing force is released and the end at which the slip is being measured (the live (stressed) or dead end). Ultimately, strand end slip contributes to the determination of strand transfer length and thus the causes of strand end slip are discussed.

It was observed that strand end slip was found to be greater for top cast reinforcement as opposed to bottom cast reinforcement (Wan et al. 2002). The reasoning behind this is consistent with the discussion regarding concrete consolidation and the effect of "top cast reinforcement" as previously presented.

The "live" end of the strand is considered to be where the strand is cut to release the prestressing force and the dead end is the other end. Tests have indicated that transfer length at the live end of the member could be as much as 15% greater than at the dead end due to strand slip (Oh and Kim 2000 and Oh et al. 2001). This increase is significant in the discussion of 'redevelopment' of severed strand prestressing force in so far as the new 'live end' of the member is the location where the strand has been severed and the prestressing force has been released. Therefore, in the region in which the strand is 'redeveloping' the prestressing force transfer will behave like a 'live end' and thus is more likely to have greater strand end slip.

Strand transfer lengths have also been found to increase with a more rapid prestressing force release rate (Kaar et al. 1963 and Steinberg et al. 2001). Kaar has shown that the transfer length for flame cut ends (which is the release method used at most precasting plants) is greater than for a more gradual release, as is evident in Figure 2-4. Another study conducted by Steinberg et al. (2001), cut strands in a manner which resulted in the release of prestressing force to be faster than flame cutting. Steinberg et al. (2001) used two methods to determine strand transfer length; 1) a manual method which analyzed strains taken from gages mounted on the member's surface before and after prestress release; and 2) LVDT readings which provided strand end slip values. Strain readings taken from gages embedded in the members verified strand transfer lengths determined from the other two methods. Regardless of the method used, all three determinations of strand transfer length resulted in values greater than that calculated based on contemporary PCI, ACI and AASHTO code provisions. The importance of the greater transfer lengths observed in test specimens subject to rapid prestressing force release rates is important in this study since a) impact damage may result in very rapid strand ruptures; and b) the technique used to cut strands in this study resulted in relatively rapid force release.

16

2.2   SEVERED STRANDS AND REDEVELOPMENT

At a distance greater than ℓ_d from observed strand damage, when strand 'redevelopment' is assumed, girder capacity is restored since a) the strand is still present in sound concrete and thus is reinforcing the section; and b) the prestress force attributed to the damaged strand is still present. This, however, is not typically taken into account in rating damaged prestressed girders where the common practice is to assume that once a strand is severed it is lost over the entire length of the girder. By accounting for 'redevelopment' and considering appropriate sections along a damaged girder, it is possible to significantly increase a girder's load rating over that obtained for the damaged section or for the entire girder assuming the loss of ruptured strands over the entire girder length.

Figure 2-5 illustrates this conceptually for a simply supported PC girder. In Figure 2-5, an undamaged girder has a moment capacity of *M*. The lines in Figure 2-5 represent damage reducing the sectional capacity to 95% - 75% of the undamaged capacity (levels still considered repairable (Kasan 2009)). The actual girder capacity (based on a uniformly distributed load) is given based on the location of this sectional damage over the half span of the girder. For instance, severe sectional damage may reduce local capacity to *0.75M*. If this damage is located at midspan (*x = 0.5L*, where L is the girder length), the girder flexural capacity is *0.75M*. If however the same damage is located at *x = 0.35L*, the overall girder load carrying capacity is *0.82M* and if *x < 0.25L*, the girder flexural capacity is unaffected. Thus, by considering the various undamaged sections away from the damage location, the load carrying capacity of the girder may be improved over the case of considering only the critical section. To permit this approach, the damaged strand must be redeveloped.

17

2.3   EXPERIMENTAL PROGRAM

In order to include the effects associated with a redeveloped strand in load rating and member assessment, the effectiveness of the 'redevelopment', indeed its existence, must be established. The following experimental program was carried out to assess strand 'redevelopment' behavior.

2.3.1   Test Girder

Tests were conducted on a girder recovered from the decommissioned Lake View Drive Bridge (Harries 2006). Originally built in 1960, the test girder was an exterior girder of an AB girder bridge having no composite topping. The girder is a 42 in. deep by 48 in. wide (1070 x 1220 mm) hollow PC box 91.2 ft (27.8 m) long (Spancrete 1960). Primary reinforcement consisted of 60 3/8 in. (9.5 mm) diameter stress-relieved 250 ksi (1720 MPa) seven wire strands placed in five layers. A section of the girder is shown in Figure 2-6b. The asphalt topping and barrier wall had been removed from the girder when it was decommissioned. The original bridge had a 39° skew. At the time of the experimental program described, the girder was supported on four timber cribs as shown in Figure 2-6a. The test region itself was in excellent shape, there was little evidence of deterioration or damage of any kind. Subsequent removal of concrete cover for instrumentation and testing (described below) revealed only 'bright' strand in sound concrete with no evidence of corrosion.

Although concrete strength of the test girder was not established in this study, the specified concrete compressive strength for all girders of the Lake View Drive Bridge was 5900 psi (40.7 MPa). Cores taken from two other girders (Harries 2006) revealed very consistent strengths of 7300 psi (50.3 MPa). A single core extracted from the test girder in a previous study

yielded a compressive strength of 8440 psi (58.2 MPa) (Naito et al. 2006). Thus the concrete is considered to be of very good quality.

Two samples of prestressing strand were removed from the test girder and the individual wires were tested. All wires were found to be in good condition with minimal corrosion. Due to the helical nature of prestressing strands, six of the seven wires are 'kinked'; only the center wires are straight and thus capable of providing accurate stress-strain relationships. A stress-strain curve obtained from one of the center (straight) wires tested is presented in Figure 2-7. Wire diameters and ultimate (rupture) stress values are provided for both center (straight) and outer (helical) wires in Table 2-1. The average ultimate strength of both center and outer wires was f_{pu} = 263 ksi (1813 MPa) having a standard deviation of 4 ksi (27.6 MPa), confirming the grade (250 ksi) and quality of the almost 50-year old strand. Concrete and steel properties described here validate the assumptions and material properties used later in the girder analysis as well as confirm the apparent excellent girder condition.

Initial prestress in all strands is reported to be f_{pi} = $0.7f_{pu}$ = 175 ksi = 1207 MPa (Spancrete 1960). Calculations of estimated prestress loss based on the method reported by PCI (1999) were $0.13f_{pu}$ = 33.7 ksi = 232 MPa, resulting in an effective prestress force of f_{pe} = $0.57f_{pu}$ = 141.3 ksi = 974 MPa. The residual stress in a single corner strand on the test girder was experimentally established to be $0.44f_{pu}$ = 110.5 ksi = 762 MPa by Naito et al. (2006). In the present study the residual stress in an interior bottom layer strand (strand H, see below) was similarly found to be $0.47f_{pu}$ = 118.3 ksi = 816 MPa (see Table 2-2).

It is noted that experimentally obtained prestress values necessarily include both the effects of prestress (f_{pe}) and the effects of applied load. The latter can be assessed based on a sections analysis and is subtracted from the experimentally obtained force in the strand to assess

the effective prestress. In this study, the only load carried by the girder is its own self weight, determined to be 909 plf (1355 kg/m). The girder is supported as shown in Figure 2-6a and the location at which strand force is determined is located only 13.6 ft (4.1 m) from the nearest support. Based on these conditions, the stress in a single lower-layer strand that is attributed to applied load (i.e.: self weight) is only 0.5 ksi (3.4 MPa).

The relatively low apparent values of effective prestress force were confirmed in two other girders from the Lake View Drive Bridge which had effective prestress forces of 101 and 96 ksi (696 and 662 MPa) (Naito et al. 2006). Additional confirmation of these values was made by direct measurements of girder camber which were all smaller than long-term calculations (PCI 1999) and fabricator drawings (Spancrete 1960) indicated (Harries 2006). No design-related reason is offered for these low values, although it is noted that both strand and concrete materials were in generally excellent shape (apart from isolated damage). Therefore the authors suggest that the initial prestress, f_{pi} may have been lower than indicated on the design drawings.

2.3.2   Test Procedure and Protocol

The basic premise of the test procedure was to intentionally sever prestressing strand while measuring the strain in the same strand at some distance from the cut. The drop in strain at a distance from the cut is an indication of the transfer of prestress between this location and that of the cut, at which the stress is now zero. In this manner the transfer length may be experimentally determined.

To access the strands for instrumentation, a shallow notch was cut transversely across the girder soffit, removing the concrete cover and exposing the surface of the lower layer of prestressing strand (Figure 2-6e). Considerable care was taken to avoid damage to the strands

and to maintain as much concrete around the strands as possible. Very small electrical resistance strain gages (micro-measurements type EA-06-062AQ-350/P) having a grid width of 0.062 in. (1.57 mm) and grid length of 0.114 in. (2.90 mm) were applied to a single wire of the partially exposed strand. To facilitate accurate alignment, the strain gage matrix was trimmed to be just greater than the grid width. The gages were applied within the notch as close as possible to the edge from which the cut distance was to be measured (distance 'x' shown in Figure 2-6d and given in Table 2-2).

Eight strands were instrumented; these were labeled A-H as indicated in Figure 2-6. Individual strands were cut at a distance ℓ_{cut} from the edge of notch. The order in which the strands were cut and the respective cut distances, ℓ_{cut}, are given in Table 2-2. In some cases, where ℓ_{cut} was sufficiently long to have little observed effect on the strain at the gage location, the strand was cut a second time at a shorter distance ℓ_{cut} (cut number 5, for instance). Strands were cut using an abrasive cut-off wheel on an 8000 rpm grinder. Each cut was accomplished in about 15 seconds. This cut speed is slightly slower than might be expected for a flame cut strand. Strain readings of all gages were taken before and after each cut. Approximately ten minutes elapsed between subsequent cuts, permitting sufficient time for any redistribution to take place. No data is reported for gage G, since this gage was damaged while making cut #1.

2.4   EXPERIMENTAL RESULTS

All results are presented in terms of stress change. Since a strand is in tension before it is cut, the result of the cut is a negative stress change. All stress change data is calculated from strain gage data assuming $E = 29000$ ksi (200 GPa). All normalized stress values reported have been

normalized based on f_{pu} = 250 ksi (1720 MPa). Figure 2-8 shows a stress history of all gages reported in this study. In each case, the significant stress drop represents that associated with cutting the strand noted. The stress change due to cutting each strand is also given in Table 2-2.

Strain data was collected for all available strands before and after each cut was made. The data was then corrected based on the initial pretest value of the strain gage. This correction accounts for the change in stress, resulting from the cut, in strands adjacent to the cut strand (i.e.: the loss of reinforcement). The corrected strain data is provided in Table 2-3. Table 2-4 provides the corresponding prestressing force change calculated from the strain data assuming E = 29000 ksi and a strand cross-section area of 0.085in^2.

As previously described, the strain gages were applied to a single helical wire of the 7-wire strand. Machida and Durelli (1973) provide a correction factor to convert strain measured in a helical wire to longitudinal strain in the strand (as represented by the strain in the center wire), based on the deviation angle of a helical wire. The deviation angle (or the lay angle) of a wire, β, is the angle between the axial direction of the helical wire and the longitudinal direction of the center wire and thus the strand (see Figure 2-9). For seven wire strand the deviation angle, β, is approximately 10°. Reworking equations proposed by Machida and Durelli (1973), the relationship between helical strand strain, ε_h, to that in the center strand strain, ε_c, is:

$$\varepsilon_c = \frac{\varepsilon_h}{\cos^2(\beta)} \qquad \text{(Eq. 2-3)}$$

Using a value of β = 10° for the deviation angle, the strain in the center wire is found to be 3.1% greater than that measured in the helical wire. This correction more accurately quantifies the prestressing force, N, in the strand when only helical strain data is available. Calculation of strand prestressing force can therefore be calculated as:

$$N = A_w E_s \varepsilon_c + 6A_w E_s \varepsilon_h \cos(\beta) \qquad\qquad \text{(Eq. 2-4)}$$

where: A_w is the area of a single strand wire; and E_s is the elastic modulus of the steel.

The resulting error in calculated prestress force when strain is measured from a helical wire and

$\beta = 10^o$ is less than 1% - in this case the actual prestress force is 0.8% less than that calculated

based on the helical wire strain. This effect is negligible for the strand considered and this

correction has not been applied to the data shown in Table 2-4.

Stress in uncut strands increase marginally (increased tension) since the act of cutting an

adjacent strand eliminates a portion of the section reinforcing, redistributing stress to the

remaining strands. For instance, based on the results of strand cut 1, the stress in the strands due

to prestress and girder dead load was 118.3 ksi (816 MPa). Strand cuts 11 and 12, also both in

the notch, yielded larger apparent stresses since these were made to a section having six and

seven fewer effective strands, respectively. Indeed, the total stress drop of strand E during the

course of testing was 143.3 ksi (988 MPa) which accounts for the increase in stress associated

with cutting the adjacent strands.

Strands that only lost some of their prestress following cutting show some further

reduction in stress with subsequent readings. This is attributed to the equilibration of transfer

forces (as described below) rather than any affect from subsequent strand cuts. Where a partial

stress drop was observed, it was not instantaneous. Upon cutting the strand at some distance ℓ_{cut},

a change in stress at the strain gage is affected. With time, the stress continues to fall as the

remaining prestress forces transfer to the member and equilibrate. This behavior is believed to

result from the progressive redistribution of bond stress along the strand in the vicinity of the cut.

Figure 2-10 shows the continued stress drop in strand A following the initial drop associated

with cutting this strand (103.6 ksi = 714 MPa). It takes about ten minutes for the stress in the

strand to re-equilibrate at a level almost 27 ksi (186 MPa) below the prestress remaining immediately following the cut; the final stress drop due to cutting strand A (cut #8) was 130.6 ksi (900 MPa) as indicated in Table 2-2.

2.4.1 Apparent Transfer Length

Figure 2-11 shows the stress change resulting from increasing cut distances. There was no observed stress change associated with any cuts made beyond $\ell_{cut} = 35d_b = 13.1$ in. $= 333$ mm. The results appear to validate the ACI transfer length equation (Eq. 2-1) which is equal to $39d_b$ in this case.

The effective prestress in the strands found in this study is lower than would otherwise be predicted: 118 ksi (816 MPa) versus a predicted value of 141 ksi (974 MPa) based on PCI calculations (see Section 2.3.1). Additionally, the cuts in this study were discrete and did not disturb surrounding concrete to a great degree. Considering the less discrete nature of real strand damage, one might expect a longer apparent transfer length *in situ*. Thus, the authors contend that the use of the AASHTO-prescribed value of $\ell_{tr} = 60d_b$ is appropriate to conservatively establish the transfer length required to reestablish prestress force at a distance beyond the extent of damaged concrete.

In this study, it has been shown that the transfer length calculation used for design remains valid for 'redevelopment' of effective prestress in severed strand. The development length of the severed strand (Equation 2-2) has not been validated but the validation of the transfer length suggests no changes in strand bond behavior and therefore no effect on development length is anticipated.

2.5   DISCUSSION AND CONCLUSIONS

The findings of this study demonstrate that severing prestressing strand is a 'local effect'. That is, the effects of the lost strand affect the section at the damage location. To either side of the damaged concrete region, the effective prestress in the strand is 'redeveloped' over the transfer length, ℓ_{tr}. This approach implies the need to consider not only the critical section of a girder but all sections along its length when rating the girder or designing repair measures for a damaged girder (Harries et al. 2009 and also discussed in Section 5.2). The localized nature of severed/exposed prestressing strands being ineffective at the damage location (and the transfer/development length away from the damage) is also supported in the failure investigation case study discussed in Chapter 4.

Although not directly studied in this investigation, effects due to concrete material properties, concrete cover and strand end slip on transfer length of a 'redeveloped' severed strand can be significant and must be considered. While this study is not (and was never intended to be) a parametric study to quantify any of the effects listed here, their influence on the transfer length of a 'redeveloped' severed strand in the experimental investigation performed are inherently included. Therefore, the conclusion that the transfer length, as prescribed by AASHTO, is sufficient to account for strand redevelopment based on the present study includes effects due to concrete material properties, concrete cover and strand end slip. The findings and conclusions discussed here remain valid in light of the inclusion of these effects. Lastly, the test results are based on a member taken out of service and thus are representative of realistic conditions expected in the field.

This particular study also identified lower-than-expected values of prestress force in the sound strands. While not affecting ultimate capacity, this would be expected to affect

serviceability of these girders. Beyond destructive tests similar to those conducted here, there is no practical method for assessing prestressing force *in situ*.

Finally, it is acknowledged that this work presents experimental data from a single decommissioned girder. The work has demonstrated that 'redevelopment' of severed strands which should occur, does, in fact, occur in a manner that is essentially intuitive. Nonetheless, opportunities to verify these results are relatively rare and should be capitalized upon when they become available.

Table 2-1 Strand Tensile Test Data.

Wire	Wire location	Wire Diameter (in.)	Measured Ultimate Stress (ksi)
A1	helical	0.1200	261.7
A2	helical	0.1240	256.0
A3	helical	0.1210	266.0
B4	helical	0.1225	260.2
B5	helical	0.1215	266.4
B6	helical	0.1205	267.1
A-center	center	0.1270	266.0
CH3A-C-1[1]	not reported	0.117	269.7
CH3A-C-2[1]	not reported	0.118	299.7
CH3A-C-3[1]	not reported	0.118	288.3
[1] values from Naito et al. 2006 1 in. = 25.4 mm; 1 ksi = 6.895 MPa			

Table 2-2 Strand cutting order, location and resulting stress change.

Cut Number (see Tables 2-3 and 2-4)	Strand	x (in.)	ℓ_{cut} (in.)	stress change at strain gage due to cut (ksi)
1	H	0.7	0 (cut in slot)	-118.3
2	F	0.6	$59.5d_b = 22.3$	none
3	E	0.5	$52.0d_b = 19.5$	-0.3
4	D	0.6	$34.7d_b = 13.0$	-0.3
5	F[1]	0.6	$16.3d_b = 6.1$	-27.0
6	C	0.6	$13.3d_b = 5.0$	-73.1
7	B	0.9	$11.5d_b = 4.3$	-112.4
8	A	0.8	$4.3d_b = 1.6$	-130.6
9	E[1]	0.5	$26.9d_b = 10.1$	-25.6
10	D[1]	0.6	$20.8d_b = 7.8$	-4.5
11	D[1]	0.6	0 (cut in slot)	-125.0
12	E[1]	0.5	0 (cut in slot)	-117.4
[1] strand recut after initial cut had little effect. 1 in. = 25.4 mm; 1 ksi = 6.895 MPa				

Table 2-3 Strain readings from testing procedure.

	time	Event #	cut location (in.)	cut strand	Strain reading, µε							
					A	B	C	D	E	F	G	H
before cut 1	10:30	1	0	H	0	0	0	0	0	0	0	0
4 wires cut 1	10:46	1	0	H	5	5	7	12	18	30		-2110
after cut 1	10:53	1	0	H	7	8	10	16	23	37		-3380
before cut 2	11:23	2	22.25	F	6	9	12	17	24	38		-
after cut 2	11:39	2	22.25	F	6	9	11	16	21	35		-
before cut 3	12:20	3	19.5	E	7	11	13	19	24	39		-
after cut 3	12:25	3	19.5	E	7	9	10	12	14	30		-
before cut 4	12:39	4	13	D	6	9	10	12	14	31		-
after cut 4	12:43	4	13	D	5	5	2	1	4	25		-
before cut 5	13:03	5	6.125	F	4	6	2	2	13	51		-
after cut 5	13:07	5	6.125	F	7	10	6	5	4	-513		-
before cut 6	13:26	6	5	C	5	13	10	6	8	-733		-
after cut 6	13:28	6	5	C	18	19	-1873	17	19	-732	GAGE	-
before cut 7	13:47	7	4.25	B	18	23	-2110	22	24	-776	FAILED	-
after cut 7	13:48	7	4.25	B	36	-2364	-2104	36	36	-772		-
before cut 8	13:56	8	1.625	A	67	-3236	-2085	42	40	-790		-
after cut 8	14:01	8	1.625	A	-3970	-3210	-2055	63	55	-801		-
before cut 9	14:16	9	10.125	E	-3855	-3234	-2119	61	32	-845		-
after cut 9	14:19	9	10.125	E	-3852	-3232	-2118	62	-588	-851		-
before cut 10	14:25	10	7.75	D	-3887	-3252	-2138	36	-711	-870		-
after cut 10	14:27	10	7.75	D	-3886	-3253	-2139	-67	-713	-873		-
before cut 11	14:37	11	0	D	-	-	-	-94	-714	-		-
after cut 11	14:39	11	0	D	-	-	-	-3722	-691	-		-
before cut 12	14:40	12	0	E	-	-	-	-3717	-693	-		-
after cut 12	14:00	12	0	E	-	-	-	-3720	-4099	-		-

1 in. = 25.4 mm

Table 2-4 Change of prestress force based on strain from testing procedure.

	time	Event #	cut location (in.)	cut strand	Change in Prestress Force, kips							
					A	B	C	D	E	F	G	H
before cut 1	10:30	1	0	H	0.00	0	0	0.00	0.00	0.00	0	0
4 wires cut 1	10:46	1	0	H	0.01	0.01	0.02	0.04	0.05	0.09		-6.18
after cut 1	10:53	1	0	H	0.02	0.02	0.03	0.05	0.07	0.11		-9.91
before cut 2	11:23	2	22.25	F	0.02	0.03	0.04	0.05	0.07	0.11		-
after cut 2	11:39	2	22.25	F	0.02	0.03	0.03	0.05	0.06	0.10		-
before cut 3	12:20	3	19.5	E	0.02	0.03	0.04	0.06	0.07	0.11		-
after cut 3	12:25	3	19.5	E	0.02	0.03	0.03	0.04	0.04	0.09		-
before cut 4	12:39	4	13	D	0.02	0.03	0.03	0.04	0.04	0.09		-
after cut 4	12:43	4	13	D	0.01	0.01	0.01	0.00	0.01	0.07		-
before cut 5	13:03	5	6.125	F	0.01	0.02	0.01	0.01	0.04	0.15		-
after cut 5	13:07	5	6.125	F	0.02	0.03	0.02	0.01	0.01	-1.50		-
before cut 6	13:26	6	5	C	0.01	0.04	0.03	0.02	0.02	-2.15		-
after cut 6	13:28	6	5	C	0.05	0.06	-5.49	0.05	0.06	-2.15	GAGE FAILED	-
before cut 7	13:47	7	4.25	B	0.05	0.07	-6.18	0.06	0.07	-2.27		-
after cut 7	13:48	7	4.25	B	0.11	-6.93	-6.17	0.11	0.11	-2.26		-
before cut 8	13:56	8	1.625	A	0.20	-9.48	-6.11	0.12	0.12	-2.32		-
after cut 8	14:01	8	1.625	A	-11.64	-9.41	-6.02	0.18	0.16	-2.35		-
before cut 9	14:16	9	10.125	E	-11.30	-9.48	-6.21	0.18	0.09	-2.48		-
after cut 9	14:19	9	10.125	E	-11.29	-9.47	-6.21	0.18	-1.72	-2.49		-
before cut 10	14:25	10	7.75	D	-11.39	-9.53	-6.27	0.11	-2.08	-2.55		-
after cut 10	14:27	10	7.75	D	-11.39	-9.53	-6.27	-0.20	-2.09	-2.56		-
before cut 11	14:37	11	0	D		-	-	-0.28	-2.09	-		-
after cut 11	14:39	11	0	D	-	-	-	-10.91	-2.03	-		-
before cut 12	14:40	12	0	E	-	-	-	-10.89	-2.03	-		-
after cut 12	14:00	12	0	E	-	-	-	-10.90	-12.01	-		-

1 in. = 25.4 mm; 1 kip = 4.448 kN
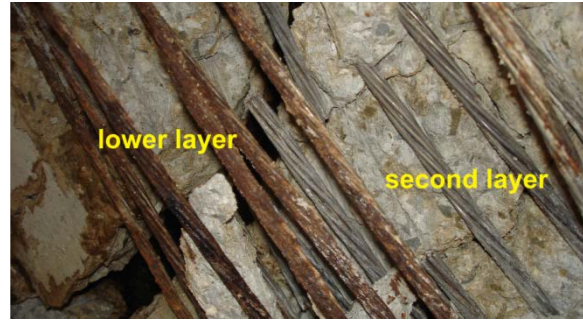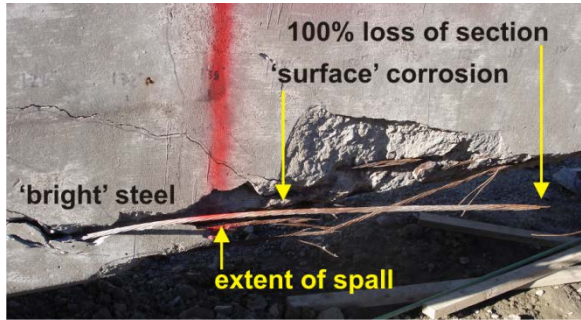
a) Progression of strand corrosion as strand is depassivated due to loss of concrete cover. Cracking at left of image is associated with load test (Harries 2009).

b) Corrosion of lower layer of strands in box girder while second layer remains bright. Strand ruptures near center of image associated with load test (Harries 2009).

c) Typical damage to strand resulting from recent vehicle impact.

d) Typical corrosion of strands resulting in significant loss of section at soffit of box girder.

Figure 2-1 *In situ* corrosion of prestressing strand.
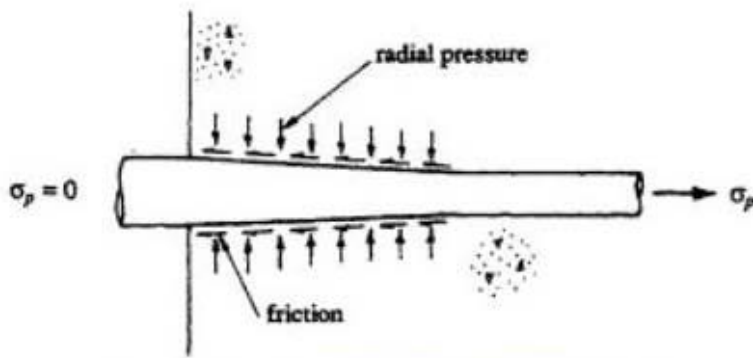
Figure 2-2 Radial Forces developed by the wire as described by the Hoyer Effect (Gilbert and Mickleborough 1990).
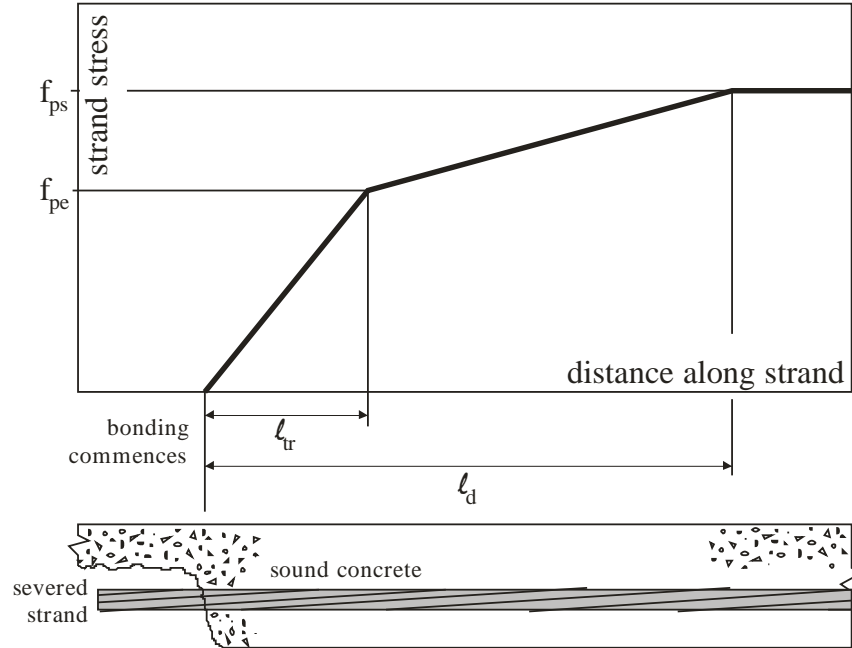
Figure 2-3: Idealized transfer and development lengths.
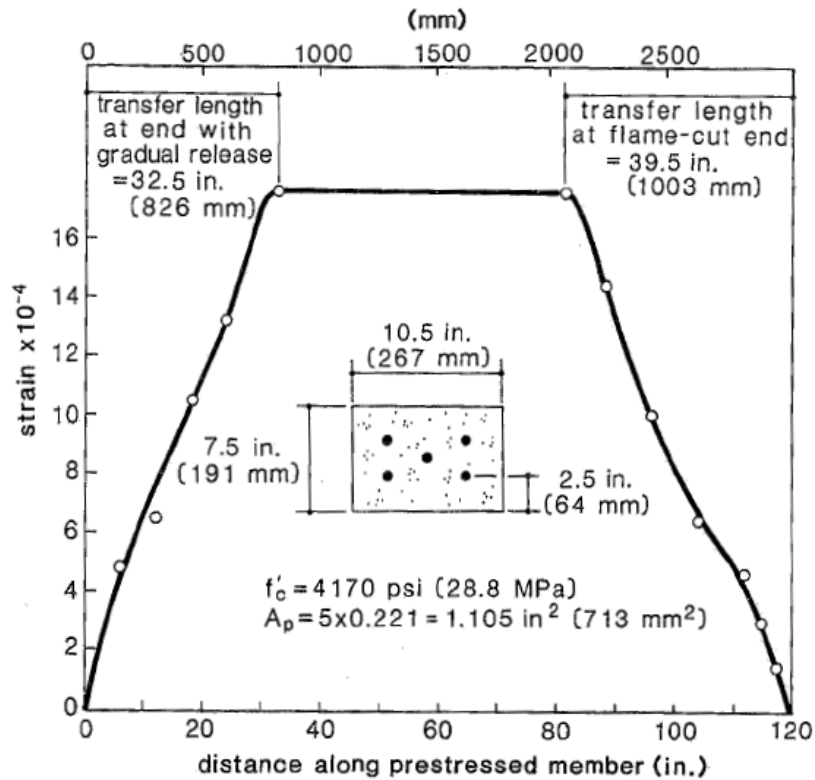
Figure 2-4 Transfer length of a 0.6 in. diameter strand in a 10 ft member illustrating different transfer lengths based on method of prestress force release (Kaar et al. 1963).
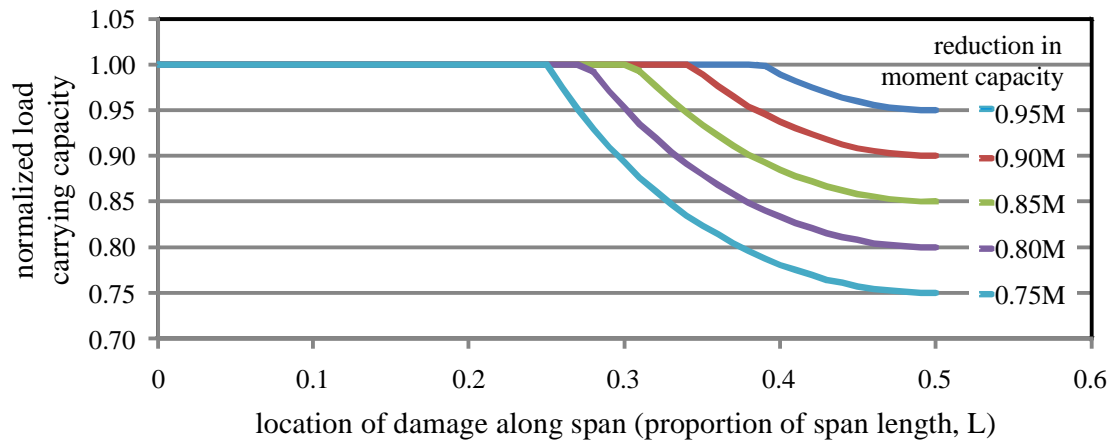
Figure 2-5 Capacity of uniformly loaded simple span girder accounting for damage.
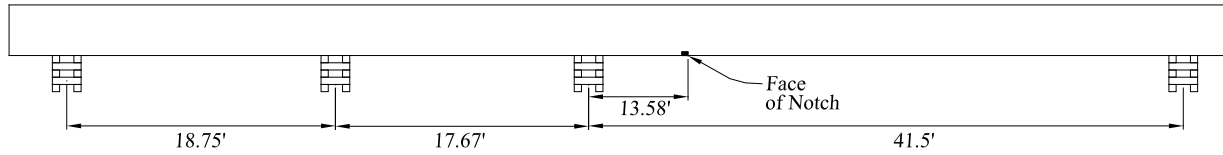
a) test girder with support conditions (1 ft = 305 mm).
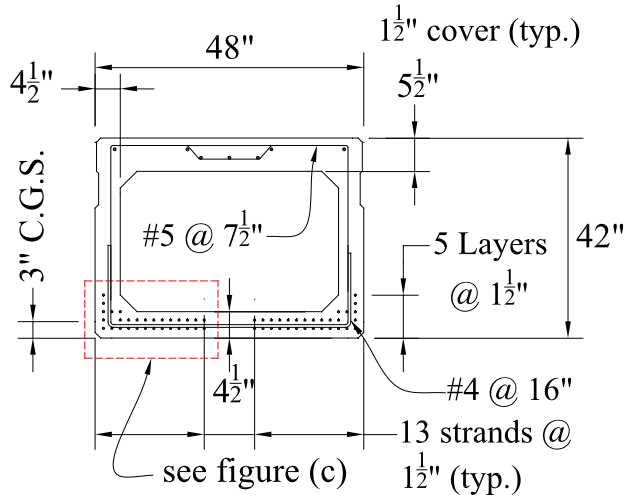
b) girder cross section (1 in. = 25.4 mm).
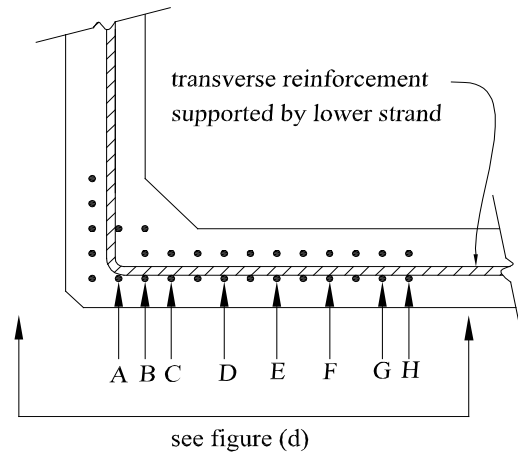
c) strand/gage nomenclature.
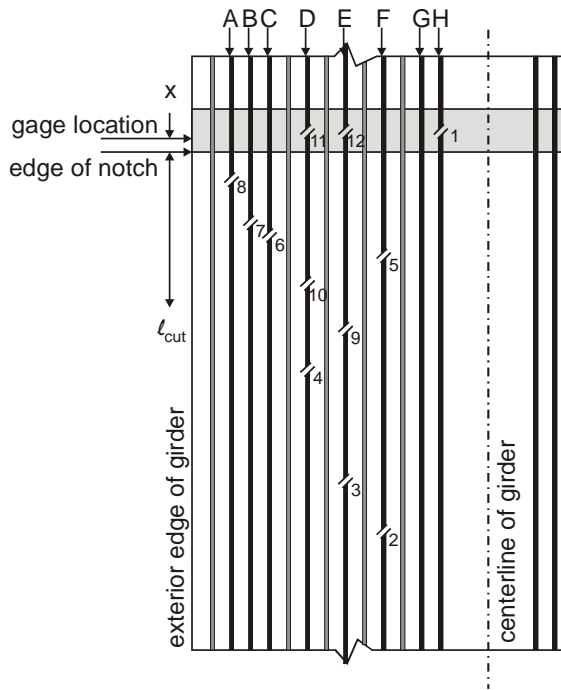
d) strands with cut location.
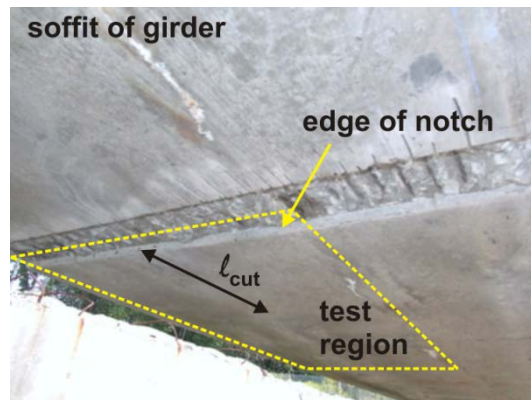
e) notch orientation.

Figure 2-6 Test and girder details.

33
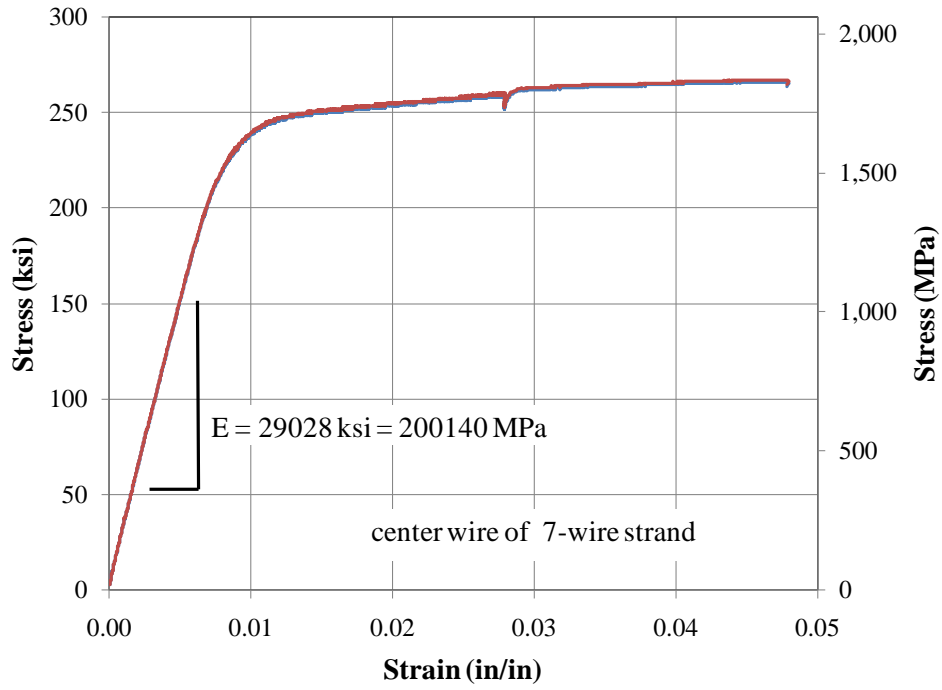
Figure 2-7 Stress-strain curve obtained from center wire of strand from test girder.
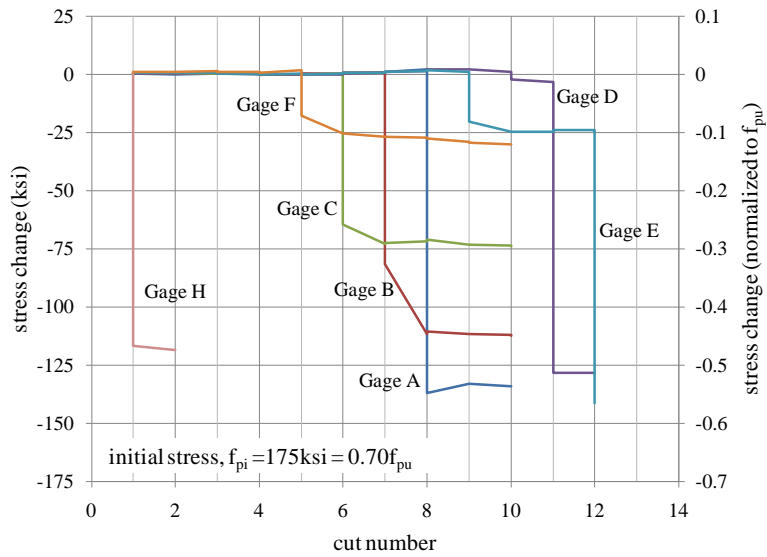
Figure 2-8 Stress change-cut number history for all gages.
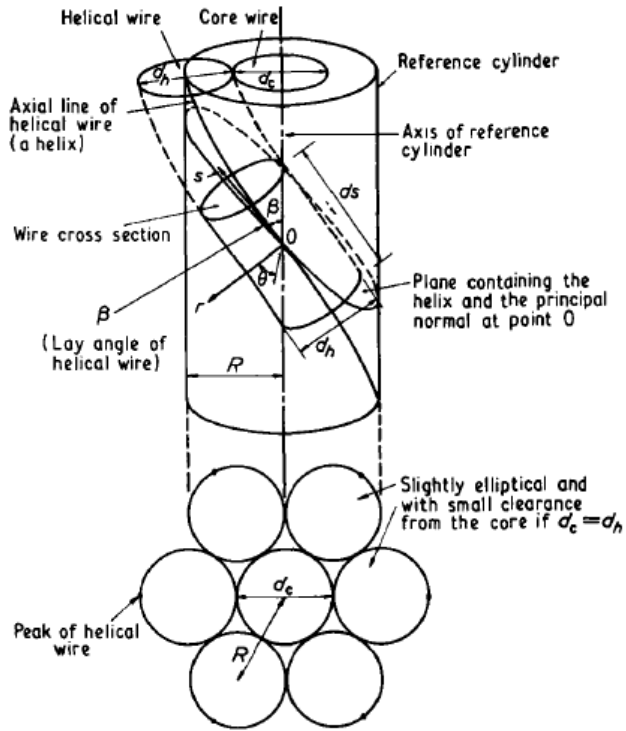
Figure 2-9 Geometry of a seven-wire strand (Machida and Durelli 1973).
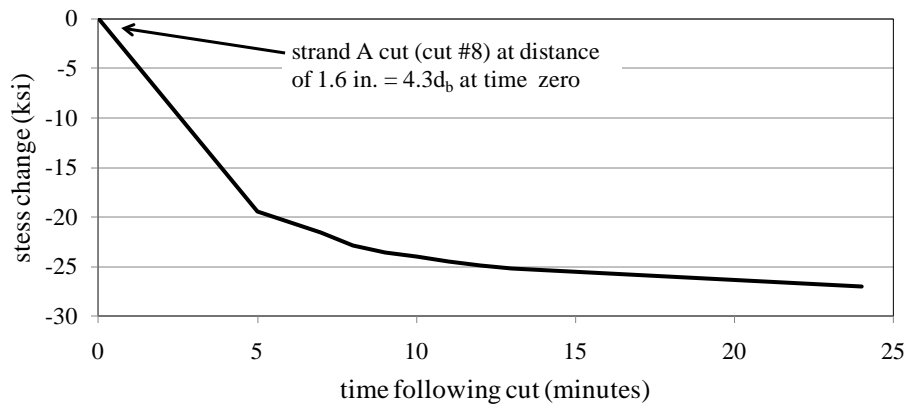
Figure 2-10 Stress change-time history for strand A **following** cut #8.

Figure 2-11 Stress drop versus cut distance.

3.0   ECCENTRICALLY LOADED GIRDER ANALYSIS

Prestressed Concrete (PC) adjacent box girder (AB) bridges are exhibiting signs of deterioration and distress as these structures 'come of age'. In Pennsylvania, there is an inventory of 1997 AB bridges; these average over 40 years old. Of these, 355 (18%) are structurally deficient based on their superstructure rating (PennDOT 2007). While prestressed concrete bridges generally perform well (in Pennsylvania, only 7.8% of prestressed bridge superstructures are rated as deficient as opposed to an inventory-wide value of 13.7%), AB bridges are the exception, representing a disproportionate number of 'problem' bridges and therefore requiring a disproportionate allocation of maintenance resources.

There are a number of documented cases (e.g.: Harries 2009) of exterior AB girders 'rolling' away from the bridge. Exterior AB girders a) often have a composite barrier wall resulting in an asymmetric section and load (torsional) condition; and b) have more strand loss (due to vehicle impact) on their lower exterior corner. These effects individually (and therefore more so in combination) have the effect of rotating the principal axes of the section as shown in Figure 3-1(b). Additionally, the flexural loading of the AB girder resulted in a biaxial response due to the rotation of the principal axes, which has been observed during testing (Harries 2006 and discussed in Chapter 4). Conventional engineering practices may utilize the composite action of the barrier wall in member assessment, when appropriate, through a uniaxial section analysis (about the horizontal axis), resulting in an increase in the apparent strength of the member.

However, properly accounting for the asymmetrical (biaxial) behavior of the composite member will provide a moment capacity of the girder about the geometric horizontal axis ($M_{x\theta}$) which will be reduced beyond that which is predicted using a typical uniaxial section analysis (M_x). In AB bridges, this effect is most pronounced in exterior girders since interior girders are restrained from rotation by the adjacent girders (Harries 2006).

Harries (2006 and 2009) demonstrated the described behavior experimentally on a 40 year old decommissioned AB girder recovered from the Lake View Drive bridge (Figure 3.2a). In this study, a 90 foot (27.5 m) long exterior AB girder having a composite barrier wall was subjected to a monotonically increasing vertical load over a test span of 84.2 ft (25.7 m). The girder had some relatively minor vehicle impact damage on its exterior face, although this was not in the midspan region. The load was controlled such that it was applied symmetrically to the 48 in. (1220 mm) wide by 42 in. (1067 mm) deep section – half to each web. The highly asymmetric section subject to a symmetric load (Figure 3.3a) exhibited significant out of plane deformation (Figure 3.3c) accompanying and coupled to the in-plane flexural deformation (Figure 3.3b). As testing progressed, the out-of-plane flexural deformation was approximately 35% of the in-plane flexural deformation as shown in Figure 3.3d. As a result, observed failure included significant crushing of both the barrier wall and AB girder immediately beneath this but not on the girder top surface across from the barrier wall (interior corner). Additionally, monitoring of strand ruptures clearly indicated an asymmetric ultimate behavior (Harries 2006).

Based on the preceding, the primary objective of this study is to develop an approach for accurately assessing of the capacity of a PC box girder having some level of discernable damage while accounting for effects of the barrier wall and permitting rotation; that is the capacity of a

damaged exterior AB girder. Examples of such damaged girders are shown in Figure 3.2; this figure also shows the range of impact damage that is seen.

3.1   SECTION ANALYSIS

Traditionally, the capacity of PC members is most simply arrived at using a uniaxial sectional analysis technique resulting in a moment-curvature behavior being defined for the section. This analysis is typically carried out considering moment about the horizontal section axis (x-axis in Figure 3.1) only. The member analysis is produced by combining multiple such plane analyses with a longitudinal (beam) analysis of the girder or bridge. This method will be referred to as 1-dimensional (1D) throughout this chapter referring to the single flexural axis considered. Such a plane sections analysis technique forms the basis for most standard analytical tools. A particularly powerful plane sections analysis tool is Program RESPONSE (Bentz 2000) which uses the modified compression field theory to accurately capture the complex effects of shear loading on a section. The drawback of such a 1D plane sections approach is that it is unable to properly model the case of an asymmetric section or a section subjected to asymmetric (torsional) loading.

Asymmetric section properties and/or loading arise in the following scenarios of interest in the present context:

1. Torsional loading due to a heavy parapet wall located eccentrically with respect to the girder shear center. This is typically the case for exterior AB girders.

2. Sectional asymmetry arising out of composite action between barrier walls, sidewalk slabs, etc. and the girder box section.

39

3. Sectional asymmetry arising from the asymmetric loss of prestressing strand (or other reinforcement). Again, due to the nature of vehicle impact damage, this is often an issue for exterior AB girders.

It is therefore recommended that biaxial section analyses be conducted to account for asymmetric section properties and/or loading (referred to hereafter as a 2D sectional analysis). For this work, only flexural behavior is discussed since the girders considered are sufficiently long to be flexure critical.

Any section subject to flexure about a non-principal axis may be conceived of as being loaded by the simultaneous application of flexural components about each of the two primary axes (referred to here as the horizontal x-axis and the vertical y-axis). The net effect of such loading is that flexural deformation has both an x- and y-component; analogous to the deformation associated with lateral flexural buckling (often incorrectly referred to as lateral torsional buckling). This is the case of a symmetric section being subject to an asymmetric load. The same effect results from an asymmetric section being subject to a symmetric load (or most asymmetric loads). In concrete design, engineers rarely consider asymmetric sections and in bridge design, loads are assumed to be symmetric, oriented about the principle axes of the members. Thus 1D sectional analysis techniques are adequate to assess the capacity of such members.

Damage to a section (specifically, asymmetric loss of prestressing strands), or the unanticipated composite behavior of appurtenances (specifically, the curb slab and barrier wall) results in an asymmetric cross section. In such a case the principal centroidal axes are rotated away from the horizontal/vertical alignment (Boresi and Sidebottom 1986). When subject to flexure about an axis other than the now-rotated principal axis, there is a coupling of principal

40

axis moments. This effect is most clearly expressed as a coupling of vertical (referred to as x-axis bending, M_x, here) and horizontal (y-axis bending, M_y) moments, and results in moment capacities lower than those traditionally calculated about the (horizontal and vertical) geometric axes of the composite section. As will be shown, this reduction can be significant. The effect on moment capacity of neutral axis rotation due to asymmetric damage to the non-composite (symmetric) section is minimal for all realistic possible cases (above member self-weight) and thus is not considered (Harries 2006).

While the foregoing discussion of flexure about non-principal axes is strictly only valid in the elastic range, this behavior may be leveraged for the related topic of section ultimate strength. Within the latter context, it is not the second moment of the areas of the cross-section that dictate the nature of the member's response to moment. Rather, it is the consideration of statical equilibrium that governs the section's response.

In an effort to identify a method of addressing such asymmetric sections with a tool suitable for the design office, while yielding results that remain compatible with present bridge rating protocols, a 2D sectional analysis approach is proposed.

Conceptually, the interaction of principal moments in a section may be presented in a moment-moment (M_x-M_y) interaction plot. Such a plot represents a failure surface whose criteria may be defined and revised to suit the capacity level (serviceability, ultimate load, etc.) considered. For a symmetric section, the M_x-M_y surface may be *schematically* represented as shown in Figure 3-1(a). In this case, the maximum flexural capacity is in bending about the x-axis (M_x) and any off-axis component of bending functionally reduces this capacity as the critical stress (whether defined by the steel or concrete) is affected by the M_y component of loading. The

effects of such biaxial bending are considered to be uncoupled in design and are conventionally expressed in the form (Park and Paulay 1975):

$$\frac{M_x}{M_{nx}} + \frac{M_y}{M_{ny}} \leq 1.0 \qquad\qquad \text{(Eq. 3-1)}$$

where M_x and M_y are the applied principal moments and M_{nx} and M_{ny} are the nominal moment capacities in each principal direction. Park and Paulay note that this linear interaction relationship is always conservative and a more elliptical interaction is appropriate particularly for lower reinforcement ratios.

Equilibrium conditions dictate that the tension and compression resultant forces resisting flexure in a section must be co-planar with the applied loading. Enforcing this equilibrium condition in an asymmetric section (Figure 3-1(b)) loaded about the horizontal x-axis requires an off-axis component of flexure be developed about the vertical y-axis. The section is therefore bending about its rotated principal axis. Figure 3-1(b) illustrates (again, schematically) the effect that the rotated principal axis has on the M_x-M_y interaction surface. It can be seen that when the composite section is subject to a moment about only the x-axis (i.e.: $M_y = 0$), the apparent capacity, $M_{x\theta}$, is less than that about the (rotated) principle axis, M_x. Such loading is described (as above) as flexure about a non-principal axis. The reduced x-axis (geometric axis but no longer the principal axis) flexural capacity results from the necessary equilibrium condition increasing the stresses in critical element longitudinal fibers. A 1D analysis will not capture this axis rotation and moment interaction and, as a result will overestimate the M_x (and M_y) moment capacity. That is a 1D analysis will return a value of M_x where $M_{x\theta}$ is the actual capacity (see Figure 3-1(b)).

3.1.1 M_x-M_y Interaction Approach to Determining Section Capacity

Previously, an uncoupled iterative approach to solving the M_x-M_y interaction behavior has been proposed for use with damaged PC box girders (Miller and Parekh 1994). In this iterative approach, for a given value of vertical curvature, the value of the horizontal curvature was varied until the calculated external horizontal (lateral) moment was zero (thus satisfying equilibrium since there is no externally applied horizontal moment). This iterative approach, although cumbersome, has predictive powers that couple the vertical and horizontal bending.

In the present work an interaction approach is adopted using a commercially available sectional analysis software package: XTRACT (Chadwell and Imbsen 2004). XTRACT has a tool referred to as an 'orbit analysis' which calculates the M_x-M_y failure envelope by rotating the assumed orientation of the principal axis of bending through 360° around the section. By applying user-defined failure criteria an M_x-M_y failure envelope is generated *based on these selected criteria*. The user then enters the envelope at the desired M_x-M_y pair and determines the section capacity. For vertical (gravity) loading on a bridge, $M_y = 0$ and the M_x capacity is assessed at this condition. In essence this is a 'trial and error' approach where the orientation of the principal axis is varied until the external equilibrium (i.e.: $M_y = 0$, in this case) is satisfied.

3.1.2   Program XTRACT

XTRACT is the commercial version of the University of California at Berkeley program UCFyber (Chadwell and Imbsen 2004). XTRACT is a biaxial nonlinear fiber element sectional analysis program. Since it is biaxial (2D in the parlance of this Chapter), it permits the input of any section shape. While XTRACT can only perform moment-curvature (M-φ) and axial load-

moment interaction (P-M) analyses about the traditional horizontal (x) and vertical (y) axes, the 'orbit analysis' tool permits an M_x-M_y failure surface to be generated based on user-specified failure criteria. The failure criteria associated with each material (concrete, reinforcing steel, prestressing steel, embedded steel section, etc.) is selected by the user (or defaults based on material properties may be selected) and the analysis proceeds considering each material. Thus, for instance, a complete M_x-M_y interaction relationship may be governed by yielding of prestressing strand in one region and crushing of concrete in another.

XTRACT provides both customizable analysis reports and an interactive mode to view results. A strong graphical interface allows the user to see the outcome of their analyses. Finally, all data is easily exported in text format for further processing. XTRACT is not able to run 'batch jobs' and thus multiple 'what if' scenarios (as done for this study) require individual runs and data processing. The ease of use (particularly in editing models) of XTRACT however makes up for the necessity of this 'brute force' approach for multiple analyses.

3.2   2D SECTIONAL ANALYSIS USING XTRACT

3.2.1   Girder Selection

A review of all PC box girder bridge structures in PennDOT Districts 11 and 12 (essentially Southwestern Pennsylvania) was performed and is summarized in Table 3-1. The intent of this exercise was to establish a snapshot of the condition of the PC AB bridge inventory in Pennsylvania. Districts 11 and 12 are representative of the state inventory as evidenced by the

ratio of 'all prestressed structures' to 'all bridges' for the state (23.3%) as compared to that of District 11 and 12 combined (22.6%), as shown in Table 3-1.

In performing this review, in-service and commonly used box girder sizes were identified and thus informed the member selection for the current study. All selected bridges were AB structures, including both composite and noncomposite (in the sense that the member is composite with the slab, not the curb slab/barrier wall) structures. Eight representative exterior girders were selected for analysis are hereafter referred to as Beams A through H. Beams A through D are 48 in. (1219 mm) wide boxes having depths of 21 in., 27 in., 33 in. and 42 in. (533 mm, 686 mm, 838 mm and 1067 mm), respectively. Similarly, Beams E through H are 36 in. (914 mm) wide boxes having the same standard depths. Dimensions and section properties of the prototype beams are provided in Table 3-2.

Dimensions of the barrier wall are based on a review of common barrier wall sizes typical of late 1960's and early 1970's construction. Harries (2006) notes that the entire curb slab/barrier wall assembly is effectively composite with the girder. Construction drawings often indicate construction joints along the curb slab/barrier wall assembly. Inspection, however, has shown that these are rarely, if ever, provided in the curb slab and are not always present in the projecting wall. Tests on an exterior girder (Harries 2006 and described above and Chapter 4) clearly indicated that composite behavior was achieved (indeed, this provided the motivation for this study). The typical sizes for barrier walls modeled in this study are given in Table 3-2; it is noted that these vary slightly for the 48 and 36 in. (1219 and 914 mm) wide beams.

3.2.2   Section Geometry

The cross sections shown in Table 3-2 were analyzed in this study. Since the strength reduction for interior girders or girders without a barrier wall is not significant (Harries 2006), only exterior girders with composite barrier walls were modeled in this study. The approach used, however, is valid for any section geometry.

The section geometry is 'drawn' and an automated discretization procedure in XTRACT divides this into triangulated fiber elements (see Figure 3-4). The concrete fiber element size for all models was 1 in. (25.4 mm), which is felt to be adequate given the complexity and size of the section. Mild steel and prestressing strand are modeled as individual fiber elements and are located exactly as they occur in the section.

The following simplifications were made in the modeling process.

1. The shear key located on the interior web of girder was not modeled.

2. No asphalt topping was included (this is non-structural in any case).

3. The barrier wall and girder concrete materials were assumed to have the same properties.

4. Nominal material properties are used (no reduction factors are applied).

Only assumption #3 is likely to affect the accuracy of the predictive capacity of the model, although since the objective is a parametric study, this is not considered a concern.

3.2.3   Concrete Material Model

A fully nonlinear concrete material model is applied to all concrete fiber elements. The model includes the tensile capacity of concrete although tension-stiffening was not considered. Figure

46

3-5(a) provides the stress-strain curve used for the concrete material. Specific concrete material properties used are as follows:

compressive strength:	f_c' = 6000 psi = 41.4 MPa
modulus of elasticity:	E_c = 4700 ksi = 32.4 GPa
tensile strength:	f_t = 479 psi = 3.3 MPa
compressive strain at f_c':	ε_c' = 0.0028
crushing strain:	ε_{cu} = 0.0060
strain at spalling:	ε_{sp} = 0.0070
maximum compressive strain:	ε_{cmax} = 0.0080
residual compressive strength:	f_{cp} = 0 psi = 0 MPa

3.2.4   Prestressing Strand

A nonlinear prestressing strand material was applied to all strand elements (Figure 3-5(b)). Regardless of diameter, each strand was assumed to be originally stressed to $0.7f_{pu}$ (175 ksi = 1207 MPa) and to retain $0.55f_{pu}$ after all losses, resulting in a prestress of 137.5 ksi (948 MPa). The prestress loss value was determined using loss calculations from Harries (2006) since the members investigated in this study are assumed to be of similar quality and age (constructed in the 1960's). Additionally, girders of this vintage utilized Grade 250 strand, hence its use in the members modeled in this study. Prestressing strand material properties are as follows:

yield stress:	f_{py} = 230 ksi = 1586 MPa
ultimate stress:	f_{pu} = 250 ksi = 1724 MPa
ultimate strain:	ε_{pu} = 0.0430
modulus of elasticity:	E_p = 29000 ksi = 200 GPa

3.2.5 Mild Reinforcing Steel

All longitudinal mild steel was modeled as A615 Grade 40 steel. The multilinear material model is shown in Figure 3-5(c) and material properties are as follows:

yield stress: $f_y = 40$ ksi $= 276$ MPa

tensile stress: $f_u = 70$ ksi $= 483$ MPa

rupture strain: $\varepsilon_{su} = 0.1200$

strain hardening strain: $\varepsilon_{sh} = 0.0150$

modulus of elasticity: $E_s = 29000$ ksi $= 200$ GPa

3.2.6 Removal of Strands

In addition to the presence of the barrier wall, the primary parameter of interest in this study is the eccentricity due to loss of prestressing strands. The following suppositions are made:

1. Strand loss is most likely at the outboard web-soffit corner of exterior girders due to mechanical damage caused by vehicle impacts followed by corrosion of the now-exposed strands. This is evident in test girders (Harries 2009) and is regularly seen in practice (Kasan 2009).

2. For exterior girders, due to the biaxial bending component resulting from the neutral axis orientation (see Figure 3-1(b)), the same outboard web-soffit corner is the critical region for tensile stresses in the section.

Thus it is physically appropriate and most critical to the section behavior to remove strands beginning at the outboard web-soffit corner (i.e.: those under the barrier wall on an exterior girder) and progress toward the inboard direction. In the analyses to follow, strands were

removed from (at most) the lower three layers only. The three digit identification of each analysis indicates the number of strands removed from the lower, second and third layers, respectively. For example, damage of 8-8-1 for Beam D indicates 8 strands removed from the lower layer, 8 from the second and 1 from the third, for a total of 17 strands removed from the section (Figure 3-6). In all cases the strands were removed from the outboard side and progressed inward. Even if vehicle impact is not the source of damage, removing strands in this manner represents a worst-case scenario since it results in the greatest girder cross section eccentricity girder as described previously.

Each beam was subjected to multiple levels of damage in order to capture the member behavior through a range of damage levels. It is important to note that in no case did the level of damage considered exceed that which would result in failure due to dead load of the member (i.e.: all damaged girders were still able to support their own weight). Tables 3-3 to 3-10 provide the induced damage for each beam as well as model predictions (as will be discussed later).

3.2.7   Criteria for Establishing Moment-Moment Failure Envelope

As described above, specific material failure criteria must be provided to establish the moment-moment (M_x - M_y) failure envelope. These criteria represent input parameters in the XTRACT model and are selected by the user. (Alternately, default values corresponding to a "serviceability" and "ultimate" load condition are automatically generated based on the material models used.) The selection of the material failure criteria results in a single envelope being generated based on the selected criteria which are related (by the user) to some load condition (in essence these criteria are 'allowable strains' or 'performance criteria' which no fiber in the section may exceed). In the present analysis, the ultimate capacity of the under reinforced (i.e.:

section response controlled by steel) PC box girder is desired, thus criteria related to the ultimate capacity were selected as follows:

concrete strain to cause failure: $\varepsilon_c = 0.003$

prestressing strand strain at failure: $\varepsilon_p = 0.010$

mild steel strain at failure: $\varepsilon_s = 0.035$

The concrete and prestressing strand values were selected to represent the initiation of concrete crushing ($\varepsilon_c = 0.003$) and a strand strain ($\varepsilon_p = 0.010$) sufficient to develop the yield capacity of the strand (230 ksi) but not approach strand rupture ($\varepsilon_{pu} = 0.043$). The mild steel strain was selected to be very high ($\varepsilon_s = 0.035$) so as not to affect the outcome of the analysis. In the sections considered, the mild steel does not play a significant role in the behavior and its failure (if the concrete and strand were still adequate) would not be catastrophic. If the mild steel were critical to the ultimate behavior, an allowable strain on the order of $\varepsilon_s = 0.006$ would be appropriate to ensure yielding but no strain hardening behavior. The criteria selected were generally observed to maximize girder capacity and thus are appropriate in assessing the ultimate load carrying capacity of the sections as described in the following section. The reader is cautioned that 'failure' in this sense is used to define the M_x-M_y envelope and should not be interpreted as implying catastrophic failure; indeed reserve deformation capacity would be expected beyond the envelope strains defined.

3.2.7.1 Sensitivity of predicted behavior to failure criteria

To reiterate, the ultimate moment capacity is determined based on user-defined limiting strain criteria, thus the ultimate moment capacity and the neutral axis rotation angle reported are only valid for the defined failure criteria. Selection of different failure criteria will yield different results. To illustrate this concept as well as verify the appropriateness of the selected failure

criteria (particularly, $\varepsilon_p = 0.010$), Beam D 6-4-0 was analyzed using strand strain failure criteria ranging from slightly greater than the long-term prestressing force ($\varepsilon_p = 0.0053$) to the onset of concrete crushing (which occurred at $\varepsilon_p > 0.015$). At values below $\varepsilon_p = 0.0047$, the strand would be unable to support the assumed level of prestress after losses of $0.55f_{pu}$ (see Section 3.2.4). The girders are under reinforced; in this case steel strand strains exceeding $\varepsilon_p = 0.015$ are required to be achieved before concrete failure (assumed to occur at $\varepsilon_c = 0.003$) will occur. Therefore strand failure strains greater than $\varepsilon_p = 0.015$ will result in no further increase in section capacity.

Figure 3-7 shows the predicted values of moment capacity and principal axis rotation as ε_p is varied. It can be seen in this figure that the ultimate capacity and the axis rotation converge to singular values as limiting strand strain increases. The selection of $\varepsilon_p = 0.010$ for all analyses is sufficient to capture the near-ultimate behavior of the sections while still respecting the under-reinforced nature of the beams (i.e.: avoiding concrete failure) and allowing for some reserve capacity.

3.3 SECTION ANALYSIS RESULTS

Tables 3-3 to 3-10 summarize both the 1D and 2D the moment capacities and neutral axis rotations determined using the criteria described in Section 3.2.7. 106 analyses are reported. The data provided in each table is defined as follows:

M_{xN} = the vertical moment capacity (i.e.: flexure about the horizontal axis) of the section (with appropriate damage) calculated assuming the neutral axis is horizontal (i.e.: $\theta = 0^o$). This capacity is equivalent to that determined from a traditional uniaxial (1-D) sectional analysis.

θ = the orientation of the neutral axis measured as a clockwise rotation from the horizontal (x-axis; Figure 3-1(b)) corresponding to the required external equilibrium condition; that is, satisfying $M_y = 0$.

$M_{x\theta}$ = the vertical moment capacity of the section having a neutral axis rotation of θ associated with the applied load case $M_y = 0$.

M_{xN0} is the special case of the vertical moment capacity of the undamaged section calculated assuming the neutral axis is horizontal (i.e.: $\theta = 0°$). In this study, $M_{xN0} = M_{xN}$ for damage case 0-0 or 0-0-0. This value is surrogate for the original design capacity of the girder.

Convergence tolerance, limits on the number of iterations (80) and the resolution of both the fiber model geometry (1 in. = 25.4 mm) and the neutral axis angle (1°) combine to result in a precision (in determining moments) that is on the order of ±20 kip-ft (±27 kN-m) for the models considered. In all cases, the value of θ is determined as the point on the interaction surface having M_y algebraically closest to zero at the ultimate capacity. $M_{x\theta}$ is then determined for this point (essentially truncating the selection of θ to the nearest whole degree). Linear interpolation between values of θ would be valid although it will not improve the precision and was not carried out. An example of a portion of the XTRACT output data for Beam D 8-8-1 illustrating this procedure is shown and annotated in Table 3-11.

3.4   INTERPRETATION OF SECTIONAL ANALYSIS PARAMETRIC STUDY

3.4.1   Capacity Determined from Uniaxial (1D) Sectional Analysis

A uniaxial (1D) sectional analysis of a member composite with the barrier wall and curb slab will overestimate the vertical flexural capacity of an asymmetric section; this is discussed below. The analyses presented nonetheless verify the intuitive conclusion: For an under-reinforced concrete section, the capacity of the damaged section, relative to the undamaged section, will be proportional to the remaining reinforcement:

$$M_{xN} = [(N - n)/N]M_{xN0} \qquad\qquad\qquad \text{(Eq. 3-2)}$$

Where n is the number of damaged (removed) strands and N is the original total number of strands in the section. The relationship expressed by Equation 3-2 was found to hold for all analyses conducted. It is noted that this relationship will only be valid while the section has sufficient capacity (i.e.: remaining strands) to carry its own dead load. If the girder capacity falls below that corresponding to its own dead load, clearly a catastrophic failure occurs.

3.4.2   Capacity Determined from Biaxial (2D) Sectional Analysis

The relationship described by Equation 3-2 only roughly holds true for biaxial (2D) analyses. The relationship is only strictly valid when the damaged strands are removed in a symmetric manner. If the strand damage is asymmetric (as is the case modeled here), application of Equation 3-2 in the context of a biaxial (2D) sectional analysis will overestimate the section capacity. This overestimation is proportional to the degree of asymmetry as expressed by the rotation of the neutral axis, θ.

3.4.3 Relationship between Biaxial (2D) and Uniaxial (1D) Sectional Analyses

The flexural capacity determined from a uniaxial (1D) analysis (M_{xN}) overestimates the vertical flexural capacity of an asymmetric section ($M_{x\theta}$). This ratio, $M_{xN}/M_{x\theta}$, is given in each of Tables 3-3 through 3-10. As one may imagine, the overestimation is related to the degree of asymmetry as expressed by the rotation of the neutral axis, θ. The results of the parametric study suggest the following factors affect the overestimation of vertical flexural capacity of an asymmetric section when predicted using a 1D analysis (M_{xN}).

3.4.3.1 Degree of damage

The overestimations of the uniaxial (1D) analysis predictions are more significant at greater levels of damage (i.e.: more strands removed) regardless of whether the strands are removed in a symmetric manner or not. Thus the rotation of the neutral axis due to asymmetric strand loss does not account for the entire overestimation. The following relationship may be established based on the parametric study conducted.

$$\mathbf{M}_{x\theta} = (\cos\theta)^{\alpha}(\mathbf{M}_{xN}) \qquad\qquad \text{(Eq. 3-3)}$$

Combining the effects expressed by Equations 3-2 and 3-3, one arrives at the relationship expressed in Equation 3-4. The advantage of Equation 3-4 is that it is written in terms of the original design capacity of the beam, M_{xN0}.

$$M_{x\theta} = \frac{N-n}{N}(\cos\theta)^{\alpha}(M_{xN0}) \qquad\qquad \text{(Eq. 3-4)}$$

In either case, it was found that α can be expressed as:

$$\alpha = 2\left(\frac{I_y}{I_x}\right) \qquad\qquad \text{(Eq. 3-5)}$$

54

Where I_y = moment of inertia of the gross girder section, including the barrier wall about the vertical y-axis and; I_x = moment of inertia of the gross girder section, including the barrier wall about the horizontal x-axis. The calculated values of α for each beam are presented in Table 3-2. The average absolute error, indicated by the ratio of member capacity calculated using Equation 3-4, $M_{x\theta}$, to XTRACT-predicted results (as seen in Tables 3-3 to 3-10), in all cases, is less than 6%.

If an empirical approach to determining the value of α is taken with the goal of minimizing absolute error, α was found to be marginally different for Equations 3-3 and 3-4 and slightly different than the relationship expressed in Equation 3-5. This implies that additional parameters play a role in the prediction of $M_{x\theta}$, particularly: a) The ultimate capacity of the section is defined based on user-selected failure criteria and thus is dependent on such criteria and; b) the section is utilized beyond its elastic range and thus will also be cracked, changing the section properties used in Equation 3-5. Therefore, approaches based on elastic mechanics will not be sufficient, but can be leveraged.

Asymmetric bending results in biaxial moments and the combination of these moments, with their directions, form the couple moment vector. The relationship to determine the angle which the resultant couple moment vector forms with the horizontal axis for a section under asymmetric bending is proportional to the ratio of moment of inertia about the vertical and horizontal axes (Beer and Johnston 1985). Since determination of the angle the resultant couple moment vector forms with the horizontal axis is similar in nature to the current study (resulting from asymmetrical bending), it is reasonable to expect Equation 3-3 and 3-4 to include a similar relationship. Therefore, it follows that α to be proportional to the ratio of moments of inertia about the vertical and horizontal axes. It is acknowledged that accuracy may be improved if an

empirical method were used to determine α. However, due to modeling restrictions and the aforementioned factors accounted for by the α parameter, determination of the ultimate capacity for an exterior box girder does not require an accuracy greater than that which is provided by Equation 3-4 and the α factor obtained from Equation 3-5. Therefore, the level of accuracy provided is felt to be sufficient for the determination of the ultimate capacity of an exterior AB girder composite with a curb slab and barrier wall.

It is apparent that the $\cos\theta$ term in Equations 3-3 and 3-4 accounts for axis rotation while the calibration factor α is a function of the girder vertical and horizontal moment of inertias. Capacities predicted using both Equations 3-3 and 3-4 and the ratio of these values with respect to the XTRACT predictions are given in Tables 3-3 through 3-10 for Beams A through H, respectively.

Using the relationships presented by Equation 3-3 and 3-4, normalized moment capacity plots were created and are provided in Figures 3-8 to 3-15. In these figures, the values of $M_{x\theta}$ determined from Equations 3-3 and 3-4 are normalized by M_{xN} and M_{xN0}, respectively, and are thus consistent with the bases for the equations.

3.4.3.2 Section geometry

The shallower girders (e.g. Beam A and E) exhibited a somewhat different relationship between uniaxial (1D) and biaxial (2D) results than did the deeper girders (e.g. Beam D and H). Largely, the difference in behavior between the shallower girders and deeper girders results from the difference between horizontal and vertical axis moments of inertia and is easily seen in a comparison of α values between Beams A and D and Beams E and H. As the shape moves towards a deeper section, the α factor decreases, in turn increasing the $(\cos\theta)^{\alpha}$ term. This suggests that the effect of the neutral axis rotation is lessened with the increase in depth.

Additionally, the variation of the α value is a result of the proportional contribution of the barrier wall to the section behavior. Since its size is essentially constant, the barrier wall corresponds to a greater portion of the gross section properties in the smaller girders.

3.4.3.3 Girder efficiency

In a further attempt to understand the effect of beam geometry, the girder efficiency, ρ, was calculated as follows (Guyon 1963):

$$\rho = \frac{I_x}{(A_g)(y_t)(y_b)} \qquad \text{(Eq. 3-6)}$$

Where I_x = moment of inertia of the gross girder section, including the barrier wall, about the horizontal x-axis; A_g = gross area of the section including the barrier wall; y_t = the distance from the neutral axis to the top of the section and; y_b = the distance from the neutral axis to the bottom of the section. The girder efficiency for Beams A through H is provided in Table 3-1. However, no correlation between girder efficiency and α parameter or the ultimate capacity was found.

3.4.3.4 Effect of Composite Barrier Wall on Undamaged Girder

Although not a focus of the present work, results from the analysis of undamaged girders (i.e.: 0-0 and 0-0-0 cases) illustrate the effect of the presence of a composite barrier wall in rotating the neutral axis of an exterior girder. As previously observed (Harries 2006), *in-situ* conditions and previous experimental results (Harries 2009) indicate that the barrier wall and curb slab act compositely with the exterior girder and thus should be included in the analysis of the structure. Additionally, the analysis is typically performed about the horizontal axis (x-axis) and the neutral axis rotation is not included. Figure 3-16a shows the ratio of the ultimate moment capacity determined using a 2D-analysis (accounting for the effects of axis rotation) compared to that

from an analysis performed about the horizontal axis (1D) for the undamaged prototype girders. It can be seen in this figure that the 1D-analysis significantly overestimates the true ultimate moment capacity of the member and that the actual capacity is between 66% and 79% of that determined from the simple analysis depending on the girder geometry. As expected, the overestimation provided by the 1D analysis is greater for the shallower members (i.e.: beam A and beam E) due to the greater proportional contribution of the barrier wall to the girder section properties and and the barrier wall's effect of shifting the neutral axis location vertically.

Although the presence of the composite barrier wall drives the rotation of the neutral axis, it also significantly increases the capacity of the exterior girder over that assumed in design; that is: with a non-composite barrier wall. The net effect is that despite the capacity reduction resulting from the neutral axis rotation, an exterior girder having a composite barrier wall has a greater capacity than that without the wall. Figure 3-16b shows the 2D-analysis of the girder having a composite barrier wall normalized by the nominal capacity of the non-composite girder. The latter may be thought of as the intended design capacity of the girder. It can be seen in this figure that the member capacity increases to between 119% and 170% of the original girder. The increase in moment capacity due to the presence of a composite barrier wall is less in deeper members; again, due to the proportional contribution of the barrier wall to the girder section properties and the barrier wall's effect of shifting the neutral axis location vertically .

This issue is further complicated when considering the possible actual load which may be carried by the exterior girder compared to the design loading. A live load moment-distribution factor of 0.3 is common for AB girder structures. When the member no longer acts in conjunction with adjacent girders (i.e.: in a transversely composite manner), the live load moment-distribution factor will increase to 0.5 (i.e.: one wheel line of the design vehicle). This

can occur when the shear key between girders deteriorates as discussed in the following section. In this case, the loss of composite behavior between adjacent girders also results in the weight of the barrier wall and curb slab to no longer be distributed to the other girders; thus the exterior girder supports the entire barrier wall and curb slab assembly. Thus it is feasible that the live load carried by the exterior girder is increased by 66% and the barrier wall dead load is increased by factor equal to half the total number of girders in the bridge. To illustrate this, Table 3-12 presents the moment demand for each prototype member when the structure is: a) acting as designed with an intact shear key and the barrier wall and curb slab dead load distributed evenly to each girder; and b) no longer behaving as designed or transversely composite (shear key ineffective) and the exterior girder is acting independently. Essentially, Table 3-12 illustrates both the 'best' and 'worst' case scenarios for moment demand of an exterior girder. Figure 3-16c shows the ratio of the potential load that may be carried by an exterior girder to that for which it is designed (ratio of worst-to-best cases).

Thus, it is not at all clear (and must be assessed on a case-by-case basis) whether the beneficial effects of assuming a composite barrier wall outstrip the deleterious effects the potential loss of composite behavior in the transverse direction. The effects of girder damage must also be considered in this assessment.

3.4.4   Exterior girders in the context of complete AB bridges

The results presented in this chapter are based on individual exterior AB girders and do not consider how these interact with the rest of the bridge. This section describes intended designed-for behavior of AB bridges, deviations from intended behavior observed in the field and therefore the appropriateness of the analyses presented in this chapter.

The exterior girder of an AB bridge (Figure 3-17) is expected to behave in a composite manner with the rest of the bridge. Two or three details are provided to ensure this, although field observations draw into question the efficacy of these details as described below:

3.4.4.1 Composite deck

Approximately 55% of AB bridges have a composite deck overlayed on the girders (Table 3-1). This deck enforces compatibility and allows the entire bridge section to behave as a single unit. It is not clear whether the presence of a composite deck alone is sufficient to resist the tendency of an exterior girder to 'roll away' from the bridge superstructure. As noted in Table 3-1, AB bridges having composite decks have significantly fewer 'structurally deficient' ratings. This study largely focused on AB bridges having non-composite decks.

3.4.4.2 Shear key

All AB bridges have a continuously grouted shear key between all girders. The shear key is located about 6 in. (152 mm) below the top of the girder, is approximately 6 in. deep and engages the AB web to a depth of about 1 in. (25 mm). The shear key is grouted after the girders are set and cannot be inspected. If the shear key is present and intact, it should be sufficient to distribute forces between girders in the manner intended by the bridge design. For an AB bridge, AASHTO (2007) calculations lead to a flexural distribution factor (DF) on the order of 0.3 for AB bridges. Without an intact shear key, this value increases to 0.5 resulting in 66% greater vertical moments being applied to the girder. Additionally, without a shear key the dead load of appurtenances (including the barrier wall) are not distributed equally across the bridge as assumed in design.

Harries (2009) reports significant anecdotal evidence that shear keys in AB bridges are often deteriorated or missing altogether: "In some cases, where shear keys were present, they were of very poorly consolidated grout… It was common to find asphalt material on the lower ledge of a shear key … indicating that the key had not been present at least since the last time the bridge was paved."

An additional detail affecting the shear key between the exterior girder and the first interior girder is that the exterior girder is often set vertically, rather than following the angle of the bridge cross slope or superelevation (this is shown in Figure 3-17). This is done typically only on the side of the bridge facing oncoming traffic (left side of Figure 3-17) and is done for purely aesthetic reasons: drivers prefer to see a vertical surface, rather than an angled one, as they pass under a bridge. The change in girder angle results in a triangular gap between the exterior and interior girders that widens with increasing depth. This widening gap makes it more unlikely that the shear key at this interface will be properly placed, intact or effective.

3.4.4.3 Tie Rods

AB bridges of the size and vintage considered here have three mild steel tie rods provided between adjacent girders (Harries 2006). These rods are typically 1 in. (25.4 mm) in diameter and located vertically in the center of the shear key. Longitudinally, these rods are located at internal diaphragms which are located near midspan and about 10-20% of the span length from each support. The tie rods are primarily used to 'pull' the girders together during construction. Tie rods may also resist some of the off-axis flexure inherent in an exterior girder; that is, they may resist the tendency of the girder to 'roll away' from the bridge. However, the relatively small rods will only resist a relatively small off axis (M_y) moment.

With the loss of shear key grout to protect them, tie rods are often found to be badly corroded (sometimes to the extent of being no longer present) at the girder interfaces (this is found upon demolition; tie rods cannot be inspected in an AB bridge). Furthermore, proof that the rods are unable to resist the tendency of the girder to 'roll away' from the bridge was clearly evident in the fact that all three tie rods of the Lake View Drive bridge exhibited tension failures despite their being in essentially very good shape (little more than surface corrosion).

As described in the previous paragraphs, the efficacy of composite decks, shear keys and tie rods in restraining exterior girders from rotation is questionable. Harries (2006) notes that the presence (inertia) of adjacent interior girders is sufficient to resist any tendency of interior girders to rotate. While an interior girder would certainly resist the tendency of an adjacent exterior girder to 'roll inward', this is not the behavior of such a girder. Thus it is rational to assume that no such restraint exists as was done in this study.

3.5   CONCLUSIONS

A parametric study which analyzed the effects of varying levels of damage to eight prototype AB beams was conducted; in all, 106 analyses were carried out. From this study, two relationships have been proposed to determine the capacity of an AB beam subject to asymmetric loading which include the composite behavior of the barrier wall assembly. These relationships relate the capacity to the more easily obtained 1D capacity predictions. While both relationships showed good predictive ability compared to the modeled values (average error less than 6%), it is believed that Equation 3-4 is a better representation of the true behavior of the beams because both damage to the structure due to lost strands and the rotation of the neutral axis are accounted

for. Additionally, this relationship is more useful in assessing an existing structure since it is based on the original undamaged, 1D capacity; essentially the original design capacity. It is noted that the α factor facilitates the adoption of a single equation to represent various member geometries.

It is common for the barrier wall and curb slab to be composite with the girder. This composite action will increase the moment capacity as compared to the original girder. However, additional loadings beyond those which the original member is intended to resist must also be considered. When including the composite action of the barrier wall and curb slab, it is prudent to assume that the entire dead load of this assembly is acting only on the exterior girder. Additionally, if the shear key is ineffective, the structure is no longer composite transversely and thus additional live load demands need to be considered. It is acceptable for the barrier wall and curb slab to be considered composite with the girder, however this new section will experience loadings different than the original member which must be accounted for in the analysis and rating of the member.
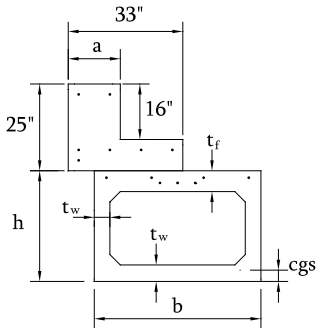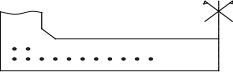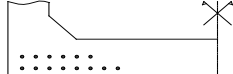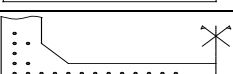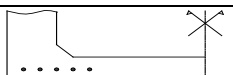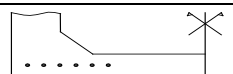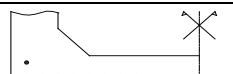
As shown in Figure 3-7, the selection of steel failure strain $\varepsilon_p = 0.010$ is sufficient to utilize the section beyond its elastic capacity and cause concrete cracking. Although all factors contributing to the capacity reduction cannot be individually quantified, the α factor accounts for these effects to a sufficiently accurate degree. Thus, Equation 3-4 provides a relationship which accurately captures the behavior and capacity of a damaged or undamaged exterior AB girder with a composite barrier wall (as was experimentally verified in Harries 2006 and reiterated in the analysis presented in Chapter 4). It is acknowledged that the expected ratio of Equation 3-4 to XTRACT-predicted results is dependent on the failure criteria selected. The failure criteria used in the current study are felt to be appropriate for an under reinforced prestressed member

while continuing to provide some reserve plastic rotation capacity As a result, the α factor is believed to be acceptable for AB girders. However, more research is required to verify the α term for other girder geometries.

Table 3-1 Summary of statewide and District 11 and 12 AB bridge inventory.

	Pennsylvania[1]			District 11[2]			District 12[3]		
		Structurally Deficient (rating < 4)			Structurally Deficient (rating < 4)			Structurally Deficient (rating < 4)	
	number of bridges	all[4]	superstructure only	number of bridges	all[4]	superstructure only	number of bridges	all[4]	superstructure only
all bridges	25203	5385 (21.4%)	3465 (13.8%)	1781	505 (28.4%)	318 (17.9%)	2345	586 (25.0%)	376 (16.0%)
all prestressed (4xxxx)	5874	887 (15.1%)	456 (7.8%)	671	188 (28.0%)	52 (7.8%)	263	71 (27.0%)	22 (8.4%)
Noncomposite AB (BMS code: 4x107)	822	350 (42.6%)	326 (39.7%)	69	19 (27.5%)	14 (20.3%)	33	9 (27.3%)	7 (21.2%)
Composite AB (BMS code: 4x207)	1175	96 (8.2%)	29 (2.5%)	95	17 (17.9%)	8 (8.4%)	40	7 (17.5%)	4 (10.0%)

[1] reported: September 10, 2007
[2] reported: December 5, 2007; District 11 includes Allegheny, Beaver and Lawrence Counties
[3] reported: December 26, 2007; District 12 includes Greene, Fayette, Washington and Westmoreland Counties
[4] SD rating resulting from any of deck, super structures or sub structure rating (culverts not considered)

Table 3-2 Prototype beam dimensions.

$f_c' = 6000$ psi
$f_{ps} = 250$ ksi
$f_y = 40$ ksi

L = length of girder (from representative bridge)
I_x = gross moment of inertia about horizontal axis
I_y = gross moment of inertia about vertical axis
A_g = gross cross sectional area
ρ = section efficiency (see Equation 3-6)

Beams A-D: strands have 1.5" vertical and horizontal clear cover (typ).

Beams E-H: strands have 1.25" vertical clear cover (typ) and 1.5" horizontal clear cover (typ).

Beam	L (ft)	h (in)	b (in)	t_w (in)	t_f (in)	a (in)	I_x (x10³ in⁴)	I_y (x10³ in⁴)	A_g (in²)	strand details and area (A_{STRAND})	cgs (in)	α (Eq. 3-5)	ρ (Eq. 3-6)	Strand Pattern (half section of box soffit drawn to scale)
A	41.5	21	48	5	5.5	15	186.8	297.9	1151	26 - 250 ksi 7/16"strand = 2.83 in² in 2 layers (22-4)	2.06	3.2	0.389	
B	55.5	27	48	5	5.5	15	266.6	336.3	1224	28 - 250 ksi 7/16"strand = 3.05 in² in two layers (16-12)	2.61	2.5	0.417	
C	71.7	33	48	5	5.5	15	368.6	369.2	1284	38 - 250 ksi 7/16"strand = 4.14 in² in three layers (16-20-2)	3.01	2.0	0.418	
D	81.7	42	48	5	5.5	15	569.0	421.4	1374	54 - 250 ksi 7/16"strand = 5.89 in² in five layers(16-26-4-2-4-2)	4.19	1.5	0.389	
E	33.2	21	36	5	5	14.5	162.5	153.3	1004	28 - 250 ksi 3/8"strand = 2.24 in² in two layers(18-10)	2.29	1.9	0.411	
F	48.3	27	36	4.5	4.5	14.5	224.8	168.0	1047	30 - 250 ksi 3/8"strand = 2.40 in² in two layers(18-12)	2.35	1.5	0.436	
G	69.5	33	36	4.5	4.5	14.5	310	185.0	1101	42 - 250 ksi 3/8"strand = 3.36 in² in six layers(16-14-6-2-2-2)	3.54	1.2	0.443	
H	47.3	42	36	4.5	4.5	14.5	467.9	206.9	1182	34 - 250 ksi 3/8"strand = 2.72 in² in three layers(16-16-2)	2.63	0.9	0.518	

1 in. = 25.4 mm; 1 kip = 4.448 kN

Table 3-3 Damage and analysis results for Beam A.

Damage	XTRACT analysis				Equation 3-3		Equation 3-4	
	M_{xN} (k-ft)	θ (deg)	M_{x0} (k-ft)	$\dfrac{M_{xN}}{M_{x0}}$	M_{x0} (k-ft)	$\dfrac{(M_{x0})_{EQ3\text{-}3}}{(M_{x0})_{XTRACT}}$	M_{x0} (k-ft)	$\dfrac{(M_{x0})_{EQ3\text{-}4}}{(M_{x0})_{XTRACT}}$
0-0	M_{xN0} = 2314	31	1526	1.52	1413	0.93	1413	0.93
1-0	2239	31	1478	1.51	1367	0.92	1359	0.92
2-0	2163	32	1354	1.60	1276	0.94	1261	0.93
3-0	2087	32	1297	1.61	1232	0.95	1208	0.93
4-0	2005	32	1241	1.62	1183	0.95	1155	0.93
5-0	1928	33	1113	1.73	1098	0.99	1064	0.96
6-0	1850	33	1058	1.75	1054	1.00	1014	0.96
7-0	1771	33	1002	1.77	1009	1.01	963	0.96
8-0	1691	33	947	1.79	963	1.02	912	0.96
9-0	1608	33	892	1.80	916	1.03	862	0.97
10-0	1528	33	836	1.83	870	1.04	811	0.97
11-0	1445	34	719	2.01	793	1.10	733	1.02
8-1	1614	34	838	1.93	886	1.06	830	0.99
8-2	1536	34	823	1.87	843	1.02	782	0.95

1 in. = 25.4 mm; 1 kip = 4.448 kN

Table 3-4 Damage and analysis results for Beam B.

Damage	XTRACT analysis				Equation 3-3		Equation 3-4	
	M_{xN} (k-ft)	θ (deg)	M_{x0} (k-ft)	$\dfrac{M_{xN}}{M_{x0}}$	M_{x0} (k-ft)	$\dfrac{(M_{x0})_{EQ3\text{-}3}}{(M_{x0})_{XTRACT}}$	M_{x0} (k-ft)	$\dfrac{(M_{x0})_{EQ3\text{-}4}}{(M_{x0})_{XTRACT}}$
0-0	M_{xN0} = 2769	31	1930	1.43	1884	0.98	1884	0.98
1-0	2681	32	1798	1.49	1776	0.99	1768	0.98
2-0	2593	32	1738	1.49	1717	0.99	1703	0.98
3-0	2504	32	1669	1.50	1658	0.99	1637	0.98
4-0	2414	33	1528	1.58	1555	1.02	1529	1.00
5-0	2326	33	1461	1.59	1498	1.03	1465	1.00
6-0	2234	33	1393	1.60	1439	1.03	1401	1.01
7-0	2144	33	1326	1.62	1381	1.04	1338	1.01
8-0	2053	33	1259	1.63	1322	1.05	1274	1.01
5-1	2239	33	1407	1.59	1442	1.03	1401	1.00
5-2	2153	34	1282	1.68	1347	1.05	1300	1.01
6-3	1973	34	1163	1.70	1235	1.06	1176	1.01
6-4	1883	35	1043	1.81	1144	1.10	1081	1.04
7-5	1704	35	928	1.84	1035	1.12	961	1.04
8-6	1521	36	807	1.88	895	1.11	815	1.01

1 in. = 25.4 mm; 1 kip = 4.448 kN

Table 3-5 Damage and analysis results for Beam C.

Damage	XTRACT analysis				Equation 3-3		Equation 3-4	
	M_{xN} (k-ft)	θ (deg)	M_{x0} (k-ft)	$\dfrac{M_{xN}}{M_{x0}}$	M_{x0} (k-ft)	$\dfrac{(M_{x0})_{EQ3\text{-}3}}{(M_{x0})_{XTRACT}}$	M_{x0} (k-ft)	$\dfrac{(M_{x0})_{EQ3\text{-}4}}{(M_{x0})_{XTRACT}}$
0-0	$M_{xN0} = 4041$	32	2949	1.37	2906	0.99	2906	0.99
1-0	3947	32	2886	1.37	2839	0.98	2830	0.98
2-0	3852	33	2736	1.41	2709	0.99	2693	0.98
3-0	3757	33	2657	1.41	2643	0.99	2618	0.99
4-0	3660	33	2578	1.42	2574	1.00	2543	0.99
5-0	3563	33	2499	1.43	2506	1.00	2468	0.99
6-0	3461	34	2338	1.48	2379	1.02	2339	1.00
7-0	3363	34	2261	1.49	2311	1.02	2266	1.00
8-0	3263	34	2183	1.49	2243	1.03	2193	1.00
5-1	3468	34	2358	1.47	2384	1.01	2339	0.99
5-2	3372	34	2291	1.47	2318	1.01	2266	0.99
6-3	3177	35	2059	1.54	2132	1.04	2069	1.01
6-4	3081	35	1985	1.55	2067	1.04	1998	1.01
7-5	2886	36	1758	1.64	1889	1.07	1810	1.03
8-6	2687	36	1611	1.67	1759	1.09	1670	1.04
8-7	2588	36	1538	1.68	1694	1.10	1601	1.04
8-8	2491	37	1399	1.78	1589	1.14	1492	1.07

1 in. = 25.4 mm; 1 kip = 4.448 kN

Table 3-6 Damage and analysis results for Beam D.

Damage	XTRACT analysis				Equation 3-3		Equation 3-4	
	M_{xN} (k-ft)	θ (deg)	M_{x0} (k-ft)	$\dfrac{M_{xN}}{M_{x0}}$	M_{x0} (k-ft)	$\dfrac{(M_{x0})_{EQ3\text{-}3}}{(M_{x0})_{XTRACT}}$	M_{x0} (k-ft)	$\dfrac{(M_{x0})_{EQ3\text{-}4}}{(M_{x0})_{XTRACT}}$
0-0-0	$M_{xN0} = 6301$	33	4913	1.28	4748	0.97	4748	0.97
1-0-0	6200	34	4743	1.31	4672	0.98	4660	0.98
2-0-0	6097	34	4663	1.31	4595	0.99	4572	0.98
3-0-0	5993	34	4568	1.31	4518	0.99	4484	0.98
4-0-0	5890	34	4473	1.32	4361	0.97	4318	0.97
5-0-0	5785	35	4285	1.35	4283	1.00	4232	0.99
6-0-0	5679	35	4191	1.36	4205	1.00	4145	0.99
7-0-0	5575	35	4093	1.36	4127	1.01	4059	0.99
8-0-0	5468	35	3998	1.37	4048	1.01	3972	0.99
5-1-0	5686	35	4210	1.35	4210	1.00	4145	0.98
5-2-0	5583	35	4133	1.35	4135	1.00	4059	0.98
6-3-0	5373	36	3852	1.39	3906	1.01	3814	0.99
6-4-0	5270	36	3763	1.40	3830	1.02	3729	0.99
7-5-0	5057	36	3575	1.41	3606	1.01	3492	0.98
8-6-0	4840	37	3298	1.47	3453	1.05	3325	1.01
8-7-0	4731	37	3208	1.47	3374	1.05	3242	1.01
8-8-0	4624	37	3119	1.48	3233	1.04	3096	0.99
8-8-1	4522	38	2957	1.53	3160	1.07	3015	1.02
8-8-2	4415	38	2883	1.53	3088	1.07	2933	1.02

1 in. = 25.4 mm; 1 kip = 4.448 kN

Table 3-7 Damage and analysis results for Beam E.

Damage	XTRACT analysis				Equation 3-3		Equation 3-4	
	M_{xN} (k-ft)	θ (deg)	M_{x0} (k-ft)	$\dfrac{M_{xN}}{M_{x0}}$	M_{x0} (k-ft)	$\dfrac{(M_{x0})_{EQ3-3}}{(M_{x0})_{XTRACT}}$	M_{x0} (k-ft)	$\dfrac{(M_{x0})_{EQ3-4}}{(M_{x0})_{XTRACT}}$
0-0	M_{xN0} = 1878	38	1271	1.48	1194	0.94	1194	0.94
1-0	1819	38	1238	1.47	1157	0.93	1152	0.93
2-0	1763	39	1145	1.54	1092	0.95	1080	0.94
3-0	1706	39	1103	1.55	1057	0.96	1039	0.94
4-0	1647	39	1062	1.55	1020	0.96	997	0.94
5-0	1588	40	973	1.63	957	0.98	930	0.96
6-0	1527	40	930	1.64	920	0.99	889	0.96
7-0	1468	40	890	1.65	885	0.99	849	0.95
8-0	1410	40	848	1.66	850	1.00	808	0.95
9-0	1348	40	806	1.67	812	1.01	768	0.95
5-1	1531	40	942	1.63	923	0.98	889	0.94
5-2	1473	41	867	1.70	863	1.00	825	0.95
6-3	1355	41	796	1.70	794	1.00	747	0.94
6-4	1297	42	723	1.79	738	1.02	687	0.95
7-5	1176	42	661	1.78	669	1.01	611	0.92
8-5	1116	43	590	1.89	616	1.04	555	0.94

1 in. = 25.4 mm; 1 kip = 4.448 kN

Table 3-8 Damage and analysis results for Beam F.

Damage	XTRACT analysis				Equation 3-3		Equation 3-4	
	M_{xN} (k-ft)	θ (deg)	M_{x0} (k-ft)	$\dfrac{M_{xN}}{M_{x0}}$	M_{x0} (k-ft)	$\dfrac{(M_{x0})_{EQ3-3}}{(M_{x0})_{XTRACT}}$	M_{x0} (k-ft)	$\dfrac{(M_{x0})_{EQ3-4}}{(M_{x0})_{XTRACT}}$
0-0	M_{xN0} = 2251	38	1632	1.38	1575	0.96	1575	0.96
1-0	2183	39	1541	1.42	1496	0.97	1491	0.97
2-0	2118	39	1489	1.42	1451	0.97	1439	0.97
3-0	2049	39	1439	1.42	1404	0.98	1388	0.96
4-0	1983	40	1339	1.48	1330	0.99	1308	0.98
5-0	1918	40	1288	1.49	1286	1.00	1258	0.98
6-0	1848	40	1238	1.49	1239	1.00	1207	0.98
7-0	1781	40	1188	1.50	1194	1.01	1157	0.97
8-0	1713	40	1137	1.51	1149	1.01	1107	0.97
9-0	1645	40	1087	1.51	1103	1.01	1056	0.97
5-1	1851	40	1250	1.48	1241	0.99	1207	0.97
5-2	1784	41	1165	1.53	1170	1.00	1131	0.97
6-3	1653	42	1034	1.60	1059	1.02	1009	0.98
6-4	1585	42	997	1.59	1015	1.02	961	0.96
7-5	1449	43	868	1.67	906	1.04	845	0.97
8-5	1381	43	820	1.68	864	1.05	798	0.97

1 in. = 25.4 mm; 1 kip = 4.448 kN

Table 3-9 Damage and analysis results for Beam G.

	XTRACT analysis				Equation 3-3		Equation 3-4	
Damage	M_{xN} (k-ft)	θ (deg)	M_{x0} (k-ft)	$\dfrac{M_{xN}}{M_{x0}}$	M_{x0} (k-ft)	$\dfrac{(M_{x0})_{EQ3-3}}{(M_{x0})_{XTRACT}}$	M_{x0} (k-ft)	$\dfrac{(M_{x0})_{EQ3-4}}{(M_{x0})_{XTRACT}}$
0-0-0	$M_{xN0}=3335$	39	2451	1.36	2464	1.01	2464	1.01
1-0-0	3262	39	2404	1.36	2410	1.00	2406	1.00
2-0-0	3191	39	2346	1.36	2358	1.01	2347	1.00
3-0-0	3119	40	2229	1.40	2265	1.02	2249	1.01
4-0-0	3046	40	2169	1.40	2212	1.02	2191	1.01
5-0-0	2973	40	2110	1.41	2159	1.02	2134	1.01
6-0-0	2897	40	2052	1.41	2104	1.03	2076	1.01
7-0-0	2823	40	1993	1.42	2050	1.03	2018	1.01
8-0-0	2748	40	1933	1.42	1996	1.03	1961	1.01
5-1-0	2902	40	2066	1.40	2108	1.02	2076	1.00
5-2-0	2828	41	1954	1.45	2018	1.03	1983	1.01
6-3-0	2682	41	1839	1.46	1913	1.04	1869	1.02
6-4-0	2610	42	1728	1.51	1828	1.06	1779	1.03
7-5-0	2459	42	1615	1.52	1722	1.07	1668	1.03
8-6-0	2310	42	1502	1.54	1618	1.08	1557	1.04
8-7-0	2237	42	1446	1.55	1567	1.08	1501	1.04
8-7-1	2167	43	1355	1.60	1489	1.10	1418	1.05
8-7-2	2094	44	1258	1.66	1410	1.12	1390	1.11

1 in. = 25.4 mm; 1 kip = 4.448 kN

Table 3-10 Damage and analysis results for Beam H.

	XTRACT analysis				Equation 3-3		Equation 3-4	
Damage	M_{xN} (k-ft)	θ (deg)	M_{x0} (k-ft)	$\dfrac{M_{xN}}{M_{x0}}$	M_{x0} (k-ft)	$\dfrac{(M_{x0})_{EQ3-3}}{(M_{x0})_{XTRACT}}$	M_{x0} (k-ft)	$\dfrac{(M_{x0})_{EQ3-4}}{(M_{x0})_{XTRACT}}$
0-0	$M_{xN0}=3233$	39	2548	1.27	2577	1.01	2577	1.01
1-0	3148	39	2485	1.27	2509	1.01	2501	1.01
2-0	3059	40	2364	1.29	2407	1.02	2394	1.01
3-0	2970	40	2291	1.30	2337	1.02	2319	1.01
4-0	2883	40	2218	1.30	2268	1.02	2244	1.01
5-0	2795	41	2098	1.33	2170	1.03	2141	1.02
6-0	2705	41	2025	1.34	2100	1.04	2067	1.02
7-0	2616	41	1952	1.34	2031	1.04	1993	1.02
8-0	2526	41	1878	1.35	1961	1.04	1919	1.02
5-1	2708	41	2038	1.33	2102	1.03	2067	1.01
5-2	2624	41	1968	1.33	2037	1.04	1993	1.01
6-3	2448	42	1780	1.38	1874	1.05	1820	1.02
6-4	2357	42	1712	1.38	1804	1.05	1747	1.02
7-5	2183	43	1531	1.43	1647	1.08	1579	1.03
8-6	2002	44	1354	1.48	1488	1.10	1414	1.04
8-7	1913	44	1287	1.49	1422	1.11	1343	1.04
8-8	1824	44	1218	1.50	1356	1.11	1272	1.04

1 in. = 25.4 mm; 1 kip = 4.448 kN

Table 3-11 Example XTRACT output.

Angle (deg)	M_x (k-ft)	M_y (k-ft)	
0	−3081	−1908	value of M_{xN} determined at $\theta = 0$ (i.e. 1D analysis).
1	−3082	−1913	
2	−3083	−1917	
...			
143	−1830	198	
144	−1908	100	
145	−1985	−4	

step 1: find entry corresponding to $M_y = 0$.
(interpolation or closest value is acceptable)

step 2: read value of θ.
(XTRACT sign convention: $\theta = 180-145 = 35^\circ$)

step 3: read value of $M_{x\theta}$.
(XTRACT sign convention removed for reporting)

|		
146	−2063	−111
147	−2143	−221
148	−2221	−334
...		
360	−3082	−1910

Table 3-12 Moment demand comparison for an exterior AB girder.

| Beam	h (in)	b (in)	L (ft)	n_g (number of girders)	Nominal Design Moments			Nominal Moment Demand	
					Beam DL (k-ft)	Wall DL (k-ft)	HS20 LL (k-ft)	As designed[1] (k-ft)	Possible In-service[2] (k-ft)
A	21	48	41.5	8	138	120	467	308	492
B	27	48	55.5	8	276	215	719	545	850
C	33	48	71.7	8	500	359	1011	893	1365
D	42	48	81.7	8	727	467	1191	1201	1789
E	21	36	33.2	12	68	76	318	176	303
F	27	36	48.3	12	157	161	589	361	613
G	33	36	69.5	12	360	333	971	707	1178
H	42	36	47.3	12	190	154	571	387	630

[1] $As\ designed = DL_{BEAM} + \dfrac{2}{n_g} DL_{WALL} + 0.3LL$

[2] $Possible\ in-service = DL_{BEAM} + DL_{WALL} + 0.5LL$

1 in. = 25.4 mm; 1 kip = 4.448 kN

(a) symmetric section **(b)** asymmetric section
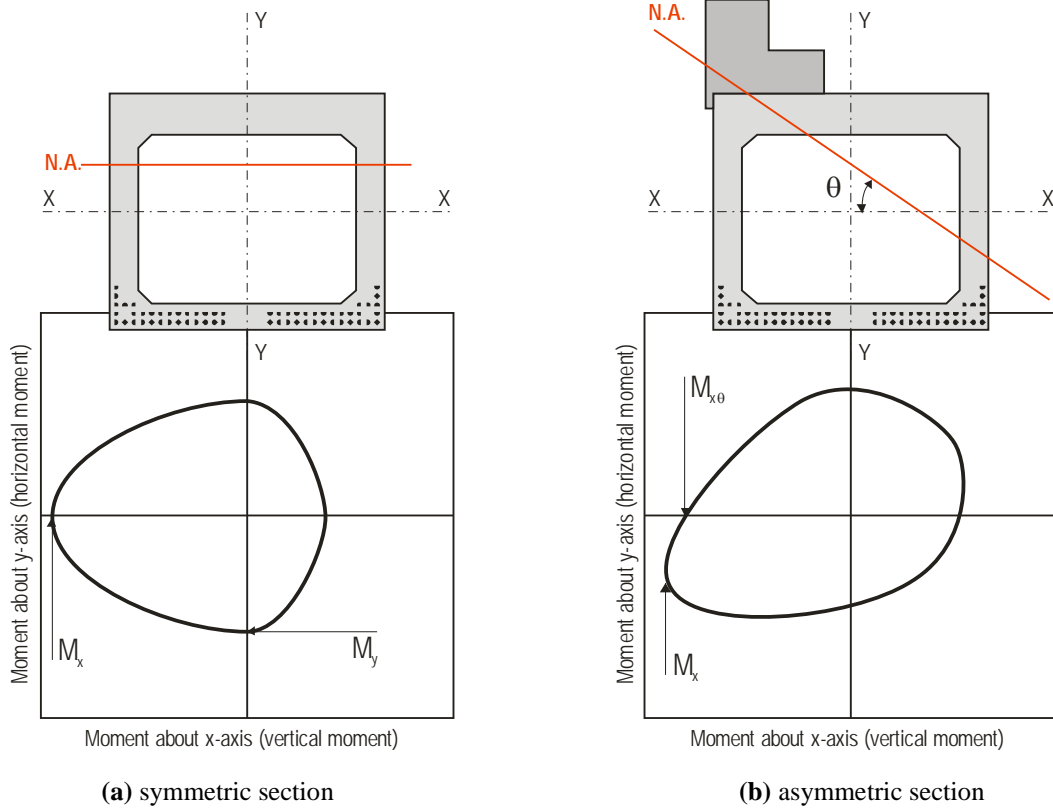
Figure 3-1 Schematic representation of moment interaction (Harries 2006).
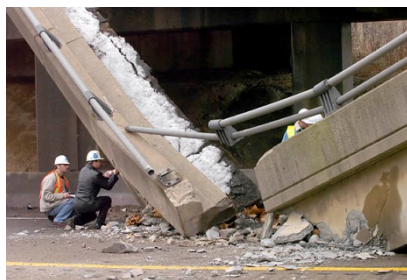
(a) Lake View Drive bridge collapsed onto I-70 December 26, 2005 (Pittsburgh Post Gazette, 12/29/05)
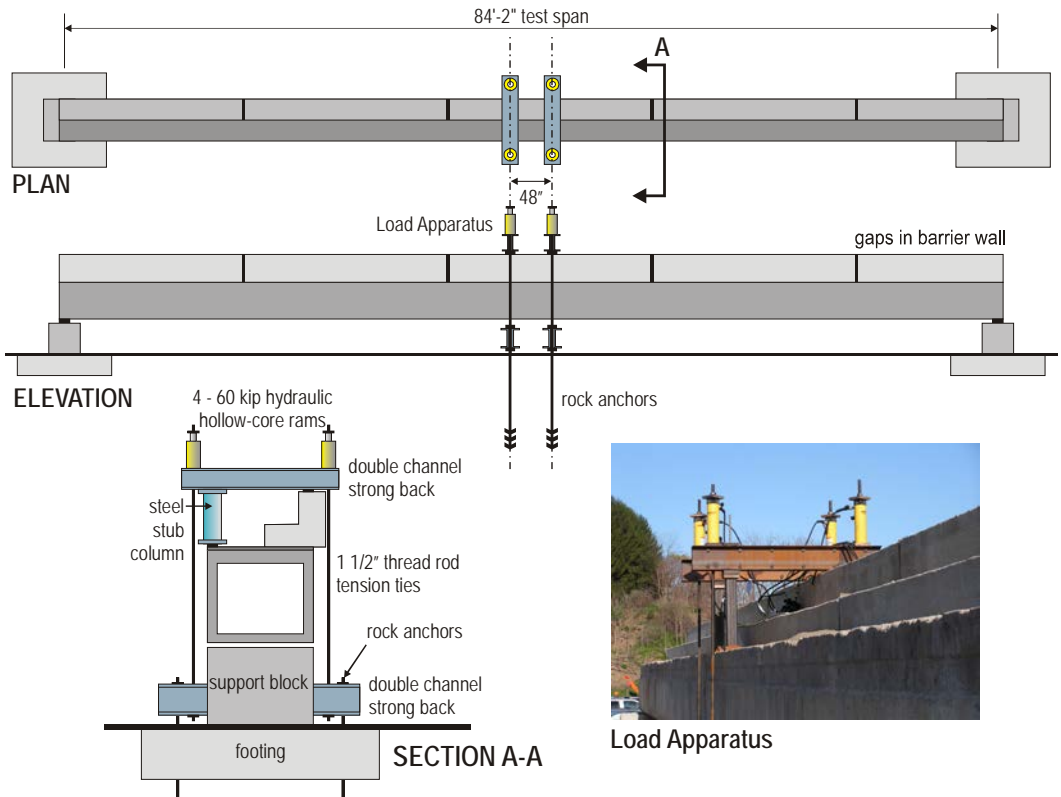
(b) Soffit and fascia of McIlvaine Road bridge over I-70 damaged by vehicle October 18, 2010 (PennDOT)
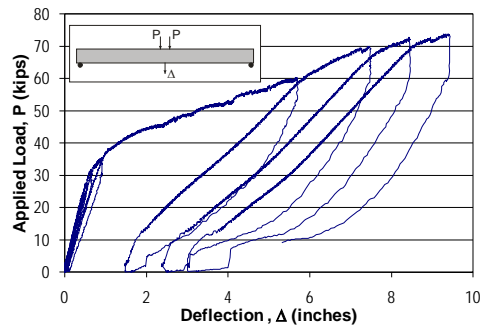
(c) Crawford Lane bridge over I-70 damaged by vehicle impact March 15, 2011 (photo by author).
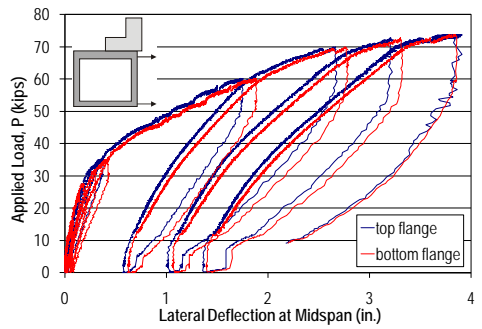
Figure 3-2 Examples of vehicle impact damage to AB girder bridges along about 22.5 miles of the I-70 corridor in southwestern Pennsylvannia.

(a) Test set-up for asymmetric EXTERIOR girder. Loading is symmetric.

(b) applied load versus vertical deflection

(c) applied load versus lateral deflection
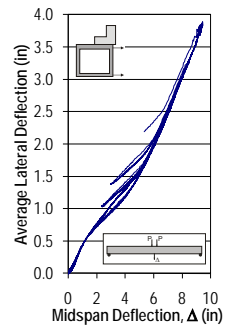
(d) lateral versus vertical deflection

Figure 3-3 EXTERIOR AB girder test (Harries 2009).
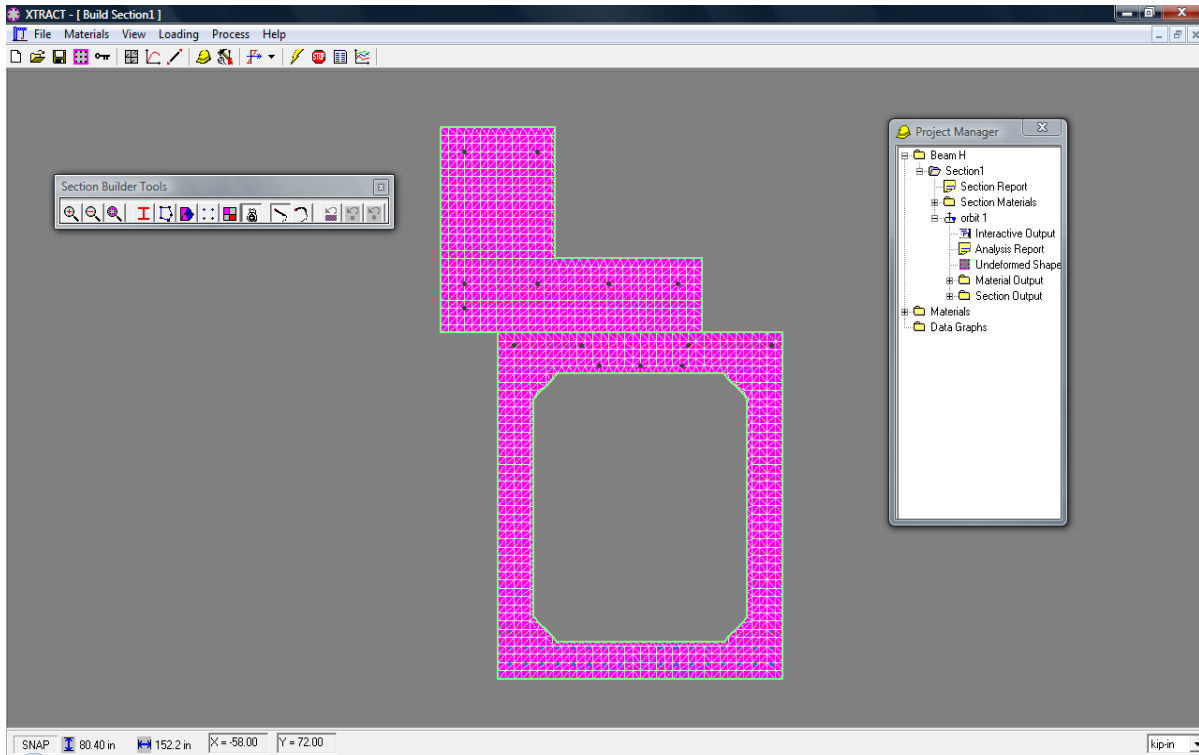
Figure 3-4 XTRACT screen capture showing Beam H.

(**a**) concrete material model.   (**b**) prestressing steel material model.   (**c**) mild steel material model.
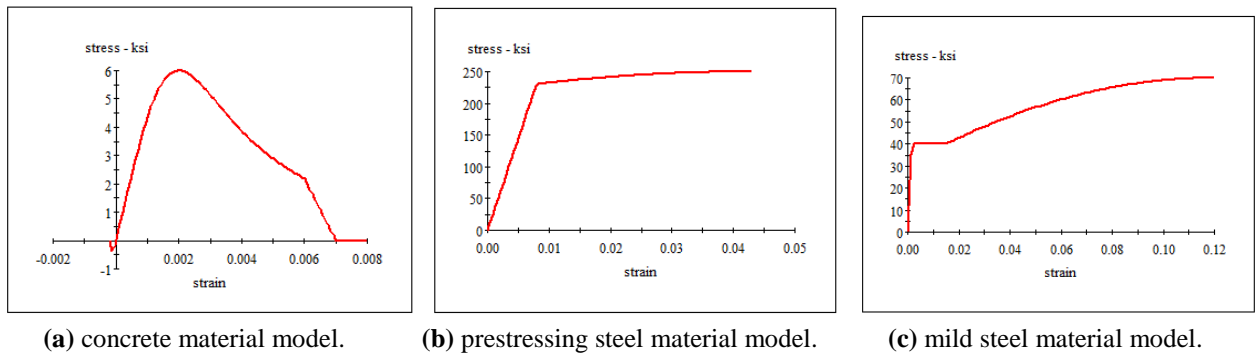
Figure 3-5 Material models used in XTRACT analyses.

(a) Beam D case 0-0-0.　　　　　　　　　　　**(b)** Beam D case 8-8-1.
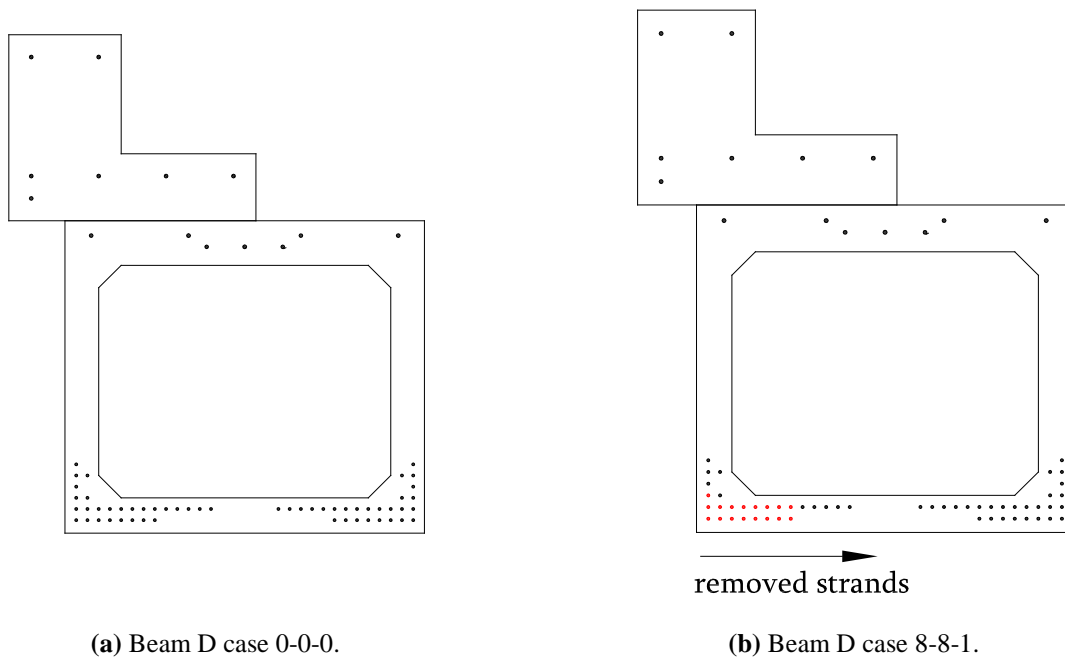
Figure 3-6 Example of damage classification.
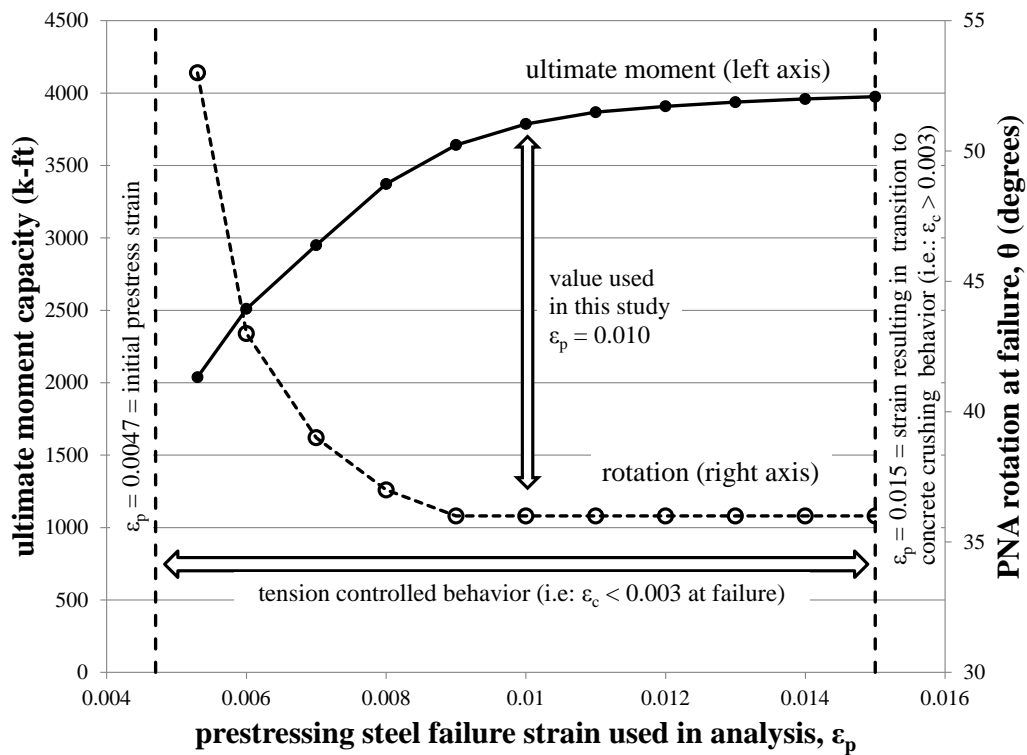
Figure 3-7 Verification of steel failure strain criteria.
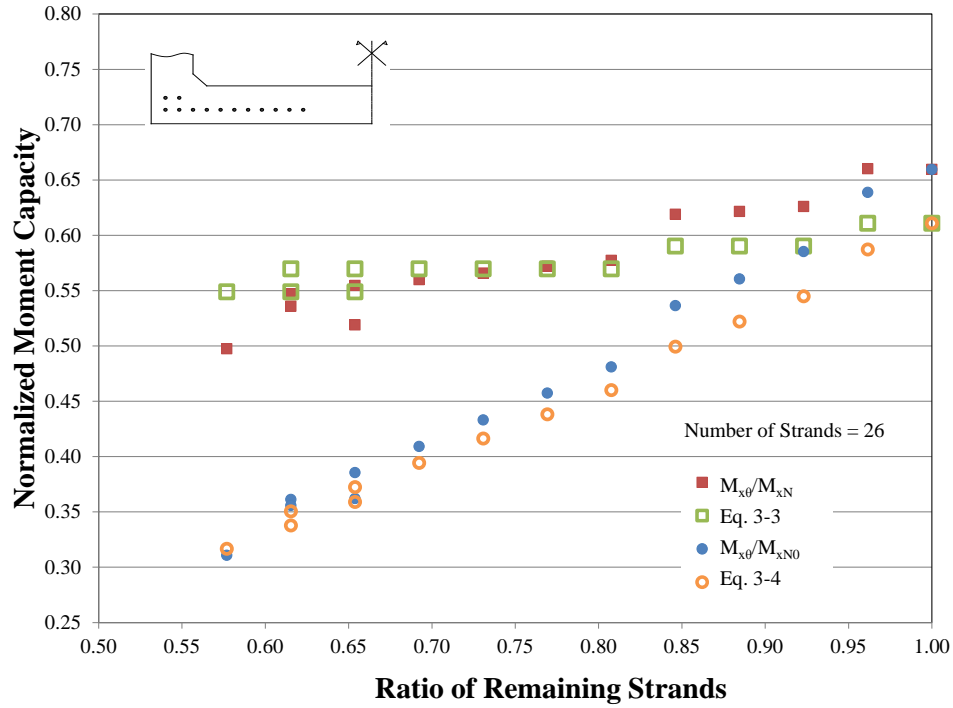
Figure 3-8 Normalized moment capacity vs. number of removed strands – Beam A.
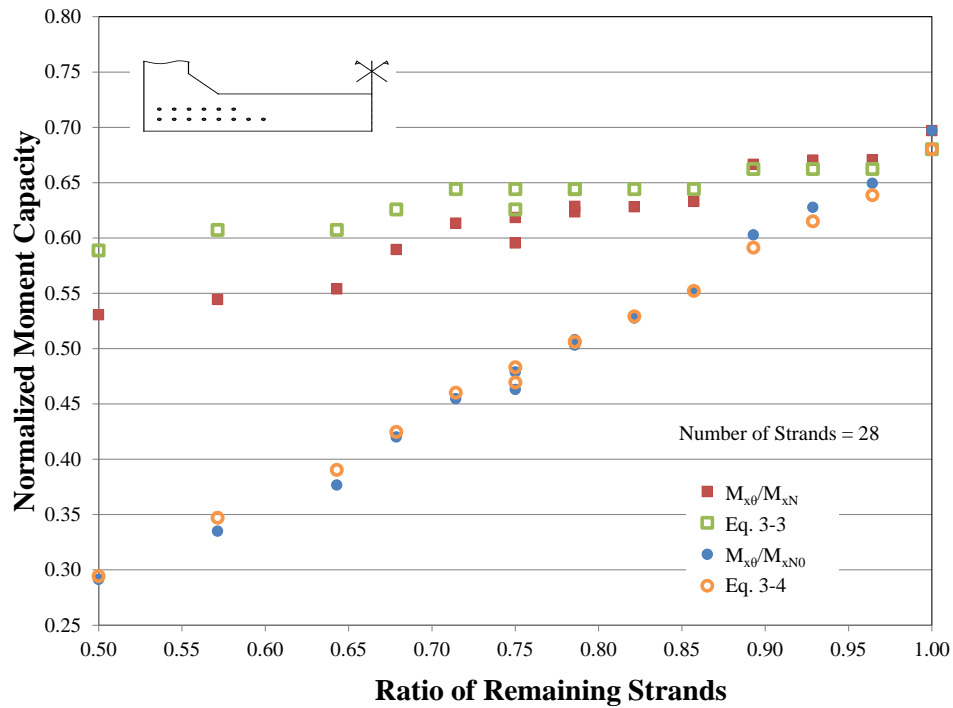
Figure 3-9 Normalized moment capacity vs. number of removed strands – Beam B.
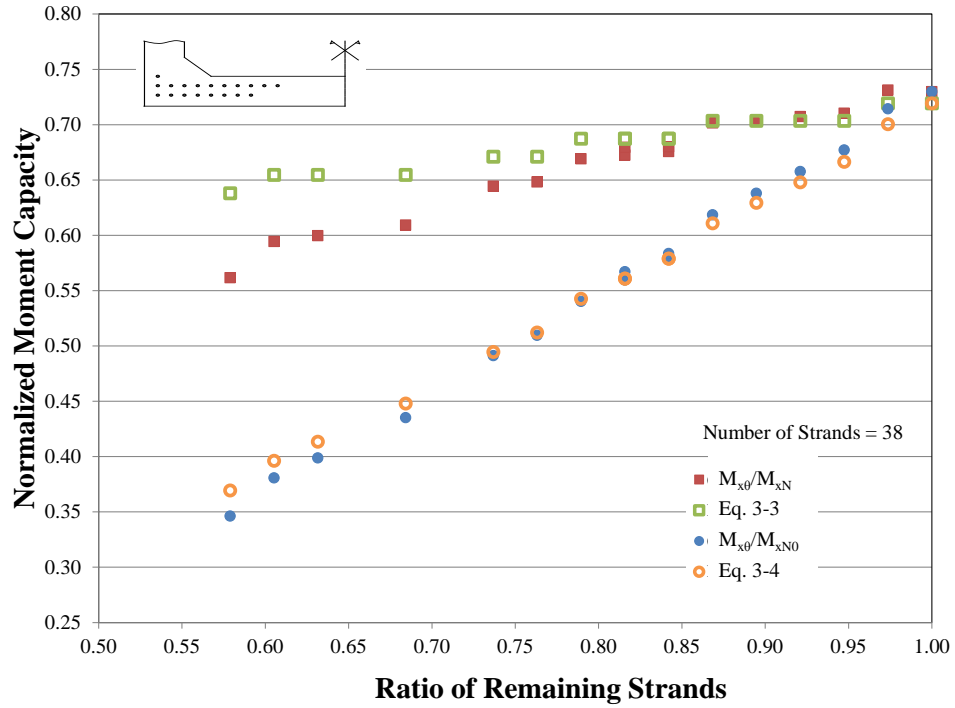
Figure 3-10 Normalized moment capacity vs. number of removed strands – Beam C.
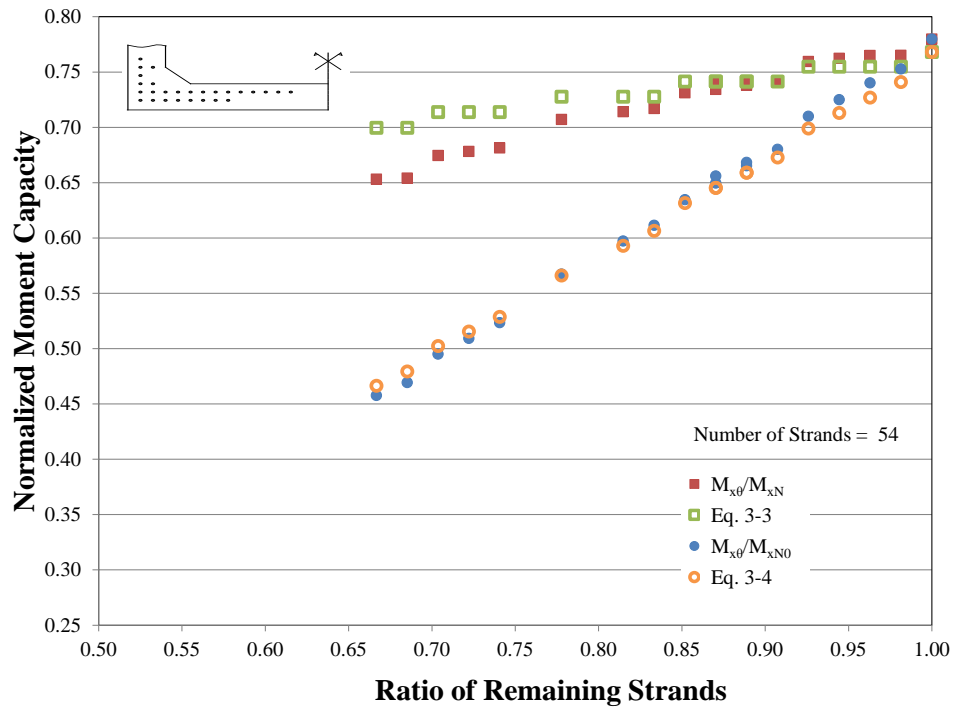
Figure 3-11 Normalized moment capacity vs. number of removed strands – Beam D.
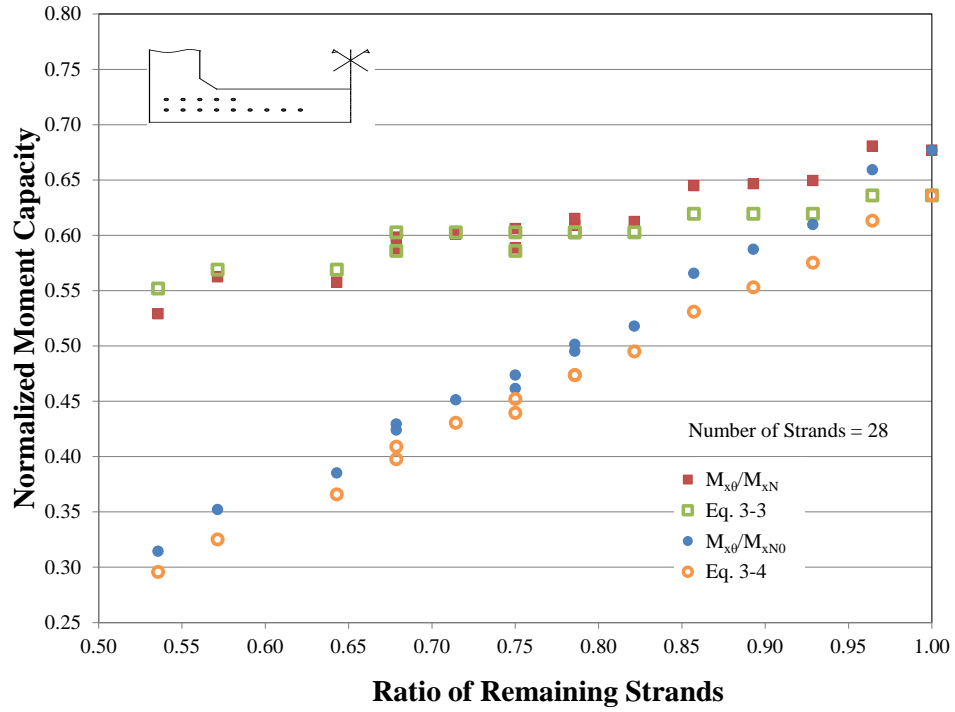
Figure 3-12 Normalized moment capacity vs. number of removed strands – Beam E.
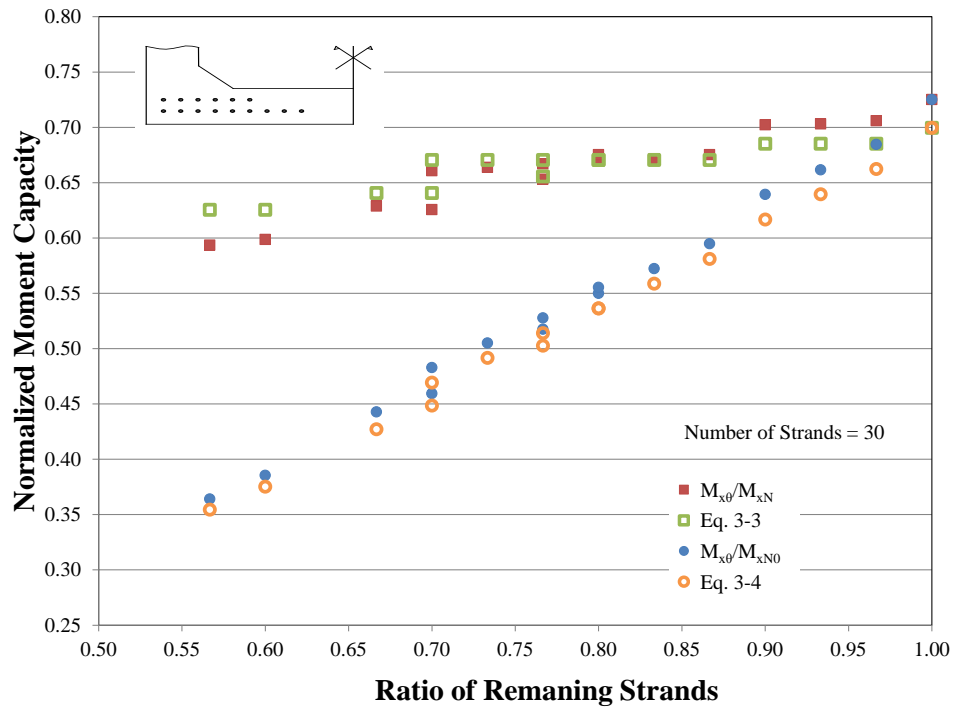
Figure 3-13 Normalized moment capacity vs. number of removed strands – Beam F.

78
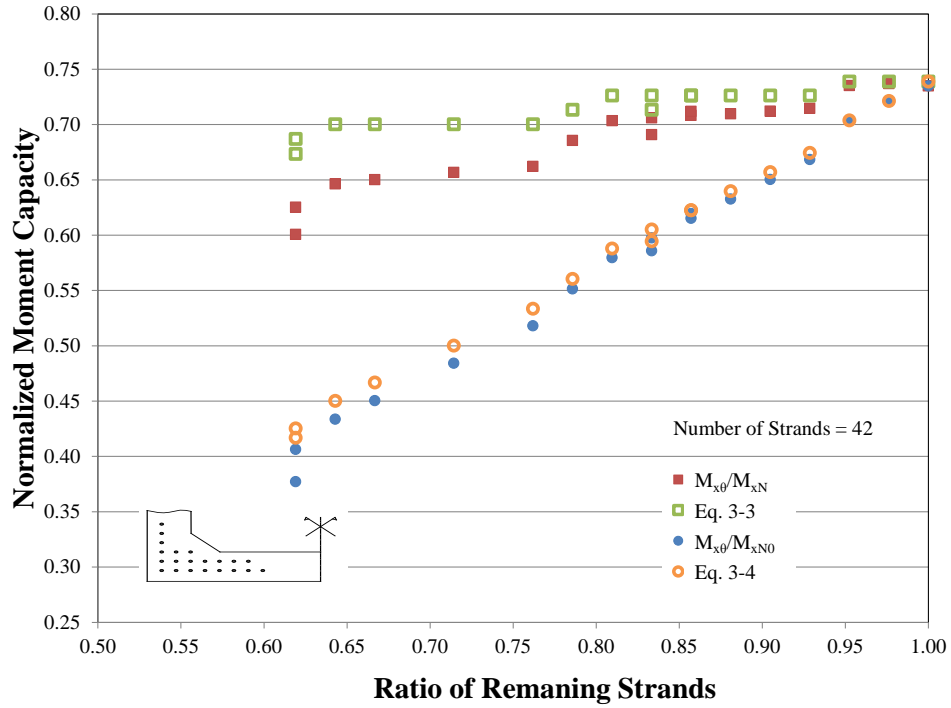
Figure 3-14 Normalized moment capacity vs. number of removed strands – Beam G.
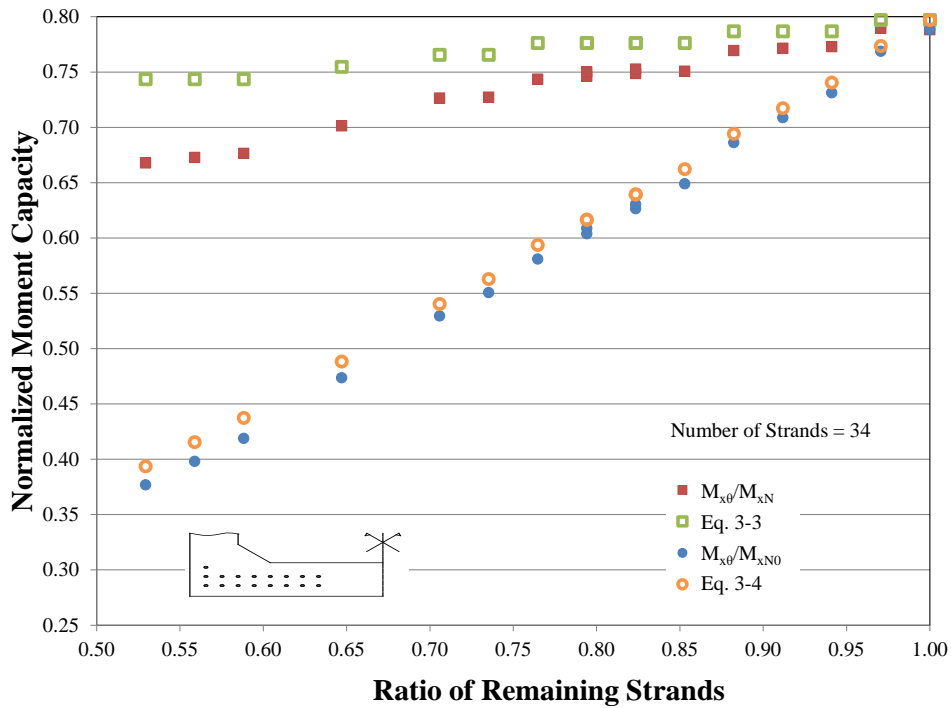
Figure 3-15 Normalized moment capacity vs. number of removed strands – Beam H.
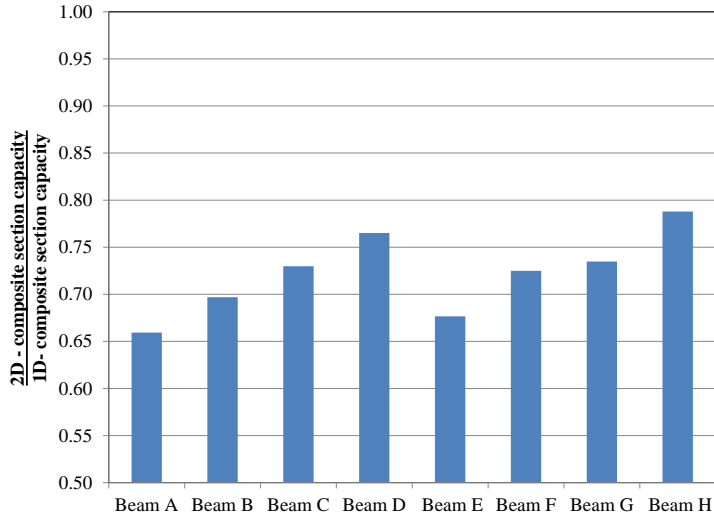
a) ratio capacity of girder with composite barrier wall analyzed considering neutral axis rotation (2D) versus that considering an analysis about the horizontal axis.
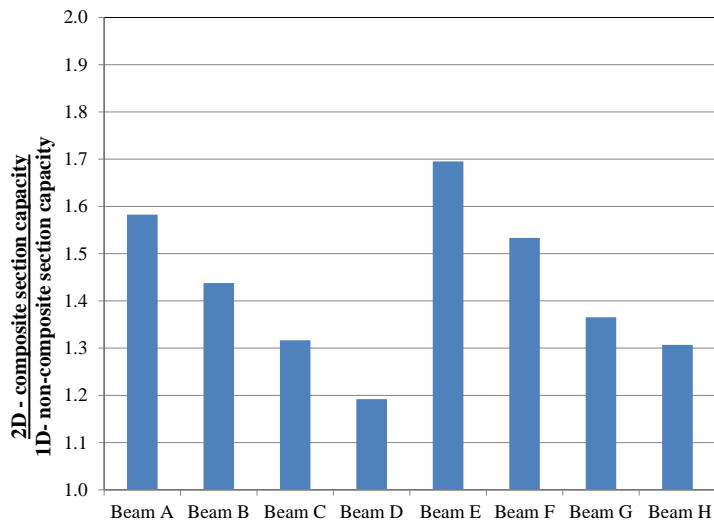
b) ratio of 2D composite barrier wall girder capacity to non composite capacity.
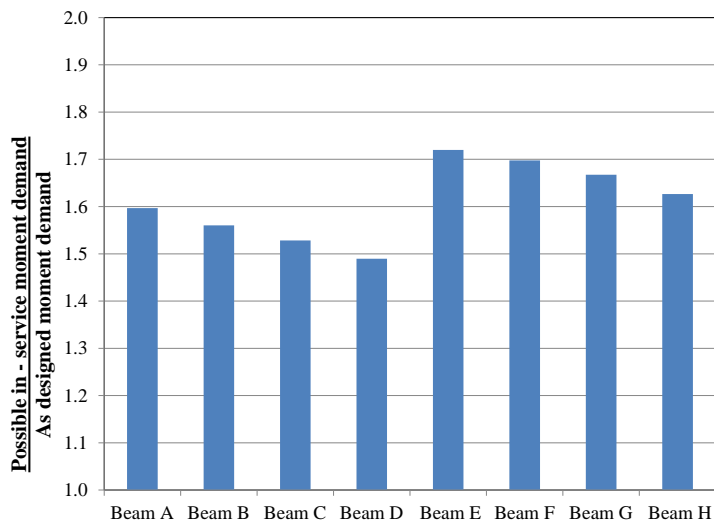
c) ratio of potential nominal load on exterior girder to nominal design load.

Figure 3-16 Capacity ratios of undamaged prototype girders.

80
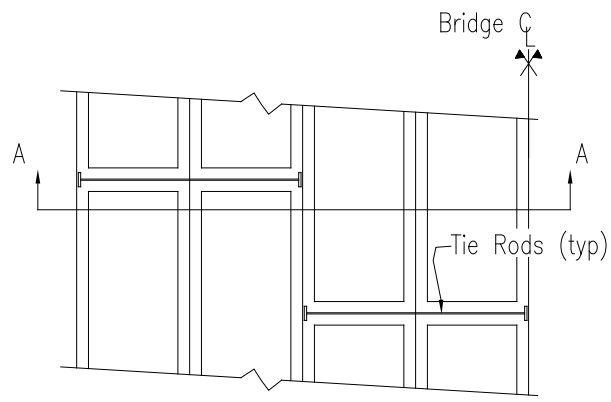
a) Plan View
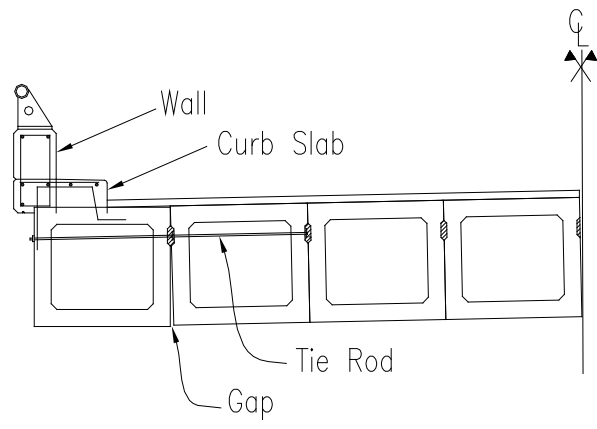
b) Section AA

Figure 3-17 Lake View Drive bridge – a typical AB girder span.

4.0 ASSESSMENT OF DAMAGED PRESTRESSED ADJACENT BOX GIRDER BRIDGES: A CASE STUDY

Recent failures of prestressed AB girder bridges – some catastrophic and others requiring posting, emergency repair measures or decommissioning – have demonstrated that this bridge type has some inherent weaknesses. This Chapter describes an approach to assessing the extant condition of damaged ABs, including those damaged by vehicle impact and corrosion. The approach described allows for the 'redevelopment' of damaged strand once it is re-established in sound concrete (described in Chapter 2) and includes the need to consider biaxial section analysis to account for significant geometric asymmetry in exterior AB girders (described in Chapter 3).The objective of this work is to discuss the implementation and, ultimately validity of more rigorous assessment techniques that account for these effects. This chapter presents the analytical assessment of a damaged exterior AB girder recovered from the decommissioned Lake View Drive bridge which partially collapsed in 2005 (Figure 3-2). Harries (2006 and 2009) report this collapse and the subsequent load testing of additional girders from the Lake View Drive structure. It was found that the ultimate capacity and behavior of this damaged 40-year old exterior AB girder was accurately predicted using the combination of multiple biaxial section analyses over the length of the member, validating the proposed assessment techniques.

4.1   DAMAGE ASSESSMENT

Visual indicators, particularly longitudinal cracking, impact damage, and exposed, corroded or severed strands identified during bridge inspection provide information vital to the condition assessment of a PC bridge. The inclusion of such damage in subsequent analyses and load rating is critical to capturing expected in-service member behavior. The following 'lessons learned' are provided to assist in the assessment of existing, damaged AB girder bridges.

4.1.1   Longitudinal Cracking

Longitudinal cracking of the soffit typically indicates strand corrosion although it is also associated with vehicle impact damage to exterior girders (Feldman et al. 1996). In either case, the lower strand layer at the location of longitudinal cracking should not be considered to contribute to girder capacity in the load rating procedure since bond of this strand has been compromised. Additional investigation of the extent of spalling in the transverse direction should be performed to determine whether adjacent strands are affected.

4.1.2   Exposed or Corroded Strands and Strand Redevelopment

As discussed in Chapter 2, exposed strands, which may or may not be corroded or severed, are typically removed from the member analysis along the entire girder length. It has been shown that severed strands will 'redevelop' their capacity and indeed maintain their prestress force in sound concrete at a distance from the damage. This redevelopment of prestressing force is conservatively represented by the prescribed strand transfer length of 60 strand diameters. Thus

in a best-case scenario, away from the damaged region, the strand retains its prestress force; in a worst-case scenario, the strand remains 'developed' in which case it still contributes to the ultimate capacity of the section as non-prestressed reinforcement.

4.1.3   125% Rule

In areas of the soffit of AB girders having concrete spalling (often resulting from impact damage) and subsequent corrosion of the lowest layer of strands, some unobservable corrosion of the second layer of strands is likely. Naito et al. (2006) report this unobserved corrosion to be 25% of strand area in addition to that of the observed damaged strands. Rigorous field investigation, including chipping away cover concrete adjacent to corroded regions to identify all potentially corroded strands is required since significant corrosion may occur prior to spalling. Additionally, minor corrosion of the second layer of strands may be expected to continue and accelerate, raising the extent of unobserved damage in girders where little or no remedial action is taken. With these issues in mind, a conservative estimate of the total strand area affected by corrosion is suggested to be taken as 50% of the strand area in addition to that of the observed damaged strands (PennDOT 2010).

4.1.4   Analysis of Eccentrically Loaded Girders

Chapter 3 discussed the issues associated with 1D- and 2D-analyses of exterior AB girders which behave compositely with the barrier wall and curb slab assembly. Particularly, the overestimation of the vertical moment capacity (M_x, about the horizontal axis) of the 1D analysis and the biaxial

behavior of an asymmetric section loaded about its non-principal axis must be accounted for appropriately in the analysis.

4.2   CASE STUDY SPECIMEN

A 90'- 2" ft. (27.5 m) long, 48 in. (1220 mm) wide by 42 in. (1067 mm) deep exterior AB girder with 60 - 3/8" (9 mm) diameter Grade 250 (1724 MPa) low-lax strands was analyzed in this study. Cross section details and strand labeling are provided in Figures 4-1a and 1b, respectively. The girder was recovered from the decommissioned Lake View Drive bridge (Figure 3-2) and was tested to failure as part of the investigation of that collapse (Figure 3-3 and Harries 2009). Prior to testing, a rigorous inspection was carried out to identify all damage locations and affected strands. Damage was classified by its location along the girder, description and the specific strands affected as shown in Table 4-1 and Figure 4-2a. This information will be used to assemble a series of plane-sections analyses along the beam length.

4.3   EXPERIMENTAL RESULTS

The exterior AB girder was subjected to a monotonically increasing vertical load over a test span of 84'-2" (25.6 m). The load, located at midspan, was spaced at 48 in. (1220 mm), representing a typical AASHTO (2010) tandem axle arrangement. The highly asymmetric section subject to a symmetric load (Figure 3-3a) exhibited significant out of plane deformation (Figure 3-3c) accompanying and coupled to the in-plane flexural deformation (Figure 3-3b). As testing

progressed, the out-of-plane flexural deformation was approximately 35% of the in-plane flexural deformation as shown in Figure 3-3d. As a result, the observed failure included significant crushing of both the barrier wall and AB girder immediately beneath this but not on the girder top flange across from the barrier wall (interior corner). Additionally, monitoring of strand ruptures clearly indicated an asymmetric ultimate behavior (Harries 2006). The ultimate capacity of the girder was observed at an applied axle load of 73.4 kips (326.5 kN) (total tandem load of 146.8 kips (653 kN)). Including the self-weight of the girder, this corresponds to a midspan moment of approximately 4285 k-ft (5810 kNm). As shown in Figure 4-2c, however, failure of the beam did not occur in the initially undamaged midspan constant moment region but rather corresponded to the locations of initial girder damage at locations D and G (see Table 4-1 and Figure 4-2a).

4.4   MODELLING THE AB GIRDER

The undamaged girder cross section and all damaged sections (see Figure 4-1a and Table 4-1) were analyzed using a commercially available fiber sectional analysis software package XTRACT (Chadwell and Imbsen 2004). As described in Chapter 3, this software has a tool referred to as an 'orbit analysis' which calculates the M_x-M_y failure envelope for a user-specified failure criteria by rotating the assumed orientation of the principal axis through 360°. From this envelope, the vertical (gravity) load carrying capacity, $M_{x\theta}$, is determined for the section. In essence this is a 'trial and error' approach where the orientation of the principal axis is varied until the external equilibrium (i.e.: $M_y = 0$, in this case) is satisfied.

Material properties are modeled as indicated in Section 3.2.3 to 3.2.5. Concrete properties were modeled after compression strength values determined from the test girder (Harries 2006). Girders of this vintage utilized Grade 250 (1724 MPa) strand and Grade 40 (276 MPa) mild steel reinforcement, hence their use in this study. All strands were assumed to be initially stressed to $0.70f_{pu}$ (175 ksi = 1207 MPa) and to retain $0.55f_{pu}$ after all losses (based on the AASHTO 2010 prestress loss calculations), resulting in a prestress of 137.5 ksi (948 MPa). This assumption is consistent with the *in situ* results obtained from another Lake View Drive girder described in Chapter 2.

4.4.1 Model Material Properties and Criteria for Establishing Moment-Moment Failure Envelope

As described in Section 3.2.7, specific material failure criteria must be provided to establish the moment-moment (M_x-M_y) failure envelope. In essence, these criteria are 'allowable strains' or 'performance criteria' which no fiber in the section may exceed and are selected based on the limit state being investigated. In the present analysis, the ultimate capacity of the under-reinforced (i.e.: section response controlled by steel) PC box girder is desired, thus criteria related to the ultimate capacity were selected. The concrete and prestressing strand values were selected to represent concrete crushing ($\varepsilon_{cF} = 0.005$) and a strand strain ($\varepsilon_{pF} = 0.015$) sufficient to develop the ultimate capacity of the strand (250 ksi = 1724 MPa; see Figure 2-7) while respecting the under-reinforced nature of the member. The mild steel strain was selected to be very high ($\varepsilon_{sF} = 0.035$) so as not to affect the outcome of the analysis. The goal of this work is to assess the effectiveness of the assessment approach to quantify the experimentally observed ultimate capacity of this girder. In this case, no conservativism is considered and failure criteria

representing significant plastic deformations are selected. If the girder were being assessed for *in situ* load rating or evaluation for repair, lower 'failure' strains would be used as done in Chapter 3.

4.5   ASSESSMENT RESULTS AND DISCUSSION

Sections analyses were performed at each damaged section (Table 4-1) and for the undamaged section. These were then 'stitched together' over the length of the girder accounting for the effects of strand redevelopment as the damaged regions transition to undamaged. The required redevelopment length was taken as $60d_b = 22.5$ in. (572 mm) in every case and the transition was assumed to be linear as shown in Figure 2-3. These analyses result in the moment capacity envelopes shown in Figure 4-2b. Both 1D and 2D analyses were conducted. The significant reduction in predicted capacity when the more rigorous 2D analysis is used is clear from Figure 4-2b. In this case, the predicted capacity from a 2D analysis is approximately 78% of that from the more conventional 1D analysis.

The pre-test inspection was extensive. Thus each 1D and 2D analysis was conducted considering only the observed damage (Table 4-1). Additional analyses were conducted to investigate the effect of applying the 125% rule (with the rigorous inspection conducted, 150% was considered needlessly conservative). The effect of applying this rule is relatively minor for the case of this relatively undamaged girder: the greatest observed strand loss was only 6 strands (of 60) at location G (contrast this to over 30 strands lost in the collapsed exterior girder shown in Figure 3-2 (Harries 2006)).

Overlaid on the moment capacity envelopes shown in Figure 4-2b are the moment demand curves resulting from loading the girder. The moment demand curve for the observed ultimate capacity of a 73.4 kip (326.5 kN) axle load just intersects the '2D- 125% strand removed' capacity at stations 30.8 and 48.2 ft. (9.4 and 14.7 m). The observed failure, shown in Figure 4-2c is remarkably consistent with this prediction (for ease of presentation each of figures 4-2a, b and c are drawn to the same horizontal scale).

The effect of accounting for strand redevelopment is clearly validated by the results shown in Figure 4-2b. Current practice of assuming that a damaged or corroded strand is removed from the analysis of the girder altogether, would have resulted in as many as 15 (of 60) strands being removed from this girder for assessment (Table 4-1). By accounting for strand redevelopment, a more rational capacity envelope is generated. In addition a more exact prediction of behavior – locating failure along the beam span – becomes possible.

The agreement between observed and predicted behaviors additionally confirms that the barrier wall assembly is in fact behaving in a composite manner with the box girder. For the damaged prototype girder considered, if the barrier wall were not present, the girder capacity would be approximately 75% of that predicted with the composite barrier wall. Care must be taken in interpreting this result however. The composite barrier wall increases the girder capacity but also results in an asymmetric section which reduces the apparent 1D capacity. Damage both further reduces the 1D capacity but also may increase the asymmetry, compounding the reduction in capacity. Finally, other factors such as degraded shear connections between adjacent girders (Harries 2009) may significantly increase the demand placed on exterior AB girders.

4.6   CONCLUSIONS

The ultimate capacity and behavior of a damaged 40-year old exterior AB girder was accurately predicted using multiple biaxial section analyses over the length of the member. The approach demonstrated accounts for geometric asymmetry resulting from the presence of a composite barrier wall and observed asymmetric strand loss. The application of the 125% rule in considering the reduction in prestressing strand area in damaged regions is also demonstrated and shown to be appropriate for the case where a rigorous inspection of damage was carried out. Finally, the appropriateness of the allowing for 'redevelopment' of damaged strand once it is re-established in sound concrete is demonstrated.

Table 4-1 Summary of girder damage.

Damage Location (see Figure 4-2a)	Affected Region (stationing from west end of girder, ft)	Damage Description	Affected Strands
A	15 - 16.5	Longitudinal crack	A12
B	@ 20	Shallow spall	none
C	@ 24	Minor impact	A1
D	25 - 31	Major impact	A1, B1, C1, D1 and A2
E	31 - 32	Exposed strands, corrosion	A2, A3, A4, A5, A6
F	@ 45	Minor impact	A1
G	48 - 55	Impact, spall and exposed and corroded strands	A8, A9, A10, A11, A12 and A13
H	68 - 61	Longitudinal crack	A1
J	61 - 64	Shallow spall	none

1 ft. = 305mm
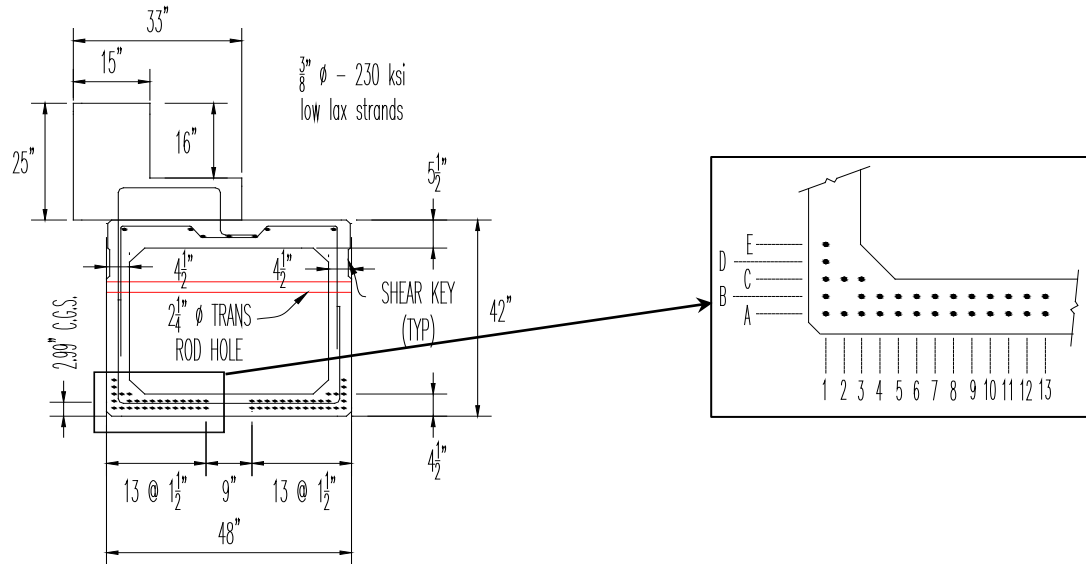
a) Cross section (dimensions in in. unless noted)   b) Strand labelling

Figure 4-1 Test girder cross section.

impact damage at D   damage at E   impact damage at F   damage at G   spalling at J
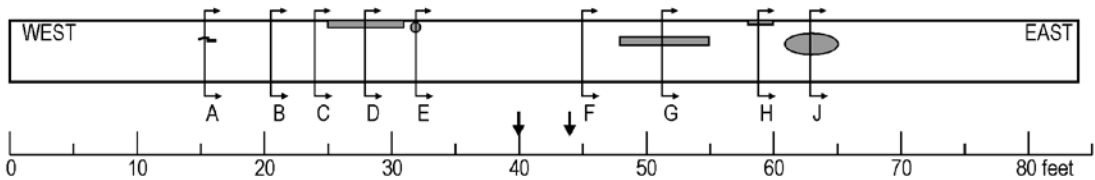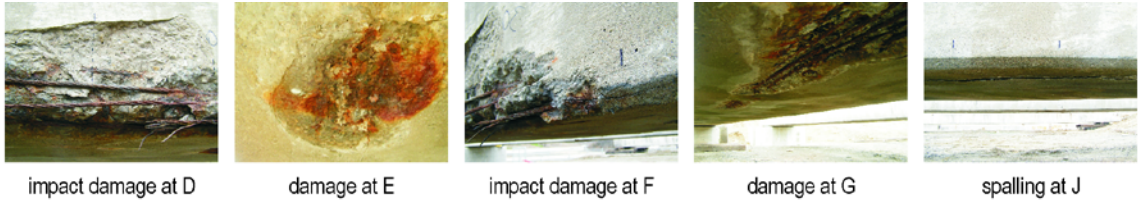
a) inverted plan showing damage locations along beam soffit
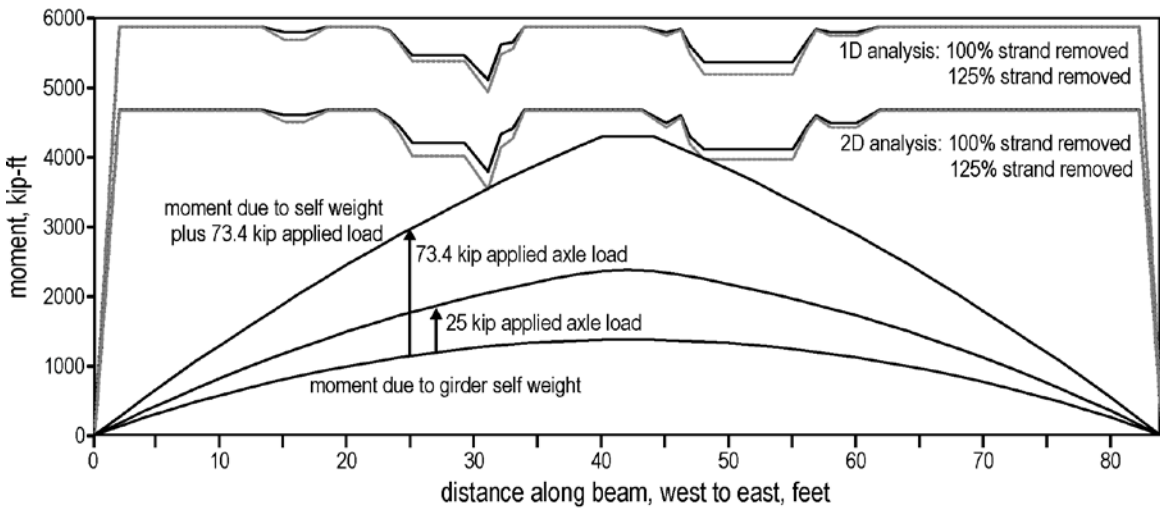
b) moment capacity calculated using 1D and 2D approaches
and moment curves due to applied loading
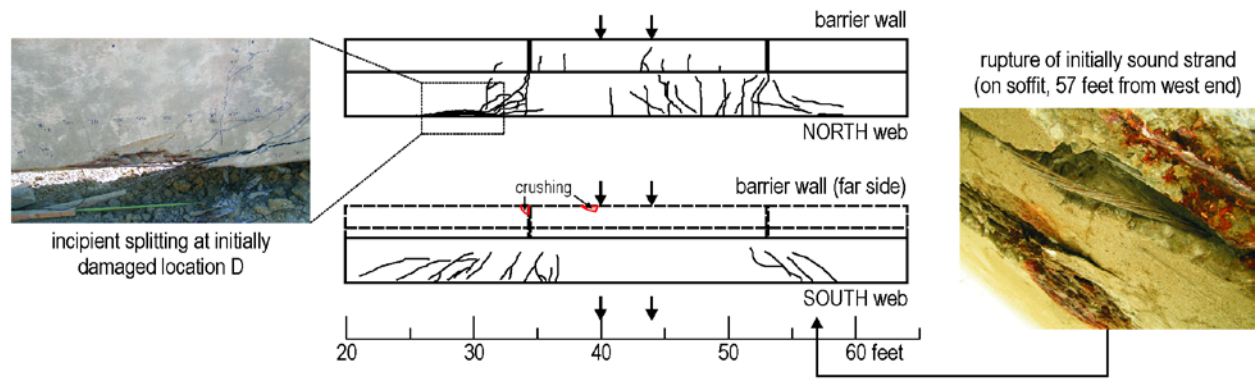
c) observed crack patterns at applied load, P = 73.4 kips

Figure 4-2 AB test girder initial damage and experimental and predicted behavior.

93

5.0   DETERMINATION OF REPAIR LIMITATIONS

Due to the significant number of vehicle impacts of prestressed concrete (PC) girders, the bridge engineering community has increased repair efforts. As a result, new repair methods and technologies (i.e.: strand splices and applications of fiber reinforced polymers (FRP)) have emerged. The use of these new repair technologies has benefitted the bridge industry by increasing the number of structures which can be repaired as opposed to being replaced or posted. Examples of such bridge repairs are presented by Tumialan et al. (2001), Schiebel et al. (2001), Klaiber et al. (2003), Herman (2005), Toenjes (2005), Kim et al. (2008), Sika (2008a), Kasan (2009), Enchayan (2010), Pakrashi et al. (2010) and Yang et al. (2011), among others. Despite these demonstrations, little attention has been paid to the selection of appropriate repair measures and the limitations of these; this is often referred to as the 'repair or replace?' question. The objective the work presented in this Chapter is to develop a methodology to approaching repair design aimed at providing justification for the solution of the 'repair or replace' question. This Chapter will present the approach to identifying repair limitations through an example of an impact-damaged AB girder bridge structure repaired with externally bonded carbon fiber reinforced polymer (EB-CFRP) plates. Additionally, a discussion regarding approaches to individual girder rating is provided due to the localized nature of impact damage where few girders of a bridge are typically affected. A portion of this discussion also acknowledges

acceptable structure postings. An illustrative example including all necessary steps and calculations is described in the following sections and presented in its entirety in Appendix A.

5.1   PROTOTYPE STRUCTURE

An 81'-2" (24.75 m) long, 48 in. wide by 42 in. deep (1220 mm by 1067 mm) precast concrete (PC) adjacent box (AB) girder is considered in this study (when composite with the deck, the overall girder depth is 45 in. (1143 mm)). The prototype girder was an exterior girder recovered from a decommissioned AB girder bridge in southwestern Pennsylvania (Figure 5-1a). The bridge was erected in 1960. Impact damage (approximately 45 in. long) is evident centered approximately 28 ft. from the girder end (see Figure 5-1b) at a location above the right lane of the carriageway passing beneath the bridge. The primary prestressing consists of 57 - 3/8" (9 mm) diameter Grade 250 (1724 MPa) low-relaxation (low-lax) strands. Cross section details of the girder are provided in Figure 5-2. Although an exterior girder, tests were conducted without a barrier wall or curb. Additional information regarding the original design of the structure can be found in the bridge cross section shown in Figure 5-3.

Damage classification and naming proceeded similar to that discussed in Section 3.2.6 and as shown in Figure 3-6. Recall, the damage multi-digit identification of each analysis indicates the number of strands removed from the lower, second, third layers, et cetera, respectively. The example provided in Appendix A describes the section AB 3-2-0 wherein 3 strands were removed from the first layer, 2 from the second and none from the third.

5.1.1 Modeling the Prototype Girder

The example in Appendix A was completed using member capacities calculated using either AASHTO- or ACI-prescribed analysis methods. In subsequent analyses, in order to rapidly analyze the girders at various damage levels, the undamaged girder cross section and all damaged and repaired sections were analyzed using a commercially available non-linear fiber sectional analysis software package XTRACT (Chadwell and Imbsen 2004). Modeling using XTRACT is discussed at length in Chapter 3. Only moment-curvature analyses are utilized for this work.

Material properties are modeled as indicated in Table 5-1. Concrete properties were modeled after design strength values of the prototype AB girder (American Marietta 1960). Girders of this vintage utilized Grade 250 strand and Grade 40 mild steel reinforcement, hence their use in this study. All strands were assumed to be initially stressed to $0.7f_{pu}$ (175 ksi) and to retain $0.57f_{pu}$ after all losses (based on the AASHTO 2010 prestress loss calculations), resulting in a prestress of 142.4 ksi. CFRP material and geometric properties are based on manufacturer's data for Sika CarboDur strips (preformed CFRP strips) (Sika 2008b) and can also be found in Table 5-1. These properties were used for convenience; the use of Sika products is not specifically endorsed in this document.

5.2 IDENTIFICATION OF THE CRITICAL SECTION FOR MOMENT

When performing a load rating analysis, ratings are based on the maximum moment demand for a particular structure; this includes the dead load of the structure (i.e. beams, diaphragms,

96

wearing surface, etc.), a 640 plf lane load (per AASHTO 2010 design specifications) and a design truck placed on the structure in a location to maximize its effect (near the center of the span for simply supported members). Conventional engineering assessment proceeds by neglecting the damaged strands in the section analysis and structure rating. In this instance of a simply supported girder, the maximum moment demand will occur when placing the truck near midspan[1]. This configuration will also often govern structural ratings. However, when rating a damaged girder where strand redevelopment is permitted (as discussed in Chapter 2), it is important to recognize the location of damage in the context of the entire structure. If damage were located elsewhere along the span, this additional potentially critical section must be investigated despite it not representing the greatest absolute demand across the span. A simple influence line approach can be used to establish the moment envelope at any location along the span. Recognizing and accounting for this effect allows the structure to be analyzed in a more rational fashion by identifying all critical section. Doing so will inform the appropriateness of the selected repair technique as well as provide a more accurate structural assessment and rating. For instance, damage may be located outside of the critical moment region and thus it is possible that a flexural repair may not be necessary.

A set of analyses was performed using the prototype girder to determine the design moment at various locations along the length of the girder. This approach requires the truck load to be located at different locations along the span to cause the maximum moment at these locations. For example, the moment demand at 30% of the span (0.3L) includes all dead load

---

[1] The location of the AASHTO HL93 vehicle to result in maximum on a simple span is such that the second axle is located 2.33 feet from the girder midspan and the third axle is on the other side of midspan; for ease of description, this is referred to as the midspan location.

effects and also locates the design truck at this location which ultimately provides the greatest moment demand at this location. The resulting moment envelope is shown in Figure 5-4. This concept is more easily visualized by considering the 'reserve' capacity: the difference between girder capacity and moment demand at any section. Figure 5-4 plots reserve capacity over the length of the girder for the undamaged AB section. All values shown in Figures 5.4 and 5.5 are factored with appropriate AASHTO load and resistance factors. It is noted that the prototype structure considered is considerably over designed – the girder capacity, even at its lowest (midspan) is almost twice the load demand. This is not uncommon for an exterior girder which will generally have lower demand than adjacent interior girders. In AB bridges, as in most simple span bridges, to reduce cost and complexity, all girders in a structure will be the same; thus exterior girders often have significant reserve capacity or over-strength.

Typically in PC girders, the moment capacity is uniform along the girder length (outside the development length). However, including the redevelopment of severed/exposed strands, away from the damage location, in the capacity analysis results in a moment capacity which varies along the length of the member (as seen in Figure 5-4). When including the damage in the analysis of the damaged prototype girder AB 3-2-0 (Appendix A), the reserve capacity along the girder length can be seen in Figure 5-4. It is important to notice in Figure 5-4 that the reserve capacity at approximately 0.35L location (location of damage) is less than that at midspan (0.5L). This effect is considerably more dramatic for increased levels of damage as can be seen for the case of AB 6-5-2-2 also shown in Figure 5.5. Therefore, when considering this girder for structural rating and repair, the critical section is at the location of damage and not midspan. The identification of the critical section of a damaged member must be determined based on design truck location and section capacity and should not be assumed to be midspan (which remains the

98

location of the greatest absolute moment demand), as illustrated in the example. Utilizing this approach should also be accompanied by the consideration of strand redevelopment (as described in Chapter 2), thus developing an accurate assessment of anticipated girder performance.

Other effects that may impact the reserve capacity include general deterioration of the girder which would have the effect of uniformly reducing girder capacity (Figure 5.4) and therefore the reserve capacity (shifting the curve in Figure 5.5 downward). Similarly, the loss of an effective shear key, as discussed in Section 3.4.4.2, will increase the live load component of the moment by approximately 67% (Figure 5.4) and therefore also reduce the reserve capacity essentially uniformly (Figure 5.5).

It should be noted that the conventional approach to assessing damaged girders is to simply assume a) the damage extends over the entire span; that is: the critical section in terms of capacity is the damaged section; and b) the demand is the greatest demand on the span; that is: the critical section in terms of demand is at midspan. This approach, while conservative , is inconsistent and inefficient, resulting in unnecessary girder replacement rather than repair in many cases.

5.3   IDENTIFICATION OF REPAIR LIMITATIONS

Limitations on what repairs are viable and the degree to which girder capacity may be recovered are inherent to each girder type and repair technique. Often, controlling factors can be identified with each repair technology and an upper bound on the effectiveness (contribution to capacity recovery) of the repair technology can be determined. Physical constraints such as girder size and shape and structure type also limit the use or efficiency of repair methods. In either case, the

'law of diminishing returns' in terms of repair efficiency is often observed as the repair effort is increased; this too informs the designer of a rational limit to the repair technology considered. Determination of these limitations ultimately informs the 'repair or replace' decision for damaged PC bridge girders.

Limitations pertaining to design and physical constraints will be discussed in the following sections, referencing the example in Appendix A, to develop an approach to answering the 'repair or replace' question. Therefore, the following sections will specifically consider 48 in. (1220 mm) wide AB girders repaired with EB-CFRP. Using a similar approach, determining limitations for other girder shapes and repair technologies will be developed further in the NCHRP 20-07 report.

5.3.1   Repair Material

Controlling factors can be identified with each repair technology and thus an upper bound of the contribution of the repair technology is determined. Beyond geometric constrains (discussed in Section 5.3.2), constraints can also be identified in the repair design methodology, as is the case for EB-CFRP. In *most* EB-CFRP repairs, CFRP debonding strain controls the repair design (Step 16 of the example). In bonded FRP-to-concrete applications, 'bond' refers to the entire FRP-adhesive-concrete interface. Debonding occurs when the strain generated in the FRP-adhesive-concrete interface exceeds its capacity and the FRP disconnects from the concrete substrate. CFRP is the most suitable FRP for structural strengthening in the parlance of this study due to its strength and stiffness properties and thus changing material is not considered. The existing

concrete substrate material cannot be modified significantly for a repair design[2]. Therefore, the only parameter which can be altered is the nature of the CFRP. In practice, particularly for bridge spans where disruption of traffic on and below the bridge are significant concerns or environmental considerations are an issue below the bridge, preformed CFRP strips are preferred to a wet lay-up CFRP application. In such a case, the preformed strips are available in only discrete sections. In this study, strips having nominal dimensions of 2 x 0.047 in. (50 x 1.2 mm) are used; these are the most readily commercially available products in North America. Thus, the only remaining design parameter is the number of layers of CFRP used. Debonding strain is inversely proportional to the square root of the number of layers. In other words, the debonding strain decreases with the increase in the number of CFRP layers resulting in a diminished efficiency in strengthening with an increased the number of layers. This is not to suggest that the use of multiple layers is not possible, it simply does not utilize the CFRP material efficiently. Therefore, to inform the limitations of this repair method in the context of the 'repair or replace' decision, EB-CFRP will typically be limited to one layer.

5.3.2   Geometry

When repairing a structure, the physical constraints regarding structure type and girder size must be considered. For AB bridge repairs employing EB-CFRPs, repairs are limited to the girder soffit only. For the AB structure in the example, the beam soffit is 48 in. wide. Even if the girder

---

[2] The design presented in Appendix A, like most such examples, assumes a sound concrete substrate or sound concrete patches restoring the original profile of the section.

web were accessible, placing CFRP on the girder web causes the centroid of the repair material to approach the neutral axis of the member, thus decreasing the lever arm and therefore utility of the web-applied CFRP. The geometric constraint limits the bonding of CFRP to the girder soffit for AB bridge structures; thus for the example girder, a maximum of 24-2 in. wide CFRP strips may be applied.

5.4   APPROACHES TO GIRDER RATING AND STRUCTURAL POSTING

AASHTO *Evaluation Manual* (2011) Eq. 6A.4.2.1-1 provides the basis for AASHTO girder rating factor, RF:

$$RF = \frac{C - \gamma_{DC}DC - \gamma_{DW}DW \pm \gamma_{P}P}{\gamma_{LL}(LL + IM)}$$
(Eq. 5-1)

Where C is the structural capacity, DC, DW, LL and IM are load effects prescribed in the AASHTO *LRFD Bridge Design Specifications* (2010), and the values of γ are LRFD load factors prescribed in Table 6A.4.2.2 of the *Evaluation Manual* (2011). These factors differ for inventory and operational rating levels. The term P represents the effects of other permanent loads on the structure and, for convenience, is neglected in the subsequent discussion.

Application of Eq. 5-1 requires an entire bridge design in all cases. Since the objective of this work is to address the degree of strengthening of individual girder elements, a variation of this equation was developed. If it assumed that the capacity of the as-built girder corresponds exactly to $RF_0 = 1$; that is: $C_0 = \gamma_{DC}DC + \gamma_{DW}DW + \gamma_{LL}(LL+IM)$, and the existing or damaged capacity is C_D, then the rating factor for the damaged structure is:

$$RF_D = \frac{C_D - \gamma_{DC}DC - \gamma_{DW}DW}{C_0 - \gamma_{DC}DC - \gamma_{DW}DW}$$
(Eq. 5-2)

Therefore analyses are effectively normalized by the AASHTO-prescribed inventory RF value (Eq. 5-1). Thus, the normalized undamaged girder rating factor $RF_0 = 1.0$ as shown in Table 5-2, showing the results of the rating exercise for the AB 3-2-0 prototype example presented in Appendix A. This formulation removes the need to calculate LL, which is a function of specific bridge geometry. If RF for the as-built structure is known (RF_0), then the C_0 term in Equation 2 may be replaced with RF_0C_0. In either case, ratings may proceed since the focus of the study is to consider the capacity of the repaired girder (C_R) relative to C_D and a target capacity C_0 (or another specified capacity). A rating factor less than unity based on Equation 5-2 does not necessarily imply structural deficiency as is the case when a rating factor less than unity is found from Equation 5-1. A value of less than unity from Eq. 5-2 simply indicates that the girder capacity is lower than the original design capacity. Thus, the decision to repair, replace or do nothing to an individual girder must still be made in the context of the entire structure.

It should be noted that the rating factors calculated in Table 5-2 use the appropriate dead load- and live load-demands according to the section being investigated. For the example in Appendix A, the critical section for the damaged structure is identified as the extreme location of damage, 0.375L or 30.3 ft. Therefore, the dead load and live load demands on the structure are determined for this location, as seen in Steps 1 and 3. However, after performing the repair, the rating factors are compared to those calculated at all other sections. As seen in Table 5-2, $RF_D =$ 2.24 at the critical location and the rating factor at 0.5L remains 2.32. Therefore, in order to restore the girders original capacity, this damage must be repaired. After performing the repair, $RF_R = 2.60$ at 0.375L. In comparing rating factors at the repaired section and 0.5L, the critical section for the repaired girder is once again at 0.5L and the rating factor for the structure are those calculated in Step 8.

This study adopts the 'repair objective' of restoring the original girder capacity, C_0; that is ensuring that $C_R \geq C_0$ or $RF_R \geq 1.0$. Different objectives are certainly possible and a repair that does not restore the original girder capacity may be acceptable, particularly if there is a great deal of overstrength (reserve capacity) in the first place. This decision must, however, be made on a case-by-case basis. Additionally, in many instances, posting the structure is acceptable and thus this option needs to be acknowledged. Regardless of the goal of the repair (undamaged capacity or an acceptable posting level), the approach to girder repair discusses here remains valid.

5.5   APPLICABILITY OF EB-CFRP REPAIRS TO AB PROTOTYPE GIRDER

To illustrate the approach described in previous sections and to assess the viability of using externally-bonded CFRP (EB-CFRP) to repair impact damaged adjacent box girders (AB), a parametric study, of sorts, was carried out.

Using the prototype example described in Section 5.1 and presented in Appendix A, a range of damage was considered. Twelve damage cases ranging from AB 3-2-0 (9% strand loss), presented in Appendix A, to AB 6-5-2-2 (26% strand loss) were considered. All analyses were conducted using XTRACT as described in Section 5.1.1. Using the fiber analysis method of XTRACT is more rigorous than the AASHTO or ACI-prescribed plane sections analysis presented in Appendix A. The difference in results is marginal; the XTRACT-derived values are about 2% greater than those based on code approaches as is shown in Table 5-2 for AB 3-2-0. Finally, all assessments were carried considering only the damaged girder; thus the rating factor derived from Eq. 5-2 was used.

As described in Section 5.3, the practical limit of the EB-CFRP repair considered is 24 2 in. wide strips. To illustrate the range of repair possible - and therefore to identify the range of repair objectives possible - four degrees of repair were considered corresponding to 25, 50, 75 and 100% of the greatest practical repair. Thus all damaged beams were assessed for their repair capacity assuming 6, 12, 18 and 24 2 in. EB-CFRP strips. Including the damaged, unrepaired girders, 65 ratings were carried out. The results of these ratings are presented in Table 5-3 in terms of both the member critical moment capacity and the resulting rating factor (Eq. 5-2).

The resulting damaged and repaired rating factors are shown graphically in Figure 5-4. In this figure, each vertical line represents a damage case. The lowest data point on each line is the rating factor for the unrepaired damaged girder, RF_D. The highest data point is the rating factor for the repair having 24-2 in. EB-CFRP strips - the maximum practical repair. Data points for each of the repairs having 6, 12 and 18 EB-CFRP strips are also shown.

A number of conclusions can be drawn from Figure 5-4 (recognizing that this is presented for 48 x 45 in. AB girders):

Considering the AB 3-2-0 example presented in Appendix A, the damaged rating factor $RF_D = 0.88$. The repair design (Appendix A) having the objective of restoring the original girder capacity ($RF_R \geq 1.0$) concluded that 15 – 2 in. EB-CFRP strips are sufficient to restore undamaged capacity, resulting in a repaired rating factor of 1.05. Maximizing the repair, using 24 EB-CFRP strips, the capacity of the repaired girder could be increased well above the original capacity to a rating factor $RF_R = 1.20$.

At the other end of the spectrum, AB 6-5-2-2 has a damaged rating factor of $RF_D = 0.65$ and its capacity cannot be fully restored even with the maximum practical EB-CFRP strips applied. In this case, the maximum repaired $RF_R = 0.97$.

Assuming the predefined objective of the 'repair or replace' question was that the repair must restore the original capacity of the girder, AB 6-5-2-2 could not be repaired and would require replacement. Interestingly, this conclusion is consistent with a rule-of-thumb used for prestressed girder repair: a girder must be replaced if strand loss exceeds 25% (Washington State DOT, reported in Kasan 2009).

Using an approach such as that presented in Figure 5-4, defining the required repair as a horizontal line at the desired capacity ($RF_R = 1.0$ was used here), one can quickly establish repair or replace criteria based on viable repairs (that may also be defined differently than done here) that fall above this line.

The same approach may also be calibrated using Eq. 5-1 although separating individual girder damage from global bridge performance is rather complex. The nature of repairable vehicle impact damage most often only affects exterior girders which raises a third alternative to the repair/replace decision. Exterior girders may simply be removed (physically or lane restricted so that they are not loaded) from the bridge altogether without affecting the load capacity of this bridge. Such an approach clearly, however, affects the traffic-carrying capacity of the span.

Plots similar to that shown in Figure 5-4 can be created for various girder types and repair technologies to illustrate the decision making criterion for the 'repair or replace' decision and will be completed in support of NCHRP 20-07.

5.6 CONCLUSIONS

A new methodology to approaching PC bridge girder repair is presented. First and foremost, when accepting strand redevelopment, it is imperative for the repair designer to identify the critical section, which may or may not be midspan. Often, the damaged section, with the design truck placed over the location of the damage is the controlling section. Next, a repair technology can be selected. Realistic and practical limitations can be identified for specific girder shapes and repair technologies. Often, girder geometry will limit the viable repair techniques. Limitations are also inherent to repair technologies. For example, for the AB girder repaired with EB-CFRP plates example discussed here, CFRP debonding controlled the repair design. Increasing the number of layers of CFRP yields diminishing returns, suggesting that it is not practical to use more than one-layer of CFRP. Equally significant, applying the CFRP to the web of the girder decreases the lever arm and uses the material inefficiently (as compared to bonding to the girder soffit). As a result, the upper bound that can be affected by EB-CFRP plates for an AB girder repair becomes apparent; it is limited to one-layer of CFRP bonded across the entire girder soffit.

For the AB 3-2-0 example presented in Appendix A, only 15 EB-CFRP strips were required to restore the original girder capacity. However, if more severe damage were considered (AB 6-5-2-2), a practical repair (24 EB-CFRP strips) would be inadequate to restore the original girder capacity and the repaired structure may require posting. A posting may be acceptable to the owner and thus this is not necessarily a shortcoming of the repair technique. Ultimately, each structure must be assessed individually and the goal of each repair must be clearly expressed. The objective of the repair is easily expressed as a target value of RF_R in Eq. 5-2. This approach also allows for easy comparison of the effectiveness of various repair types. In some instances, the damage location or the damage severity may yield an RF_D which is greater than RF_0 for the

undamaged structure. This suggests that the damage does not need to be structurally repaired; however, corrosion mitigation and patching and painting practices (as suggested in Kasan 2009) should be followed to arrest further corrosion and damage. Following this methodology, the lower bound of an effective structural repair for the member can be determined. This lower bound solution is to only repair the girder aesthetics (patching and painting) and take preventative measures to mitigate further damage. Lower bound solutions do not include structural repair measures.

The approach to girder repair described in this Chapter is significantly different than most conventional practice. A new paradigm to select and evaluate and identify the 'upper-bound' contribution of girder repair technologies has been provided and illustrated through an AB girder repaired with EB-CFRP plates. Employing this approach will benefit repair designers and state transportation agencies by providing rational criterion for the selection and application of repair technologies.

Table 5-1 Modeled Material Properties.

	Concrete	Grade 250 Prestressing Steel	Grade 40 A615 Reinforcing Steel	CFRP
modulus of elasticity	E_c = 4,227 ksi	E_p = 28,500 ksi	E_s = 28,500 ksi	E_f = 23,200 ksi
tensile yield strength	-	f_{py} = 230 ksi	f_y = 40 ksi	-
tensile ultimate stress	-	f_{pu} = 250 ksi	f_u = 70 ksi	f_f = 406 ksi
tensile ultimate strain	-	ε_{pu} = 0.0430	ε_{su} = 0.1200	ε_f = 0.017
strain hardening strain	-	-	ε_{sh} = 0.0150	-
compressive strength	f_c' = 5.5 ksi	-	-	-
strain at fc'	ε_c = 0.0028	-	-	-
crushing strain	ε_{cu} = 0.0060	-	-	-
spalling strain	ε_{sp} = 0.0070	-	-	-
ultimate compressive strain (f_c = 0)	ε_{cmax} = 0.0080	-	-	-
failure criteria used in analysis	ε_{cF} = 0.003	ε_{pF} = 0.015	ε_{sF} = 0.035	ε_{fF} = 0.0059

Table 5-2 Comparison of Rating Factor Calculation Methods for AB 3-2-0 presented in Appendix A.

	M_n (kft)	AB320 M_{DAM} (kft)	EB-CFRP 15 strips M_R (kft)	Inventory RF_0	RF_D	RF_R	Operating RF_0	RF_D	RF_R
Conventional[1] (AASHTO/ACI) at 0.5L	3511	3218	3562	2.32	2.32	2.32	3.01	3.01	3.01
Conventional[1] (AASHTO/ACI) at 0.375L				2.55	2.24	2.60	3.31	2.91	3.37
XTRACT fiber analysis[2] at 0.5L	3573	3275	3698	1.00	1.00	1.00	1.30	1.30	1.30
XTRACT fiber analysis[2] at 0.375L				1.00	0.88	1.05	1.30	1.14	1.36

[1]Equation 5-1.
[2]Equation 5-2.

Table 5-3 Capacity and Inventory Rating Factor for EB-CFRP Repaired AB Girders.

	AB Damage Case												
	320	420	422	530	4222	631	641	42222	6322	652	752	6522	65222
strand loss	9%	10%	14%	14%	18%	18%	19%	21%	23%	23%	25%	26%	30%
C_R (kft)	3275	3213	3102	3090	2899	2972	2913	2998	2811	2795	2731	2689	2586
RF_R	0.88	0.86	0.81	0.81	0.73	0.76	0.74	0.77	0.70	0.69	0.66	0.65	0.59
EB-CFRP 6 strips	3316	3253	3142	3132	2937	3015	2956	3039	2854	2840	2777	2734	2633
	0.90	0.87	0.83	0.82	0.75	0.78	0.75	0.79	0.71	0.71	0.68	0.66	0.61
EB-CFRP 12 strips	3571	3511	3398	3388	3193	3270	3210	3293	3111	3096	3033	2988	2888
	1.00	0.98	0.93	0.93	0.85	0.88	0.85	0.89	0.82	0.81	0.78	0.77	0.72
EB-CFRP 18 strips	3826	3764	3653	3640	3445	3526	3465	3546	3363	3350	3288	3243	3143
	1.10	1.08	1.03	1.03	0.95	0.98	0.96	0.99	0.92	0.91	0.89	0.87	0.82
EB-CFRP 24 strips	4080	4018	3907	3894	3698	3780	3719	3799	3618	3604	3543	3498	3395
	1.20	1.18	1.13	1.13	1.05	1.08	1.06	1.09	1.02	1.01	0.99	0.97	0.93

C_0=3573kft; RF_0=1.0

a) prototype girder *in situ*(photo from PennDOT inspection report dated August 8, 2007).

b) impact damage location, considered in the Appendix A example.

Figure 5-1 Prototype AB Girder.
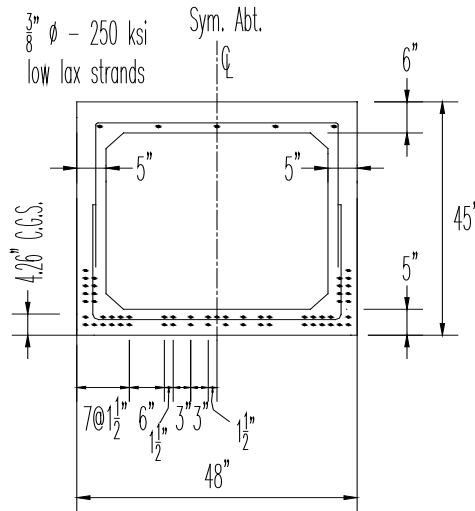
Figure 5-2 Prototype AB Girder Cross Section.
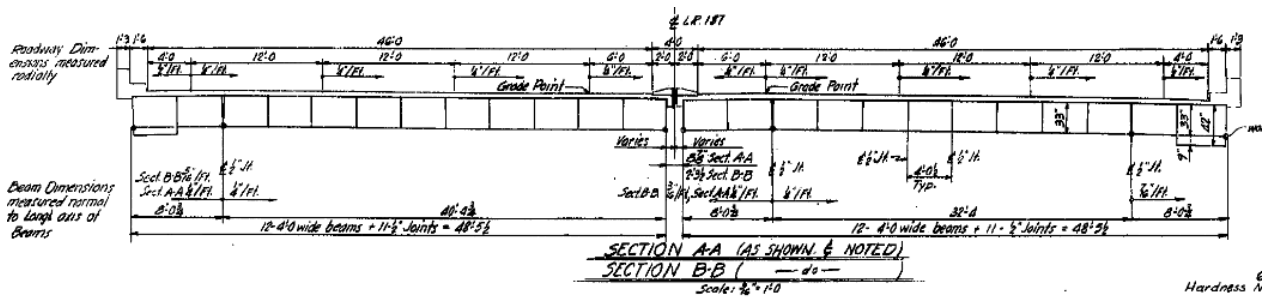
Figure 5-3 Prototype AB Bridge Cross Section.

110
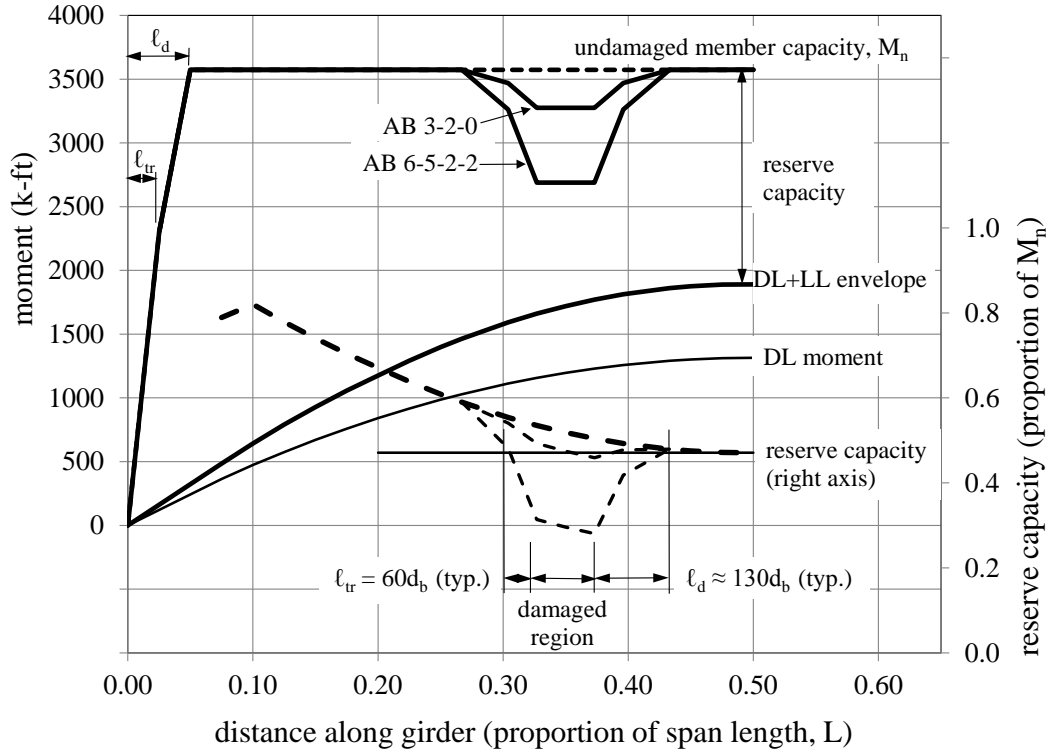
Figure 5-4 Girder Moment Envelopes.
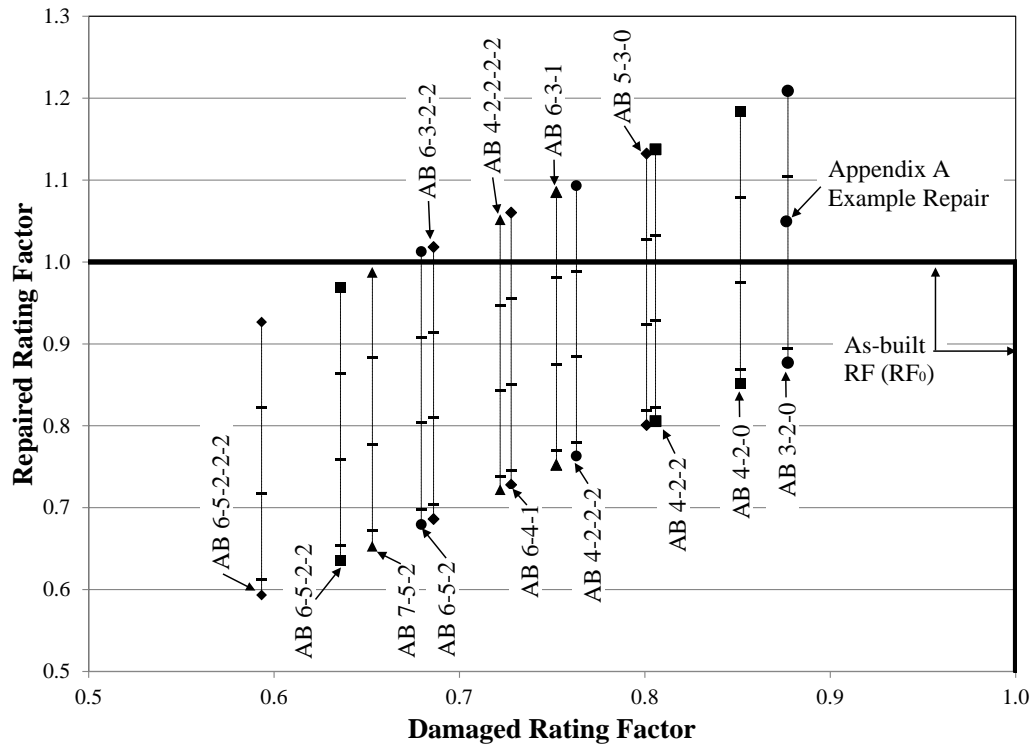
Figure 5-5 Repaired versus Damaged Rating Factor Plot.

111

6.0 CONCLUSIONS AND FUTURE WORK

An overview of the conclusions and findings from each aspect of this dissertation are reiterated here. Additionally, topics identified which require further investigation beyond this work are noted in Section 6.2.

6.1.1 Redevelopment length

The findings of this study demonstrate that severing prestressing strand is a 'local effect'. That is, the effects of the lost strand affect the section at the damage location. To either side of the damaged concrete region, the effective prestress in the strand is 'redeveloped' over the transfer length, ℓ_{tr}. This approach implies the need to consider not only the critical section of a girder but all sections along its length when rating the girder or designing repair measures for a damaged girder (Harries et al. 2009).

6.1.2   Eccentrically Loaded Girder Analysis

A parametric study which analyzed the effects of varying levels of damage to eight prototype AB beams was conducted; in all, 106 analyses were carried out. The relationship proposed by Equation 3-4 represents the true behavior of the asymmetric members because both damage to the structure due to lost strands and the rotation of the neutral axis are accounted for. Additionally, this relationship is useful in assessing an existing structure since it is based on the original undamaged, 1D capacity; essentially the original design capacity.

It is common for the barrier wall and curb slab to be composite with the girder. This composite action will increase the moment capacity as compared to the original girder. However, additional loadings beyond those which the original member is intended to resist must also be considered, such as the entire dead load of the barrier wall and curb slab assembly is acting only on the exterior girder and additional live load demands resulting from ineffective shear keys. It is acceptable for the barrier wall and curb slab to be considered composite with the girder, however this new section will experience loadings different than the original member which must be accounted for in the analysis and rating of the member.

6.1.3   Assessment of a Damaged Prestressed Concrete Bridge Girder: Case study

The techniques described in Chapters 2 and 3 were used in an analysis to predict the failure of a damaged 40-year old exterior AB girder. The ultimate capacity and behavior of the AB girder was accurately predicted using multiple biaxial section analyses over the length of the member. The approach demonstrated accounts for geometric asymmetry resulting from the presence of a composite barrier wall and observed asymmetric strand loss. The application of the 125% rule in considering the reduction in prestressing strand area in damaged regions is also demonstrated and shown to be appropriate for the case where a rigorous inspection of damage was carried out. Finally, the appropriateness of the allowing for 'redevelopment' of damaged strand once it is re-established in sound concrete is demonstrated. This analysis demonstrated the applicability of the techniques described in Chapters 2 and 3 and compares analytical to experimental results of a full-scale girder. The analytical results matched the experimental results to a considerable degree and thus confirming their validity.

6.1.4   Determination of Repair Limitations

A new methodology to approaching prestressed concrete bridge girder repair is presented. First, when accepting strand redevelopment (Chapter 2), it is imperative for the repair designer to identify the critical section, which may or may not be midspan. Often, the damaged section, with the design truck placed over the location of the damage is the controlling section. In some instances, the damage location or the damage severity may yield a rating factor (RF_D) which is greater than that for the undamaged structure (RF_0). This suggests that the damage does not need

to be structurally repaired; however, corrosion mitigation and patching and painting practices should be followed to arrest further corrosion and damage. Additionally, the lower bound of an effective structural repair for the member can be determined. This lower bound is the 'do nothing' solution to the 'repair or replace' question addressing impact-damaged girders.

Realistic and practical limitations can be identified for specific girder shapes and repair technologies, which in turn, dictate the applicable repair technology. For the EB-CFRP AB 3-2-0 example, the limitations of this repair technique are: a) complete utilization of girder soffit; and b) limited to one layer on CFRP. Geometrically, the bridge type limits access to the webs. Additionally, application of FRP material to the webs decreases the lever-arm, in turn using the material less efficiently. Most EB-FRP repair designs are governed by plate debonding failures. The debonding strain of FRP is inversely proportional to the square root of the number of FRP layers. Therefore, these repairs were limited to one layer to retain good debonding behavior. The approach demonstrated in the example presented can assist in determining rational repair technique limitations based on member geometry and repair technology.

If the repair technology's contribution is maximized and the girder still does not acheive the original girder's capacity, a structure posting may be required. Posting may be acceptable to the owner and thus this is not necessarily a shortcoming of the repair technique. An expression was developed (Equation 5-2) to address a single girder rating factor (RF). This expression allows the designer to quickly 'rate' the effectiveness of the selected repair technique since it refers to the original girder capacity. This basis is useful in the context of impact damaged prestressed concrete bridge members by allowing for easy comparison of the effectiveness of different repair techniques. Conveniently, Equation 5-2 can be utilized with a target capacity

different than the original member capacity, thus allowing for the repair to be customized to the project needs.

6.2 TOPICS FOR FURTHER INVESTIGATION

6.2.1 Additional Considerations for Quantifying Redevelopment Length

Although not directly studied in this investigation, effects due to concrete material properties, concrete cover, strand diameter and *in situ* prestress force on transfer length of a 'redeveloped' severed strand can be significant and must be considered. A parametric study to quantify any of the effects listed here and their influence on the transfer length of a 'redeveloped' severed strand in the experimental investigation completed should be performed to quantify these effects.

6.2.2 Eccentrically Loaded Girder Analysis

The α factor presented in Eq. 3.5 is believed to be acceptable for adjacent box girder girders. However, more research is required to establish the α term for other girder geometries. It should be noted that the method presented in Chapter 3 can be utilized and adapted to determine this term and the corresponding capacity equation for other girder shapes. Additionally, an effort should be made to identify measures which can be taken to reduce or negate the eccentric loading effect on the exterior girder.

6.2.3 Prestressing Strand Assessment

The redevelopment length of severed prestressing strand experimental program also identified lower-than-expected values of prestress force in the sound strands. While not affecting ultimate capacity, this would be expected to affect serviceability of these girders. Beyond destructive tests similar to those conducted here, there is no practical method for assessing prestressing force *in situ*. However, it is recommended that prestressing loss calculations be revisited, including an experimental program to reevaluate the accuracy of code prescribed prestressing force loss calculations.

Although not specifically addressed in this study, non-destructive testing and similar evaluation techniques need to be advanced in order to quantify the extent of corrosion for prestressing strands, *in-situ*. Such information would allow for a more accurate assessment of *in-situ* members and greatly benefit repair designers.

6.2.4 Repair Technology Limitations

The approach to impact-damaged girder repair presented in Chapter 5 can be applied to other girder shapes and repair techniques, but however, is not specifically completed in this document. This is the goal of a study currently in progress (NCHRP 20-07) by teams at the University of Pittsburgh (Dr. Kent Harries and the author) and the University of Cincinnati. This work will expand upon the number of girder types and repair technologies investigated in similar fashion.

APPENDIX A

ADJACENT BOX GIRDER BRIDGE EXAMPLE

This example presents the capacity calculation, rating and subsequent repair methodology and

calculations for the impact damaged AB girder described in Section 5.1, repaired with externally

bonded CFRP. The example is intended to be illustrative rather than definitive.

GIVEN CONDITIONS

Span Length:	81 ft. simple span
Critical Section Location (see Section 5.2):	0.375L = 30.4 ft.
Year Built:	c1960
Concrete Compressive Strength:	f'_c = 5.5 ksi (P/S beam)
Prestressing Steel:	3/8 in. diameter, 250 ksi low-lax strands
Mild-reinforcing steel:	Grade 40
Number of beams:	12
Skew:	0 degrees
Damage Description:	Impact damage occured to the exterior girder and is 45 in. long and centered at 28.4 ft. from girder end. See Figure 5-2 for cross section details.

SECTION PROPERTIES		calculated from bridge drawings
48 in. x 42 in. adjacent box beams: A_{cg} = 742 in^2 I_x = 181,800 in^4 S_b = 9,619 in^3 S_t = 7,870 in^3	Composite Section Properties: $A_{cg,C}$ = 886 in^2 $I_{x,C}$ = 255,300 in^4 $S_{b,C}$ = 11,197 in^3 $S_{t,C}$ = 11,500 in^3	

STEP 1: DEAD LOAD ANALYSIS

Components and Attachment: DC (per girder)

$$\text{Beam Self Weight: } \left(\frac{742"}{144} \times 0.150 \right) = 0.773 \text{k/ft}$$

$$\text{Composite Deck Slab: } \left(\frac{3" \times 576"}{144} \times 0.150 \right) \frac{1}{12 \text{ girders}} = 0.150 \text{k/ft}$$

$$\text{Parapet (exterior): } \left(\left(\frac{42" \times 15"}{144} + \frac{16" \times 9"}{144} \right) \times 0.150 \right) \frac{1}{12} = 0.068 \text{k/ft}$$

$$\text{Parapet (center): } \left(\frac{0.5" \times 24" \times 8"}{144} \times 0.150 \right) \frac{1}{12} = 0.008 \text{k/ft}$$

$$\text{Total DC: } 0.999 \text{ k/ft}$$

Wearing Surface: DW (per girder)

$$\text{Asphalt thickness = 2 in.: } \left(\frac{2" \times 576"}{144} \times 0.144 \right) \frac{1}{12} = 0.096 \text{k/ft}$$

At 0.5L	**At 0.375L**
Moment due to DC:	Moment due to DC:
$M_{DC} = \dfrac{0.999 \times 81^2}{8} = 819.3 \text{ kft} \leftarrow$	$M_{DC} = \dfrac{0.999 \times 30.3 \times (81 - 30.3)}{2} = 767.3 \text{ kft} \leftarrow$
Moment due to DW:	Moment due to DW:
$M_{DW} = \dfrac{0.096 \times 81^2}{8} = 78.7 \text{ kft} \leftarrow$	$M_{DC} = \dfrac{0.096 \times 30.3 \times (81 - 30.3)}{2} = 73.7 \text{ kft} \leftarrow$

STEP 2: LIVE LOAD ANALYSIS Type F cross section; effective shear keys are present	LRFD T4.6.2.2.1-1
COMPUTE LIVE LOAD DISTRIBUTION FACTORS FOR INTERIOR GIRDERS *Compute Live Load Distribution Factors* $$N_b = 12$$ $$k = 2.5(N_b)^{-0.2} = 2.5(12)^{-0.2} = 1.52 \geq 1.5$$	LRFD T4.6.2.2.2b-1
For closed thin wall shapes: $$A_0 = \text{Area enclosed by the centerlines of elements}$$ $$A_0 = (48-2.5-2.5) \times (45-3-2.5) = 1698.5 \text{ in}^2$$ $$S = \text{length of a side element}$$ $$J = \frac{4A_0^2}{\sum \dfrac{s}{t}} = \frac{4 \times 1698.5^2}{\dfrac{(48-5)}{5} + \dfrac{(48-5)}{6} + \dfrac{2(45-3-2.5)}{5}} = 365{,}563 \text{ in}^4$$	LRFD C4.6.2.2.1-3
Distribution Factor for Moment – Interior Girders, g_{int} One Lane Loaded: $$g_{int,m1} = k\left(\frac{b}{33.3L}\right)^{0.5}\left(\frac{I_x}{J}\right)^{0.25} = 1.52\left(\frac{48}{33.3(81)}\right)^{0.5}\left(\frac{255{,}300}{365{,}563}\right)^{0.25} = 0.185$$ Two Lanes Loaded: $$g_{int,m2} = k\left(\frac{b}{305}\right)^{0.6}\left(\frac{b}{12L}\right)^{0.2}\left(\frac{I_x}{J}\right)^{0.06} = 1.52\left(\frac{48}{305}\right)^{0.6}\left(\frac{48}{12(81)}\right)^{0.2}\left(\frac{255{,}300}{365{,}563}\right)^{0.06} = 0.269$$ $$g_{int} = g_{int,m2} = 0.269 \leftarrow$$	LRFD T4.6.2.2.2b-1
Distribution Factor for Moment – Exterior Girders, g_{ext} One Lane Loaded: $$g_{ext,m1} = e \times g_{int,m1}$$ $$e = 1.125 + \frac{d_e}{30} = 1.125 \geq 1.0 \text{ with } d_e = 0$$ $$g_{ext,m1} = 1.125 \times 0.185 = 0.208$$ Two Lanes Loaded: $$e = 1.04 + \frac{d_e}{25} = 1.04 \geq 1.0$$ $$g_{ext,m2} = 1.04 \times 0.269 = 0.280$$ $$g_{ext} = g_{ext,m2} = 0.280 \leftarrow$$	LRFD T4.6.2.2.2d-1
STEP 3: MOMENT DEMAND	

STEP 3: MOMENT DEMAND		
Maximum Live Load (HL-93) Moment at 0.5L	*Maximum Live Load (HL-93) Moment at 0.375L*	
Design Lane Load = 525 kft Design Truck = 1169 kft Design Tandem = 962 kft IM = 33% M_{LL+IM} = LL + TRUCK*IM M_{LL+IM} =525 + 1.33 x 1169 = 2080 kft g x M_{LL+IM} = 0.280 x 2080 = 582.4 kft	Design Lane Load = 492 kft Design Truck = 1099 kft Design Tandem = 759 kft IM = 33% M_{LL+IM} = LL + TRUCK*IM M_{LL+IM} =492 + 1.33 x 1099 = 1954 kft g x M_{LL+IM} = 0.280 x 1954 = 547.1 kft	LRFD T3.6.2.1-1

STEP 4: COMPUTE NOMINAL FLEXURAL RESISTANCE $$f_{ps} = f_{pu}\left(1 - k\frac{c}{d_p}\right)$$ $f_{pu} = 250$ ksi and $k = 0.28$ for low lax strands d_p = distance from extreme compression fiber to C.G. of prestressing tendons original cg strands = 4.3 in; $d_p = 45 - 4.3 = 40.7$ in For rectangular section behavior: with $A_{ps} = 57 \times 0.08 = 4.56\text{in}^2$; $b = 48\text{in}$; $f_c^{'} = 5.5\text{ksi}$; and $\beta = 0.78$ Assume $A_s = A_s^{'} = 0\ \text{in}^2$. $$c = \frac{A_{ps}f_{ps} - A_s f_s - A_s^{'}f_s^{'}}{0.85f_c^{'}\beta_1 b + kA_{ps}\dfrac{f_{pu}}{d_p}} = \frac{4.56 \times 250 - 0}{0.85 \times 5.5 \times 0.78 \times 48 + 0.28 \times 4.56 \times \dfrac{250}{40.7}} = 6.23\text{in}$$ $a = \beta_1 c = 0.78 \times 6.23 = 4.9$ in < 6 in Therefore, rectangular section behavior assumption is valid $$f_{ps} = 250\left(1 - 0.28\frac{4.9}{40.7}\right) = 241.6\text{ksi}$$ $$M_n = A_{ps}f_{ps}\left(d_p - \frac{a}{2}\right) = 4.56 \times 241.6\left(40.7 - \frac{4.9}{2}\right) \times \frac{1}{12} = 3511\text{ kft}$$	LRFD Eq. 5.7.3.1.1-1 LRFD Eq. TC5.7.3.1.1 -1 LRFD 5.7.2.2 LRFD Eq. 5.7.3.1.1-4 LRFD Eq. 5.7.3.2.2-1

STEP 5: EFFECTIVE PRESTRESS

Determine Effective Prestress, P_{pe}**:**

$$P_{pe} = A_{ps} \text{ x } f_{pe}$$

Total Prestress Losses:

$$\Delta f_{pT} = \Delta f_{pES} + \Delta f_{pLT} \text{ immediately before transfer}$$

Effective Prestress:

f_{pe} = Initial Prestress – Total Prestress Losses

Loss Due to Elastic Shortening, Δf_{pES} :

$$\Delta f_{pES} = \frac{E_p}{E_{ct}} f_{gcp}$$

$$f_{gcp} = \frac{P_i}{A} + \frac{P_i e^2}{I} - \frac{M_D e}{I}$$

Initial Prestress immediately prior to transfer = $0.7f_{pu}$.
For estimating P_i immediately after transfer, use $0.90(0.7f_{pu})$.

$$P_i = 0.90 \text{ x } (0.7 \text{ x } 250) \text{ x } 57 \text{ x } 0.08 = 718.2 \text{ kips}$$

$A_{cg} = 742 \text{ in}^2;\quad I_x = 181,800 \text{ in}^4;\quad e = 22.8 - 4.3 = 18.5 \text{ in}$

M_D = moment due to self-weight of the member

$$M_D = \frac{0.773 \times 81^2}{8} = 634 \text{ kft}$$

$$f_{gcp} = \frac{718.2}{742} + \frac{718.2 \times 18.5^2}{181,800} - \frac{634 \times 12 \times 18.5}{181,800} = 0.968 + 1.352 - 0.774 = 1.546 \text{ksi}$$

$$K_1 = 1.0$$

$$w_c = 0.140 + 0.001f'_c = 0.140 + 0.001(5.5) = 0.146 \text{ kcf}$$

$$E_c = 33000 K_1 (w_c)^{1.5} \sqrt{f'_c} = 33000 \times 1.0 \times (0.146)^{1.5} \sqrt{5.5} = 4317 \text{ ksi}$$

$$E_p = 28,500 \text{ ksi}$$

$$\Delta f_{pES} = \frac{28,500}{4317} \times 1.546 = 10.2 \text{ksi} \leftarrow$$

	LRFD Eq.

LRFD Eq.
5.9.5.1-1

LRFD Eq.
5.9.5.2.3a-1

LRFD
T5.9.3-1
LRFD
C5.9.5.2.3a

LRFD
5.4.2.4
LRFD Eq.
5.4.2.4-1

Approximate Lump Sum Estimate of time-Dependent Losses, Δf_{pLT} :
Includes creep, shrinkage and relaxation of steel.

$$\Delta f_{pLT} = 10.0 + \frac{f_{pi} A_{ps}}{A_{cg,C}} \gamma_h \gamma_{st} + 12.0 \gamma_h \gamma_{st} + \Delta f_{pR}$$

with H = 70%; γ_h = 1.7-0.01H = 1.7 - 0.01(70) = 1.0

$$\gamma_{st} = \frac{5}{(1+f'_c)} = \frac{5}{(1+5.5)} = 0.77$$

Δf_{pR} = an estimate of relaxation loss = 2.5 ksi; f_{pi} = 0.70 x 250 = 175 ksi

$$\Delta f_{pLT} = 10.0 + \frac{175 \times 4.56}{886}(1.0)(0.77) + 12.0(1.0)(0.77) + 2.5 = 22.4 \text{ ksi}$$

Total Prestress Losses, Δf_{pT}**:**

$$\Delta f_{pT} = \Delta f_{pES} + \Delta f_{pLT} = 10.2 + 22.4 = 32.6 \text{ ksi} \leftarrow$$

LRFD
5.9.5.3-1

LRFD Eq.
5.9.5.3-2
LRFD Eq.
5.9.5.3-3

LRFD Fig.
5.9.5.1-1

STEP 6: MAXIMUM REINFORCEMENT The factored resistance (φ factor) of compression controlled sections shall be reduced in accordance with LRFD 5.5.4.2.1. This approach limits the capacity of over-reinforced (compression controlled) sections. The net tensile strain, ε_t, is the tensile strain at the nominal strength determined by strain compatibility using similar triangles. Given an allowable concrete strain of 0.003 and depth to the neutral axis c = 4.9 in. and a depth from the extreme concrete compression fiber to the center of gravity of the prestressing strands, d_p = 40.7 in. $$\frac{\varepsilon_c}{c} = \frac{\varepsilon_t}{d-c} \rightarrow \frac{0.003}{4.9} = \frac{\varepsilon_t}{40.7-4.9}$$ $\varepsilon_t = 0.022 > 0.005$ Therefore the section is tension controlled. $$\varphi = 1.0, \text{ for flexure}$$	EVAL. MANUAL C6A.5.5 EVAL. MANUAL C5.7.2.1 LRFD 5.7.2.1 & 5.5.4.2 LRFD 5.5.4.2
STEP 7: MINIMUM REINFORCEMENT Amount of reinforcement to develop M_r equal to the lesser of $1.33M_u$ or $1.2M_{cr}$ $$M_r = M_n = 3511 \text{ kft}$$ $$M_u = 1.75(582.4) + 1.25(819.3) + 1.5(78.7) = 2161 \text{ kft}$$ $$1.33M_u = 1.33(2161) = 2874 \text{ kft}$$ $$M_r > 1.33M_u \text{ (3511 kft > 2874 kft)}$$ Therefore, minimum reinforcement check is satisfied	LRFD 5.7.3.3.2 LRFD 5.7.3.2
STEP 8: LOAD RATING OF UNDAMAGED GIRDER RF$_R$ *Critical section for undamaged simple span girder is at MIDSPAN.* Assemble γ factors for both Inventory and Operating Levels: Inventory: γ_{DC} = 1.25; γ_{DW} = 1.50; γ_{LL+IM} = 1.75 Operating: γ_{DC} = 1.25; γ_{DW} = 1.50; γ_{LL+IM} = 1.35 Assume P = 0 k. Inventory: $$RF = \frac{\varphi C - \gamma_{DC}DC - \gamma_{DW}DW \pm \gamma_P P}{\gamma_{LL}(LL+IM)} = \frac{3511-1.25(819.3)-1.50(78.7)}{1.75(582.4)} = 2.32 \ \leftarrow$$ Operating: $$RF = 2.32\frac{1.75}{1.35} = 3.01 \ \leftarrow$$	EVAL. MANUAL T6A.4.2.2-1 EVAL. MANUAL Eq. 6A.4.2.1-1

STEP 9: DAMAGED CAPACITY

Damage occurs at 0.35L

Determining the damaged capacity will follow the same procedure the nominal capacity, but will include the effects of the lost strands at the damaged section.

LRFD Eq. 5.7.3.1.1-1

$$f_{ps} = f_{pu}\left(1 - k\frac{c}{d_p}\right)$$

f_{pu} = 250 ksi and k = 0.28 for low lax strands

d_p = distance from extreme compression fiber to C.G. of prestressing tendons

$$d_p = 45 - 4.5 = 40.5 \text{ in}$$

5 strands (of 57) have been lost, therefore: A_{ps} = 52 x 0.08 = 4.16in^2

LRFD Eq. 5.7.3.1.1-4

$$c = \frac{A_{ps}f_{ps} - A_s f_s - A_s' f_s'}{0.85f_c'\beta_1 b + kA_{ps}\frac{f_{pu}}{d_p}} = \frac{4.16 \times 250 - 0}{0.85 \times 5.5 \times 0.78 \times 48 + 0.28 \times 4.16 \times \frac{250}{40.5}} = 5.70 \text{ in}$$

$$a = \beta_1 c = 0.78 \times 5.70 = 4.4 \text{ in} < 6 \text{ in}$$

Therefore, rectangular section behavior assumption is valid

$$f_{ps} = 250\left(1 - 0.28\frac{4.4}{40.5}\right) = 242.4 \text{ ksi}$$

LRFD Eq. 5.7.3.2.2-1

$$M_n = A_{ps}f_{ps}\left(d_p - \frac{a}{2}\right) = 4.16 \times 242.4\left(40.5 - \frac{4.4}{2}\right) \times \frac{1}{12} = 3218 \text{ kft}$$

STEP 10: LOAD RATING OF DAMAGED GIRDER, RF$_D$

Critical section for damaged girder is at 0.375L (see Section 5.2).

Inventory:

EVAL. MANUAL Eq. 6A.4.2.1-1

$$RF = \frac{\varphi C - \gamma_{DC}DC - \gamma_{DW}DW \pm \gamma_P P}{\gamma_{LL}(LL + IM)} = \frac{3218 - 1.25(767.3) - 1.50(73.7)}{1.75(547.1)} = 2.24$$

Operating:

$$RF = 2.24\frac{1.75}{1.35} = 2.90 \text{ OK} \leftarrow$$

STEP 11: DEFINE OBJECTIVE OF REPAIR

Restore undamaged moment capacity: M_n = 3511 k-ft

Capacity of damaged girder without repair: M_{3-2-0} = 3218 k-ft

Capacity will be restored with the use of externally bonded CFRP plates.

All equation, figure and table references for FRP repair design are from ACI 440.2R-08, unless otherwise noted.

STEP 12: CALCULATE FRP SYSTEM DESIGN MATERIAL PROPERTIES

ACI T9.1

$$C_E = 0.85$$

$$f_{fu} = C_E \times f_{fu}^* = 0.85 \times 406 = 345 \text{ ksi}$$

$$\varepsilon_{fu} = C_E \times \varepsilon_{fu}^* = 0.85 \times 0.017 = 0.0145 \text{ in/in}$$

STEP 13: ASSEMBLE BEAM PROPERTIES

Assemble geometric and material properties for the beam and FRP system. An estimate of the area of FRP (A_f) is chosen here. If the section capacity does not meet the demand after the completion of all steps in this procedure, the FRP area is iterated upon.

$E_c = 4.23 \times 10^6$ psi	$A_{ps} = 4.16$ in^2
$A_{cg,C} = 886$ in^2	$E_{ps} = 28.5 \times 10^6$ psi
$h = 45$ in	$\varepsilon_{pe} = 0.0050$
$y_t = 22.2$ in	$P_e = 592,400$ lb
$y_b = 22.8$ in	cg strands = 4.5 in
$e = 18.3$ in	$d_p = 40.5$ in
$I_{x,C} = 255,300$ in^4	$A_f = 0.463$ in^2 (assumed)
$r = 17.0$ in	$E_f = 23.2 \times 10^6$ psi
	$d_f = 45.0235$ in

STEP 14: DETERMINE STATE OF STRAIN ON BEAM SOFFIT, AT TIME OF FRP INSTALLATION

The existing strain on the beam soffit is calculated. It is assumed that the beam is uncracked and the only load applied at the time of FRP installation is dead load. M_D is changed to reflect a different moment applied during CFRP installation. If the beam is cracked, appropriate cracked section properties may be used. However, a cracked prestressed beam may not be a good candidate for repair due to the excessive loss of prestress required to result in cracking.

$$\varepsilon_{bi} = \frac{-P_e}{E_c A_{cg}}\left(1 + \frac{e y_b}{r^2}\right) + \frac{M_D y_b}{E_c I_g}$$

$$= \frac{-592400}{4.23 \times 10^6 \times 886}\left(1 + \frac{18.5 \times 22.8}{(15.6)^2}\right) + \frac{((819.3 + 82.0) \times 12000) \times 22.8}{4.23 \times 10^6 \times 255300} = -0.0002 \text{ in/in}$$

STEP 15: ESTIMATE DEPTH TO NEUTRAL AXIS

Any value can be assumed, but a reasonable initial estimate of c is ~ 0.2h. The value of c is adjusted to affect equilibrium.

$$c = 0.2 \times 45\text{in} = 9.0 \text{ in}$$

STEP 16: DETERMINE DESIGN STRAIN OF THE FRP SYSTEM

The limiting strain in the FRP system is calculated based on three possible failure modes: FRP debonding (Eq. 10-2), FRP rupture (Eq. 10-16) and FRP strain corresponding to prestressing steel rupture (Eq. 10-17). The strain in the FRP system is limited to the minimum value obtained from (Eq. 10-2), (Eq. 10-16) and (Eq. 10-17).

FRP Strain corresponding to FRP Debonding: | ACI Eq. 10-2

$$\varepsilon_{fd} = 0.083\sqrt{\frac{f_c'}{nE_f t_f}} = 0.083\sqrt{\frac{5500}{1 \times 23.2 \times 10^6 \times 0.047}} = 0.0059\,\text{in/in}$$

FRP Strain corresponding to Concrete Crushing: | ACI Eq. 10-16

$$\varepsilon_{fe} = \frac{\varepsilon_{cu}(d_f - c)}{c} - \varepsilon_{bi} = \frac{0.003 \times (45.0235 - 9.0)}{9.0} - (-0.0002) = 0.0122\,\text{in/in} \le \varepsilon_{fd}$$

FRP Strain corresponding to PS Steel Rupture: | ACI Eq. 10-17

$$\varepsilon_{fe} = \frac{(\varepsilon_{pu} - \varepsilon_{pi})(d_f - c)}{(d_p - c)} - \varepsilon_{bi} \le \varepsilon_{fd}$$

where | ACI Eq. 10-18

$$\varepsilon_{pi} = \frac{P_e}{E_p A_p} + \frac{P_e}{E_c A_c}\left(1 + \frac{e^2}{r^2}\right) = \frac{592400}{28.5 \times 10^6 \times 4.16} + \frac{592400}{4.23 \times 10^6 \times 886}\left(1 + \frac{(18.5)^2}{(17.0)^2}\right) = 0.0053\,\text{in/in}$$

$$\varepsilon_{fe} = \frac{(0.035 - 0.0053)(45.0235 - 9.0)}{(40.5 - 9.0)} - (-0.0002) = 0.0341\,\text{in/in}$$

Therefore, the limiting strain in the FRP system is ε_{fd} =0.0059 in/in and the anticipated mode of failure is FRP debonding.

STEP 17: CALCULATE THE STRAIN IN THE EXISTING PRESTRESSING STEEL

The strain in the prestressing steel can be calculated with the following expression: | ACI Eq. 10-22

$$\varepsilon_{ps} = \varepsilon_{pe} + \frac{P_e}{E_c A_c}\left(1 + \frac{e^2}{r^2}\right) + \varepsilon_{pnet} \le 0.035$$

Prestressing Steel Strain corresponding to concrete crushing: | ACI Eq. 10-23a

$$\varepsilon_{pnet} = 0.003\frac{(d_p - c)}{c} = 0.003\frac{(40.5 - 9.0)}{9.0} = 0.0105\,\text{in/in}$$

$$\varepsilon_{ps} = 0.0050 + \frac{592400}{4.23 \times 10^6 \times 790}\times\left(1 + \frac{(18.5)^2}{(17.0)^2}\right) + 0.0105 = 0.0158\,\text{in/in} \le 0.035$$

Prestressing Steel Strain corresponding to FRP rupture or debonding: | ACI Eq. 10-23b

$$\varepsilon_{pnet} = (\varepsilon_{fe} + \varepsilon_{bi})\frac{(d_p - c)}{(d_f - c)} = (0.0059 - 0.0002)\frac{(40.5 - 9.0)}{(45.0235 - 9.0)} = 0.0050\,\text{in/in}$$

$$\varepsilon_{ps} = 0.0050 + \frac{592400}{4.23 \times 10^6 \times 886}\times\left(1 + \frac{(18.5)^2}{(17.0)^2}\right) + 0.0050 = 0.0104\,\text{in/in} \le 0.035$$

Therefore, FRP debonding represents the expected failure mode of the system and ε_{ps} = 0.0104 in/in.

STEP 18: CALCULATE STRESS LEVEL IN THE PRESTRESSING STEEL AND FRP	ACI Eq. 10-24
$$f_{ps} = 28500 \times \varepsilon_{ps} \quad (\text{when } \varepsilon_{ps} \leq 0.0076)$$ $$\text{or}$$ $$f_{ps} = 250 - \frac{0.04}{\varepsilon_{ps} - 0.0064} \quad (\text{when } \varepsilon_{ps} \geq 0.0076)$$ $\varepsilon_{ps} = 0.0104 > 0.0076$ therefore use $f_{ps} = 250 - \dfrac{0.04}{(0.0104) - 0.0064} = 239.9 \, \text{ksi}$ $$f_{fe} = E_f \times \varepsilon_{fe} = 23.2 \times 10^6 \times 0.0059 = 136.9 \text{ ksi} \leftarrow$$	ACI Eq. 10-9
STEP 19: CALCULATE EQUIVALENT STRESS BLOCK PARAMETERS From strain compatibility, the strain in the concrete at failure can be calculated as: $$\varepsilon_c = (\varepsilon_{fe} + \varepsilon_{bi}) \frac{c}{(d_f - c)} = (0.0059 - 0.0002) \times \frac{9.0}{45.0235 - 9.0} = 0.0014 \, \text{in/in}$$ The strain ε_c' corresponding to f_c' is calculated as: $$\varepsilon_c' = \frac{1.7 f_c'}{E_c} = \frac{1.7 \times 5500}{4.23 \times 10^6} = 0.0022 \, \text{in/in}$$ Using ACI 318-08, the equivalent stress block factors can be calculated as: $$\beta_1 = \frac{4\varepsilon_c' - \varepsilon_c}{6\varepsilon_c' - 2\varepsilon_c} = \frac{4 \times 0.0022 - 0.0014}{6 \times 0.0022 - 2 \times 0.0014} = 0.712$$ $$\alpha_1 = \frac{3\varepsilon_c'\varepsilon_c - \varepsilon_c^2}{3\beta_1\varepsilon_c'^2} = \frac{3 \times 0.0022 \times 0.0014 - (0.0014)^2}{3 \times 0.713 \times (0.0022)^2} = 0.703$$	
STEP 20: CALCULATE THE INTERNAL FORCE RESULTANTS $$c = \frac{A_p \times f_{ps} + A_f \times f_{fe}}{\alpha_1 \times f_c' \times \beta_1 \times b} \frac{4.16 \times 239.9 + 0.463 \times 136.9}{0.703 \times (5500/1000) \times 0.712 \times 48} = 8.03 \, \text{in} > 6 \, \text{in} \leftarrow$$ c is found to be greater than the height of the flange (6 in), so c needs to be recalculated accounting for the neutral axis extending into the web. This calculation yields c = 15.2 in.	ACI Eq. 10-25
STEP 21: ACHIEVE EQUILIBRIUM The value of c calculated in Step 20 must be equal to that of the c value assumed in Step 15. If not, the value of c must be iterated upon until these values are equal. Upon iteration of c, flexural strength must be checked as in Step 22. If the calculated strength is not sufficient, the area of FRP reinforcement must be increased and Step 15 through Step 22 must be repeated, as is the case with this design. A_f is increased to 1.389in^2 and the process repeated. By iteration, c = 11.5 in. $\leftarrow$	

|	
STEP 22: CALCULATE THE FLEXURAL STRENGTH CORRESPONDING TO THE PRESTRESSING STEEL AND FRP COMPONENTS The nominal capacity of the section is found as: $$M_n = M_{np} = \psi M_{nf}$$ The corresponding contribution of prestressing steel and FRP, respectively, are found as: $$M_{np} = A_p f_{ps}\left(d_p - \frac{\beta_1 c}{2}\right) = 4.16 \times 239.7 \times \left(40.5 - \frac{0.737 \times 11.5}{2}\right) = 36159\,\text{kin}$$ $$M_{nf} = A_f f_{fe}\left(d_f - \frac{\beta_1 c}{2}\right) = 1.389 \times 136.8 \times \left(45.0235 - \frac{0.737 \times 11.5}{2}\right) = 7750\,\text{kin}$$ $$\psi = 0.85$$ The nominal section capacity of the *repaired girder* is: $$M_n = M_{REP} = (36159 + (0.85)7750)\frac{1}{12} = 3562\,\text{kft} \leftarrow$$	ACI Eq. 10-26
STEP 23: CALCULATE REPAIR RATING FACTOR, RF_R Inventory: $$RF_R = \frac{\varphi C - \gamma_{DC}DC - \gamma_{DW}DW \pm \gamma_P P}{\gamma_{LL}(LL+IM)} = \frac{3562 - 1.25(767.3) - 1.50(73.7)}{1.75(547.1)} = 2.60 \leftarrow$$ Operating: $$RF_D = 2.60\frac{1.75}{1.35} = 3.37 \leftarrow$$ ***The Inventory and Operating Rating Factor are compared to those calculated at all other sections in this example. The critical section is once again at MIDSPAN and the girder rating factors are those calculated in Step 8.***	
STEP 24: DESIGN SUMMARY Use 15 – 2 in wide CFRP strips. 	
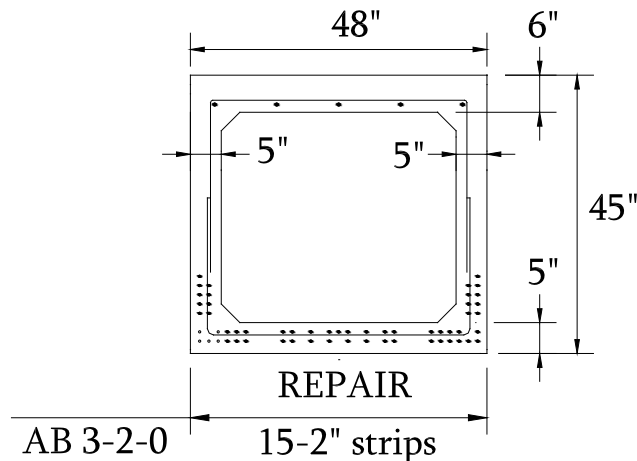
BIBLIOGRPAHY

American Association of State Highway and Transportation Officials (AASHTO). 2007. *LRFD Bridge Design Specifications*, 4th Edition and Interims, Washington, D.C.

American Association of State Highway and Transportation Officials (AASHTO). 2011. *Manual for Bridge Evaluation*, 2nd Edition, Washington, D.C.

American Concrete Institute (ACI) Committee 222. 2001. *ACI 222.2R-01 Corrosion of Prestressing Steels*, ACI, Farmington Hills MI, 43 pp.

American Concrete Institute (ACI) Committee 318. 2008. *ACI 318-08 Building Code Requirements for Structural Concrete and Commentary*, ACI, Farmington Hills MI, 43 pp.

American Concrete Institute (ACI) Committee 440. 2008. *ACI 440.2R-08 Guide for the Design and Construction of Externally Bonded FRP Systems for Strengthening Concrete Structures*, ACI, Farmington Hills MI,76pp.

American Marietta Company. 1960. L.R. 187 Bridge at STA. 316+18.25 Drawings (4 sheets). Approved by PADoH October 26, 1960.

Beer, F.P. and Johnston, E.R. 1985. *Mechanics of Materials: SI Edition*. McGraw-Hill Ryerson, Ltd, Canada.

Bentz, E. 2000. RESPONSE 2000 – Reinforced Concrete Sectional Analysis using the Modified Compression Field Theory, version 1.0.5.

Boresi, A.P. and Sidebottom, O.M. 1986. *Advanced Mechanics of Materials*, John Wiley and Sons, Ltd.

Enchayan, R. 2010. Repair of Damaged Prestressed Concrete Girder, *Presentation at the AASHTO Midwest Bridge Preservation Conference*, October 13, 2010, Detroit, MI.

Federal Highway Administration (FHWA). 2007. National Bridge Inventory (NBI), <www.fhwa.dot.gov/Bridge/nbi.htm> (accessed 02/12/10).

Feldman, L.R., Jirsa, J.O., Fowler, D.W. and Carrasquillo, R.L. 1996. Current Practice in the Repair of Prestressed Bridge Girders, Report No. FHWA/TX-96/1370-1. The University of Texas at Austin, 69 pp.

Gilbert, R.J. and N.C. Mickelborough. 1990. *Design of Prestressed Concrete*. Span Press, Oxfordshire, United Kingdom.

Guyon, Y. 1963. *Prestressed Concrete*, John Wiley and Sons, Inc., New York, NY.

Harries, K.A. 2006. Full-scale Testing Program on De-commissioned Girders from the Lake View Drive Bridge, Pennsylvania Department of Transportation Report FHWA-PA-2006-008-EMG001. 158 pp.

Harries, K.A. 2009. Structural Testing of Prestressed Concrete Girders from the Lake View Drive Bridge, *ASCE Journal of Bridge Engineering*. 14(2). 78-92.

Harries, K.A., Kasan, J. and Aktas, C. 2009. Repair Methods for Prestressed Girder Bridges, Pennsylvania Department of Transportation Report FHWA-PA-2009-008-PIT 006. 169 pp.

Herman, T. 2005. A Tale of Two Bridges, *Bridges Magazine*, Nov/Dec. 2005, 14-16.

Hoyer, E. 1939. Der Stahlsaitenbeton [piano-string-concrete], Otto Elsner, Berlin, 136 pp.

Kaar, P.H., La Fraugh, R. W. and Mass, M. A. 1963. Influence of Concrete Strength on Strand Transfer Length, *PCI Journal*, 8(5), 47-67.

Kasan, J.L. 2009. Structural Repair of Prestressed Concrete Bridge Girders. MSCE Thesis, University of Pittsburgh, Pittsburgh, Pennsylvania, 161 pp.

Kim, Y.J., Green, M.F. and Fallis, G.J. 2008. Repair of Bridge Girder Damaged by Impact Loads with Prestressed CFRP Sheets, *ASCE Journal of Bridge Engineering*, 13(1), 15-23.

Klaiber, F.W, Wipf, T.J. and Kempers, B.J. 2003. Repair of Damaged Prestressed Concrete Bridges using CFRP, Mid-Continent Transportation Symposium Proceedings, Center for Transportation Research and Education, Ames, IA.

Marrey, B. and Grote, J. 2003. The Story of Prestressed Concrete from 1930 to 1945: A Step Towards the European Union. Proceedings of the First International Congress on Construction History, Madrid, January 2003.

Miller, R.A. and Parekh, K.J. 1994. Destructive Testing of Deteriorated Prestressed Box Beam Bridge, *Transportation Research Record*, Number 1460, pp 37-44.

Mitchell, D., Cook, W. D., Khan, A. A. and Tham, T. 1993. Influence of High Strength Concrete on Transfer and Development Length of Pretensioning Strand. *PCI Journal*, May-June, 52-66.

Naito, C., Sause, R., Hodgson, I., Pessiki, S. & Desai, C. 2006. Forensic Evaluation of Prestressed Box Beams from the Lake View Drive over I-70 Bridge, ATLSS Report No. 06-13, Lehigh University, Bethlehem, PA. 62 pp.

Oh, B. H. and Kim, E. S. 2000. Realistic Evaluation of Transfer Lengths in Prestensioned, Prestressed Concrete Members, *ACI Structural Journal*, 97 (6), 821-830.

Oh, B.H., Kim, E.S. and Kim, K.S. 2001. Correct Prediction of Transfer Lengths in Pretensioned Prestressed Concrete Structures. Transactions, *SMiRT 16*, Washington D.C.

Pakrashi, V., Kelly, J., Harkin, J., Farrell, A., Nanukuttan, S. 2010. Emergency Rehabilitation of Brownsbarn Bridge. BCRI2010 Joint Symposium: Bridge and Infrastructure Research in Ireland (BRI) and Concrete Research in Ireland (CRI). Cork, Ireland.

Park, R. and Paulay, T. 1975. *Reinforced Concrete Structures*, John Wiley and Sons, 773 pp.

Pennsylvania Department of Transportation (PennDOT). 2007. Bridge Inventory December 2007. PennDOT, Harrisburg, PA, USA.

Pennsylvania Department of Transportation (PennDOT). 2010. *Bridge Safety and Inspection Manual*, 2nd Ed. (PennDOT Publication 238). Harrisburg, PA, 482 pp.

Precast/Prestressed Concrete Institute (PCI). 1999. *PCI Design Handbook*, 5th edition, Chicago, IL.

Schiebel, S., Parretti, R. and Nanni, A. 2001. Repair and Strengthening of Impacted PC Girders on Bridge A4845 Jackson County, Missouri, Report No. RDT01-017, Missouri Department of Transportation, Jackson City, MO.

Sika. 2008a. Case Study: Hopkin and Clinton Street Bridge Rehabilitation. Sika Corporation, USA.

Sika. 2008b. Prestressing System for Structural Strengthening with Sika CarboDur CFRP Plates. Sika Corportion, USA.

Spancrete. 1960. Washington County L.R. 798-1 Bridge at STA. 1205+50.00 Drawings (3 sheets). June 28, 1960. Approved by PADoH August 10, 1960.

Steinberg, E., Beir, J. T. and Sargand, S. 2001. Effects of Sudden Prestress Force Transfer in Pretensioned Concrete Beams, *PCI Journal*, January-February, 64-75.

Tabatabai, H. and Dickson, T.J. 1993. The History of the Prestressing Strand Development Length Equation, *PCI Journal*, 38(6), pp 64-75.

Toenjes, C.A. 2005. Repair of Prestressed Concrete Girders with Carbon Fiber Reinforced Polymer Wrap. Presentation at the International Bridge, Tunnel and Turnpike Association (IBTTA) Facilities Management Workshop, May 14-18, 2005, Toronto, Ontario. <http://www.ibtta.org/files/PDFs/Toenjes_Chris.pdf>. Accessed 10/6/11.

Chadwell, C.B. and Imbsen, R.A. 2004. XTRACT: A Tool for Axial Force - Ultimate Curvature Interactions. Proceedings of the ASCE Structures Congress, Nashville, TN. May 2004.

Tumialan, J.G., Huang, P., Nanni, A. and Jones, M. 2001. Strengthening of an Impacted PC Girder on Bridge A10062 St Louis County, Missouri, Report No. RDT01-013, University of Missouri-Rolla, Rolla, MO.

Wan, B., Petrou, P., Harries, K.A. and Hussein, A.A. 2002. "Top Bar" Effects in Prestressed Concrete Piles, *ACI Structures Journal*, 99(2), pp 208-214.

Yang, D. Merrill, B.D. and Bradberry, T.E. 2011. Texas' Use of CFRP Repair to Concrete Bridges. *Recent Advances in Maintenance and Repair of Concrete Bridges: ACI SP-277*, Ed. Yail. J. Kim, 39-48.